Inaugural - Dissertation

zur Erlangung der Doktorwürde
der
Naturwissenschaftlich-Mathematischen Gesamtfakultät
der Ruprecht-Karls-Universität
Heidelberg

vorgelegt von
Diplomphysiker Sören Doose
aus Kiel
Tag der mündlichen Prüfung: 31.10.2003

Single-Molecule Characterization of Photophysical and Colloidal Properties of Biocompatible Quantum Dots

Gutachter: Prof. Dr. Jürgen Wolfrum
Prof. Dr. Shimon Weiss

Zusammenfassung

Kolloidale Halbleiter-Nanokristalle stellen eine neue Klasse von Fluoreszenzsonden für biologische Anwendungen dar. Aufgrund ihrer besonderen optischen Eigenschaften — durchstimmbares, schmales Emissionsspektrum, kontinuierliches Anregungsspektrum, hohe Photostabilität und lange Fluoreszenzlebensdauern (in der Grössenordnung von 10 ns) — eignen diese sich besonders für Experimente, die lange Beobachtungzeiten, Detektion von mehreren Farben oder eine zeitlich selektierte Detektion erfordern.

Photophysikalische Eigenschaften von CdSe oder CdTe Kern, CdSe/ZnS Kern/Schale und oberflächenmodifizierten Nanokristallen sind auf Ensemble- und Einzelmolekülebene untersucht worden.

Eine Vielzahl von Syntheserouten und Oberflächenmodifikationen, die Löslichkeit in wässrigen Medien und Markierung von biologischen Makromolekülen ermöglichen, sind Voraussetzung für biologische Anwendungen. Aufgrund der hohen Empfindlichkeit auf Oberflächenzustände haben chemische Modifikationen grosse Auswirkungen auf die photophysikalischen Eigenschaften, die genau kontrolliert werden müssen. Fluoreszenz von Nanokristallen wurde mittels Einzelmolekülmethoden charakterisiert, Intensitätsfluktuationen untersucht und eine nicht fluoreszierende Subpopulation entdeckt, die über lichtinduzierte Prozesse reaktiviert werden kann.

Konfokale Scanning-Stage-, Epifluoreszenz- und Total-Internal-Reflection- Mikroskopie wurden verwendet, um auf Glass immobilisierte Nanokristalle zu beobachten. Messung der Fluoreszenzlebensdauern ergaben Werte von ca. 20 ns für einzelne Nanokristalle, wobei Abweichungen von einem monoexponentiellen Verhalten sichtbar wurden. Durch die Beobachtung von Photon-Antibunching konnte nachgewiesen werden, dass diese Eigenschaften charakteristisch für einzelne Teilchen sind.

Fluoreszenz-Korrelations-Spektroskopie (FCS) fand Verwendung, um photophysikalische und kolloidale Eigenschaften von Nanokristallen in Lösung zu untersuchen.

Es wurde gezeigt, dass FCS eine wertvolle Methode darstellt, um Information zu Synthese und Oberflächenmodifikationen zu gewinnen. FCS ermöglicht die Messung der Konzentration fluoreszierender Teilchen, einer mittleren Intensität und der Teilchengrösse. Aus diesen kann die Fluoreszenzintensität pro Teilchen abgeleiten werden, was mit Ensemblemethoden nicht erreicht werden kann, solange eine Subpopulation von absorbierenden aber nicht emittierenden Teilchen präsent ist. Das Verhältnis von dunklen zu fluoreszierenden Teilchen wurde bestimmt und Änderungen der Konzentration durch lichtinduzierte Aktivierung beobachtet. Mit FCS gemessene Teilchengrössen wurden mit Messungen mittels Transmissionselektronenmikroskopie verglichen und gute Übereinstimmung für Teilchen von 7 nm gefunden.

Es wurde beobachtet, dass die Korrelationsamplitude von der Anregungsenergie abhängt, was durch Einflüsse von Sättigung und optischen Kräften (optical trapping) erklärt werden kann. Für die Polarisierbarkeit ergaben sich Werte, die zwei Grössenordnungen über Literaturwerten liegen, die auf Messungen mit nicht-resonanten Wellenlängen basieren.

Monte-Carlo Simulationen (MCS) wurden durchgeführt, um Korrelationsfunktionen unter dem Einfluss von Intensitätsschwankungen (Blinken), die einem Potenzgesetz folgen, zu berechnen. Zu diesem Zweck wurden Diffusion durch ein konfokales Beobachtungsvolumen, Absorptions-Emissions-Zyklen mit definierten Zeitkonstanten und Blinken in die MCS integriert. Einflüsse von Sättigung, Grössenverteilungen, photochemische Zersetzung und Blinken konnten simuliert und mit experimentellen Daten verglichen werden.

MCS reproduzieren zwei Effekte, die durch den Einfluss von Blinken auf FCS Kurven experimentell beobachtet werden: (i) deutliche Abweichung von einem Diffusionsmodell bei hohen Anregungsenergien; (ii) keine Abweichungen von diesem Modell bei niedrigen Anregungsenergien. Simulationen ergaben, dass FCS für gewisse Potenzgesetze nicht vom Blinken beeinflusst wird.

Abstract

Colloidal semiconductor nanocrystals (NCs) have recently been introduced as novel fluorescent labels for various biological applications. Their unique optical properties — tunable narrow emission spectrum, broad excitation spectrum, high photostability and long fluorescent lifetimes (on the order of tens of nanoseconds) — make them attractive probes in experiments involving long observation times, multicolor and time-gated detection.

Photophysical properties were investigated at the ensemble and single-molecule level for CdSe or CdTe core, CdSe/ZnS core-shell and surface-modified NCs. The use of NCs as fluorescent probes in biological applications requires various synthesis routes and surface modifications to enable solubility in aqueous solution and to allow labeling of biological macromolecules. Due to NC's sensitivity to surface-defects chemical treatments have a significant influence on photophysical properties and need to be thoroughly monitored. Single-molecule fluorescence detection was used to characterize NC fluorescence, observe intermittency in the emission (blinking), and unravel a non-fluorescent subpopulation of NCs whose fluorescence can be restored through photo-induced activation.

Stage-scanning confocal, epifluorescence and objective-type total-internal-reflection microscopy, were applied to observe surface-immobilized NCs. Fluorescence lifetimes were determined to be around 20 ns for single particles showing deviations from a mono-exponential decay. This observation was proven to be characteristic of single particles by monitoring photon antibunching.

Fluorescence correlation spectroscopy (FCS) was used to characterize photophysical and colloidal properties in solution. It was shown to be a powerful technique to rapidly evaluate information on synthesis and surface modifications. These are essential to achieve water-solubility and bio-conjugation and dramatically influence the optical performance. FCS allows measuring concentration of fluorescent parti-

cles, an average brightness and particle size. From these observables, the brightness per particle can be estimated, something not possible in ensemble measurements due to the presence of absorbing but dark particles. The ratio of dark to fluorescent NCs was estimated and concentration changes due to photo-induced activation were observed. Particle sizes measured by FCS were compared to transmission electron microscopy and found in good agreement down to 7 nm.

The correlation amplitude was observed to be excitation power dependent which was attributed to saturation and optical trapping effects. An electronic polarizability was evaluated and found to be two orders of magnitude larger than reported for measurements at non-resonant wavelength.

Monte-Carlo simulations (MCS) were performed to compute autocorrelation functions under the influence of power-law blinking. Diffusion through a confocal volume, excitation-emission cycles with defined rate constants and on/off blinking were incorporated into MCS and used to investigate influences of saturation, size-distributions, photobleaching and blinking. The results were compared to experimental data of various NCs.

Simulations account for both types of experimentally observed effects of blinking in FCS curves: significant deviation from a diffusion-model observed at high excitation powers; and no deviation from a diffusion-model despite the existence of blinking, observed at low excitation powers. Simulations showed that blinking does not influence FCS data for certain power law parameters.

Acknowledgments

I am grateful to all the people who helped me through good and bad times during my dissertation work.

I am very thankful to Prof. Jürgen Wolfrum and Prof. Markus Sauer for introducing me to the fascinating field of single-molecule fluorescence spectroscopy and supporting my stay abroad for much longer than initially planed.

Prof. Shimon Weiss I would like to thank just as much for welcoming me in his group, convincing me a few times to stay a bit longer, and for providing an excellent research environment. I enjoyed being part of two very different laboratories in Berkeley and Los Angeles.

I also enjoyed being part of a group from which I learned in many ways: Xavier Michalet and Achilles Kapanidis showed me the quirks of scientific work and taught me that one can never be critical enough; Xavier also helped me enter the world of LabView; Fabien Pinaud, Malte Pflughoefft and James Tsay provided lots of NC samples together with chemical explanations; Ted Laurence explained numerous details about optics and computers; Laurent Bentolila helped me appreciate biology from the inside but also outdoors; Jun-Ichi Hotta taught me how to use an optical tweezer; Thilo Lacoste and Alois Sonnleitner introduced me to the peculiarities of TIR; and all the others made having coffee, well, *once* a day, so much more fun: Nam Ki Lee, Emmanuel Margeat, Nathalie Grassmann, Xiangxu Kong, Markus Jäger, Sam On Ho, Kambiz Hamadani, Eyal Nil, Tsing Hua Her, Brian Campbell. I would like to thank Lori Stinson for being so cheerful (especially in the morning) even when dealing with letters concerning visa issues.

I would also like to thank the guys in Germany for having welcomed me in their group once and many times again: Dirk-Peter Herten, Hannes Neuweiler, Christian Müller, Chong Woo Park, Kjung-Tae Han, Andreas Schulz, Volker Buschmann, Anja Dietrich, Hannes Barsch and all the others in the physical-chemistry department.

I am especially thankful to Philip Tinnefeld for his support in fighting black bears and a few other obstacles, to Achilles Kapanidis and Elke Reuter who kept me afloat whenever life and research wasn't going so great and to Olaf Körner and Ann-Catrin Pahl for providing lots of motivation.

My greatest thanks goes to my family, Hans-Otto and Meike, my grandparents, uncles and aunts, who played a much bigger role than the amount of hours we spend together would suggest. Without their love and encouragement this work would never have been finished.

I would like to thank Xavier, Shimon, Achilles, Malte, Natalie and James for critical comments on the manuscript, Tenaya Sims for putting up with my paper chaos in the middle of the living room and Olaf for his indispensable help with LaTeX.

And last not least I am very grateful for financial support provided by the Boehringer Ingelheim Fonds.

Abbreviations

ADC	Analog-to-Digital Converter
AFM	Atomic Force Microscopy
APD	Avalanche Photodiode
CCD	Charge-Coupled Device
CLSM	Confocal-Laser-Scanning-Microscopy
CW	continues laser emission
DP	Detection Profile
EMCCD	Electron-Multiplying Charge-Coupled Device
EP	Excitation Profile
FCS	Fluorescence Correlation Spectroscopy
FIDA	FLuorescence Intensity Distribution Analysis
FIMDA	Fluorescence Intensity Multiple Distribution Analysis
FISH	Fluorescence-In-Situ-Hybridization
FRET	Förster Resonance Energy Transfer
GFP	Green-Fluorescent-Protein
ICCD	Image-Intensified Charge-Coupled Device
MAFID	Moment Analysis of Fluorescence Intensity Distribution
MCP	Micro-Channel-Plate
NC	Nanocrystal
NI	National Instruments
NSOM	Near-Field Scanning Optical Microscopy
OP	Observation Profile
PAID	Photon Arrival-Time Interval Distribution
PCH	Photon Counting Histogram
PMP	Photomultiplier Tube
PSF	Point-Spread-Function

QE	Quantum Efficiency
QY	Quantum Yield
RMS	Root-Mean-Square
SBR	Signal-to-Background Ratio
SNR	Signal-to-Noise Ratio
STD	Standard Deviation
TEM	Transmission Electron Microscopy
TIR	Total-Internal-Reflection

List of Figures

Contents

1

Introduction

A rainbow in the sky, glowing algae in the sea or flickering northern lights are just a few examples of colorful impressions in nature. A world in black and white would not be nearly as beautiful and much less exciting. Color influences our emotions as much as it is used to express them. Blue and rose periods are part of everyone's life. The explanation of color by electromagnetic waves with a defined frequency reveals a different world with just as many wonders, worth of exploration. But color can also serve as a tool, and help to explore nature's beauty, when it is hidden from our senses or buried in the details. One such tool which utilizes color is fluorescence microscopy. Fluorescence, the emission of light by matter when being exposed to light of a different color, has been known since the first report by Herschel *[Herschel, 1845]* about the appearance of a blue color in quinine, an ingredient in tonic water, when illuminated by sun light. Stokes unveiled the advantageous characteristic that fluorescence typically occurs at lower energy or longer wavelength than that of absorption *[Stokes, 1852]*. This so-called Stokes-shift enables the observation of fluorescing molecules, or fluorophores, with a sensitivity and specificity that cannot be achieved with other optical methods. Fluorescence contributed in many ways to new discoveries. Spectroscopy helped unravel molecular details about fluorophores

and small molecules. Fluorescent probes are used as reporters in biochemical assays or chemical sensors.

Tremendous impact on biological research was achieved in combination with light microscopy. The invention of optical microscopy — Hans and Zacharias Janssen are credited with making the first compound microscope (a multiple lens assembly) around 1595 — enabled Anton van Leeuwenhoek to be the first person to see and identify bacteria. Optical microscopy grew more successful with technical developments that increased contrast between specimens. But since all non-fluorescence imaging-techniques, such as dark-field, phase-contrast or Nomarski's differential interference contrast (DIC), have to rely on variations in the index of refraction, they do not provide any means to distinguish individual objects any other than by their shape. To resolve more details and emphasize certain materials or species, staining agents were used to specifically color tissue, cells and organelles of interest. But the ultimate limit of resolution and sensitivity was only reached using fluorescence microscopy. By eliminating excitation light, leaving visible only emitting objects, background can almost be completely removed and the contrast dramatically increased. In addition, it became possible to observe individual objects that are smaller than the diffraction limit.

With the advent of molecular biology and an improved understanding of labeling chemistries, fluorescence microscopy further developed to make use of its full potential for observing the biological world at high resolution and with highest sensitivity.

In fact fluorescence microscopy is the only optical method that allows reaching the ultimate limit of sensitivity, that is the observation of individual molecules. Until this very recent achievement, non-optical methods were the first successful means to explore single-molecules. For example scanning tunneling *[Binning et al., 1982]*, atomic force *[Binning et al., 1986]* and electron microscopy achieved molecular or even atomic resolution of surfaces, and the patch clamp technique enabled the observation of ion translocation through single ion channels embedded in a cell membrane *[Neher and Sakmann, 1976]*. The limitations of these techniques to biological applications are obvious: the patch clamp technique can only observe electrical currents and thus investigate ion-channels, scanning tunneling and atomic force microscopy are limited to surface observations, difficult to perform in aqueous solvents and can only be performed at rather slow imaging speeds (seconds to minutes). In spite of a vast amount of fascinating images provided through electron microscopy and the tremendous impact electron microscopy has on biological research, it suffers from

similar limitations, is mostly performed in vacuum and at low temperature *[Burgess et al., 2003]*. None of these methods can tackle the growing demand to observe fast dynamics (microseconds to seconds) on a molecular scale in a non-invasive way and possibly even in a live cell environment.

Since the genome has been deciphered for a steadily increasing number of species, several thousand genes have been identified. But genes only contain the information that is needed to synthesize proteins, the functional units of life. Crystallography has provided structural information for a large number of proteins with astonishing resolution up to 1 Å. At the same time it is clear that functioning of cellular machinery and regulatory mechanisms depend on the interplay of many different protein components. A recent investigation identified several hundred protein complexes in the yeast organism *[Gavin et al., 2002; Ho et al., 2002]*. This means that functionality is not at all entirely defined by either the genetic code, or the structure of individual proteins. Protein-protein interactions therefore have attracted ever more interest over the last few years and fluorescence microscopy is an important tool for functional as well as structural analysis of macromolecules in the cell.

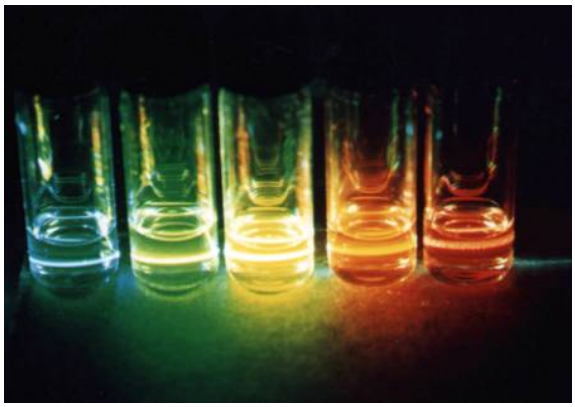

Figure 1.1: Concentrated solutions of CdSe/ZnS NCs with different radii and thus different emission wavelength. The particles are excited by an Argon laser (488 nm); particle radii are determined by transmission electron microscopy (form left to right, with corresponding emission wavelength): $\sim$ 1.5 nm (500 nm), $\sim$ 2.5 nm (530 nm), $\sim$ 3.5 nm (570 nm), $\sim$ 5 nm (605 nm), $\sim$ 6 nm (620 nm). Absorption and emission spectra are shown in Figure 4.1.

Fascinating examples can easily be named. Molecular machines that turn chemical energy into motion and make cells move, contract or divide, work more efficient

than the best engine, human beings have ever constructed. Protein-DNA complexes perform the most demanding tasks in terms of accuracy: the replication of DNA including proofreading, performed at a rate of 50 or more bases per second, transcription to read out the genetic code and make it available in the form of RNA, or translation to synthesize sequences of amino-acids from RNA. The direct investigation of such processes is complicated and many challenges are waiting on the path to finally observe and characterize such processes in vivo.

Even though textbooks usually present us a picture of individual molecules interacting with each other and performing specific actions over time, experimental evidence is still mostly based on ensemble measurements. Due to the fact that an ensemble of e.g. transcription complexes, is extremely difficult if not impossible to synchronize, single-molecule methods are often the only means to directly observe dynamic behavior of such complexes or variations in their composition. Also probing properties molecule by molecule can reveal sub-populations that are hidden in ensemble measurements due to the inherent averaging. Single-molecule methods lead to new information about any system for which the ergodic hypothesis is not applicable, meaning that an ensemble average does not provide the same result as a time average for one ensemble member. And this is the case for many biological macromolecules or protein complexes due to inhomogeneity in their structure or composition.

Fluorescence microscopy has developed into a variety of specialized techniques enabling single-molecule detection and spectroscopy. Applying a selective excitation scheme to single molecules at cryogenic temperatures, Moerner's and Orrit's group were the first to actually detect fluorescence from single molecules *[Moerner and Orrit, 1999]*. Confocal laser scanning microscopy (CLSM) helped not only to resolve the third dimension and image tissue layer by layer with improved resolution, but also to decrease background contributions from out of focus areas. Since background reduction turned out to be an essential task for the observation of single molecules in solution, confocal microscopy is the technique of choice for solution-based applications. The principle of evanescent wave excitation from either tapered fiber tips or total-internal-reflection (TIR) at interfaces provides another way to limit the excitation volume and with it some major background sources. TIR provided the means for the first successful observation of single antibodies, labeled with several hundred fluorophores, by *Hirschfeld [1976]*. This work pointed out one major limitation in fluorescence: organic fluorophores encounter irreversible photo-destruction

after the emission of a few million photons. This and other characteristics are emphasized by *Lakowicz [1999]* when he writes: "the probe is everything.". In addition to optical methods, the development of new fluorescent probes has experienced a tremendous advance over the last decades. The use of dye lasers stimulated the search for stable organic dyes emitting over the whole visible spectrum. Biological applications pushed the development of fluorophores emitting in the near IR, a wavelength range, where autofluorescence from naturally fluorescent proteins is essentially eliminated. Also fascinating is the controlled expression of green, yellow or red fluorescent proteins, fused to proteins of interest, in living cells.

In addition to various organic fluorophores, colloidal semiconductor nanocrystals (NCs), or quantum dots, have recently been introduced as biocompatible labels *[Michalet et al., 2001]*. Unique photophysical properties render NCs especially suitable for observations in the live cell: (i) a narrow emission spectrum that can be tuned throughout the visual wavelength range by varying the size of the NCs during synthesis; (ii) a broad absorption spectrum enabling multi-color detection schemes with a single wavelength excitation source; (iii) a fluorescence lifetime of 20–30 ns, 10 times longer than the lifetime of naturally-occurring fluorescent proteins (autofluorescence), allowing background reduction by a time-gated detection (selection of photons that are emitted with a certain delay to excitation); and (iv) a large total number of emitted photons (100–1000 times larger than for rhodamine fluorophores), prerequisite for observations at timescales of minutes and hours.

The first successful biological experiments using NCs to stain cells or specifically label actin filaments, antibodies and receptors have just been demonstrated *[Bruchez et al., 1998; Chan and Nie, 1998]*. These applications demonstrate the demand for extremely stable, multi-color probes. Unfortunately there are drawbacks, that become increasingly severe for site-specific labeling and single-particle experiments. NCs exhibit (like most single fluorophores) intermittency in their emission (blinking); but unlike organic fluorophores, the off-times are on the order of the experimental observation time. This behavior, together with the overall brightness, is strongly influenced by the specific protocol used in the synthesis, and chemical modifications of the NC surface, which are essential to any bioconjugation scheme. In addition, the overall size of several nanometers, which can easily be increased to several tens of nanometers for the preparation of bright, water-soluble and functional NCs, limits the applicability to site-specific labeling of biomolecules due to steric reasons.

Ongoing research on the synthesis and bioconjugation of colloidal NCs requires methods to monitor optical behavior each time a chemical modification is made to NCs. Current methods include UV/VIS and fluorescence spectrophotometers, liquid chromatography, and electrophoresis. In parallel, colloidal properties are monitored by powder x-ray diffraction, electron or atomic force microscopy.

Fluorescence correlation spectroscopy (FCS) is another optical technique, which monitors signal fluctuations. First introduced by *Magde et al. [1974]* it has matured over the last ten years through the combination with confocal microscopy. Single-molecule sensitivity allows identification of molecular species in terms of their diffusion behavior and other processes that cause fluctuations in the emission. Diffusion and rate constants can be extracted, as long as a theoretical model to fit experimental data is available. FCS and related techniques have been used to monitor macromolecular interactions in vitro and in vivo.

This thesis presents some of the unique photophysical properties of colloidal semiconductor NCs reaching from ensemble to single-particle concentrations. To turn NCs into exceptional fluorescent probes with a wide range of biological applications, a fast and reliable feedback loop between NC preparation, including chemical modifications and optical characterization, was developed using confocal fluorescence microscopy techniques. For the first time one-photon fluorescence correlation spectroscopy was used to collect information about colloidal and photophysical properties of semiconductor NCs in solution. An application is presented where FCS helps gathering information about photo-induced activation in solution and compare the results to single-particle measurements on a surface. Time-gated FCS is implemented and performed on NCs to reduce background contributions from organic impurities and increase signal to background ratios. This enables the determination of NC concentrations even in the presence of strong autofluorescence as in live cells. The influence of power-law distributed blinking on FCS data is explored via Monte-Carlo simulations and compared to experimental data. The developed methods are routinely used in our laboratory to provide a fast and reliable characterization of NCs in solution after alteration of photophysical properties by synthesis and surface modifications.

The second chapter will first give an overview of recent developments in fluorescence microscopy and review modern techniques that allow achieving single-molecule sensitivity (State of the Art and Theoretical Aspects). The prospects using NCs as novel fluorescent labels are explored, the origin of their unique optical properties

is explained, and FCS, a technique that is particularly useful for characterization of fluorescence in solution, is presented. In the following chapter (Experimental Concepts) experimental details are emphasized, which are relevant to this work. Samples and sample preparation methods are specified and technical details for the developed computer simulations are given. Then experimental results are presented (Results and Discussion), leading from ensemble characteristics of colloidal NCs to single-particle properties for surface-immobilized particles. Finally solution-based characterization using FCS is demonstrated to investigate photophysical as well as colloidal properties of NCs. Monte-Carlo simulations are presented as a tool to interpret the influence of blinking and, in rare cases, photobleaching on FCS data. The final chapter gives an overview of future applications how to use the developed methods, with an emphasis on biological applications (Conclusion and Outlook).

2

State of the Art and Theoretical Aspects

2.1 Fluorescence Microscopy

From the advent of natural sciences in the 16th century, the general approach of understanding nature was more and more diversified into specialized disciplines like physics, chemistry and biology. The last few decades marked the beginning of an opposite trend: the overlap of different fields leads to multidisciplinary approaches. This fact is illustrated by hybrid names for research areas, such as biophysical chemistry or bioinformatics, as well as scientific journals, e.g. Physical Chemistry Chemical Physics. Biology for example developed into a variety of research areas that either make use of fancy physical techniques (X-ray, NMR), explore the chemistry of DNA or proteins or use the maximum available computation power to interpret genetic information.

One technique that has had great impact on biology and later on material sciences is optical microscopy. Invented in the 16th century by the Janssens in Middleburg, Holland, it has evolved into a number of imaging systems with ever better resolving

power. Methods were developed to increase contrast and allow the observation of greater detail. Phase contrast, Nomarski's differential interference (DIC) or Hoffmann's contrast make use of variation in the index of refraction or it's influence on the light's polarization. In addition to these transmitted-light microscopy techniques, stains were used to identify specific objects and distinguish them from less interesting background. In particular fluorescent stains allowed increasing specificity and enabled the observation of objects that are smaller than the diffraction limit set by the observed wavelength.

2.1.1 Fundamentals of Fluorescence

Fluorescence, the process of emitting a photon during the relaxation from an energetically higher to a lower electronic state, has been extensively investigated in atomic physics. The rise of quantum mechanics at the beginning of the 20th century allowed explaining experimental observations in great detail.

Due to the tremendously increasing complexity that arises in molecules built up from a large number of atoms, an exact prediction of available electronic states and the transition probabilities or moments between them is impossible. Nevertheless theories with various degrees of approximation have been developed to give insight into the photophysics of increasingly complex molecules.

In organic molecules interactions with UV and visible light can lead to the absorption of photon energy by localized molecular units, called chromophores. The energy diagram for electrons in chromophores can very often be approximated in a way that resembles the electronic energy structure for atoms. The ground state S_0 corresponds to an electron configuration with the lowest possible energy. After excitation the molecule resides in the first or higher excited state S_n for a certain duration. It then can relax back into the ground state by emitting a photon with an energy $\Delta E = \hbar\nu$ which equals the energy difference between S_0 and S_1. Through interaction with phonons, the molecule can also enter long lasting triplet states T_n via phonon-assisted intersystem crossing. Transitions from singlet to triplet states are quantum-mechanically forbidden when spin interactions are ignored. Therefore intersystem crossing rates as well as deactivation rates of triplet states are about two orders of magnitude lower than rates for radiative relaxation from singlet states.

The larger a molecule, the more complex its vibrational modes become. Vibrational energy levels are spaced by energies much less than the difference between

electronic states. Since photon-absorption occurs much faster than molecular vibrations, the thermal equilibrium with respect to vibrational modes is disturbed with every absorption process. A Boltzmann-distribution for the vibrational modes of the excited state is restored at a sub-pico second timescale, leaving the molecule in its vibrational ground state of the electronically excited state for the longest time.

From an experimenters point of view such a simplified description often can be sufficient to put observations into the context of molecular mechanisms. Jablonski established the illustration of absorption and emission processes as depicted in Figure 2.1. In this scheme additional pathways can easily be visualized that cause non-radiative relaxation processes and reduce the number of excitations contributing to the fluorescence signal.

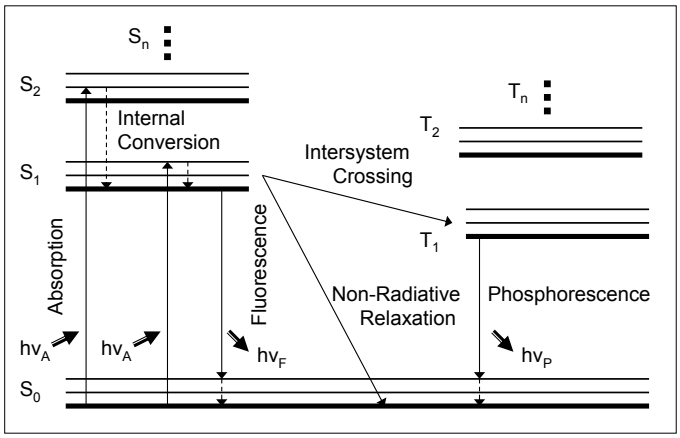

Figure 2.1: Jablonski Diagram: Absorption and emission processes are depicted as excitation from a ground to the first or second excited electronic state. Each electronic state is split into various vibrational states, which are populated according to a Boltzmann-distribution. Relaxation from electronic states can be due to fluorescence, intersystem crossing to a long-lived triplet state, followed by phosphorescence, or non-radiative processes like internal conversion, quenching by and energy transfer to near-by molecules.

A common characteristic of fluorescence, which can be used as an observable, is its intensity: the number of emitted photons per time unit. It depends on the number of absorbed photons per time (excitation power density, absorption cross section) and how many of the excited states relax radiatively (quantum yield). Other characteristics that can be turned into useful observables to obtain information from

a different perspective, have been inverstigated: spectrum, fluorescence lifetime, and polarization state.

Spectrum Fluorescence intensity always depends on the detected wavelength. The exact emission spectrum is the property that renders fluorescence such a powerful tool, mainly because the emission is shifted relative to the absorption spectrum by the so called Stokes shift. The complexity of fluorescent molecules results in the fact that in addition to electronic transitions, there are always vibrational modes interacting with electronic energy levels. As depicted in the Jablonski diagram (Figure 2.1), each excitation into an excited electronic state S_1, is followed by vibrational relaxation into the vibrational ground state of S_1. In other words, energy is converted from Coulomb energy into vibrational energy and eventually dissipated into heat. Vibrational relaxation occurs on time scales of picoseconds (10^{-12} s). Since the lifetime of an excited electronic state is on the order of nanoseconds (10^{-9} s), contributions from vibrational relaxation to the fluorescence lifetime are negligible. Furthermore as fluorophores usually decay to excited vibrational levels of the electronic ground state S_0 more energy is lost to vibrations causing an even larger Stokes shift. At the same time these rapid relaxation processes render emission spectra independent of the excitation wavelength, an observation that is known as Kasha's rule.

A third general feature of emission spectra in most fluorophores is expressed in the so called mirror rule. This rule expresses the fact that the emission spectrum representing the $S_1 \rightarrow S_0$ transition generally is a mirror image of the corresponding absorption spectrum. It can be explained by the similarity of vibrational energy levels in the ground and excited electronic state. According to the Frank-Condon principle all electronic transitions occur without change in the position of nuclei. This results in similar probabilities for corresponding transitions between particular vibrational energy levels in ground and excited electronic states:

$$Prob(S_0^0 \rightarrow S_1^2) \approx Prob(S_1^0 \rightarrow S_0^2), \quad \text{with } S^{\text{vibrational energy level}}_{\text{electronic energy level}}. \tag{2.1}$$

Lifetime and Quantum Yield The lifetime of an excited electronic state is influenced by any process depopulating that state with a certain rate constant k. In addition to the emission of photons, non-radiative processes can take place that convert the energy in other ways then into photons, leaving only a characteristic

amount of absorbed photons to be converted into fluorescence. The ratio describing how many absorbed photons are emitted is called fluorescence quantum yield, QY. In the case that all depopulation processes follow an exponential decay (N being the population number) and thus can be described by a rate constant $k_i = 1/\tau_i$, the overall depopulation process follows a sum of these rate constants

$$N(t) = N_0 \prod_i \exp(-k_i t) = N_0 \exp(\sum_i -k_i t) = N_0 \exp(-\frac{t}{\tau_f}). \tag{2.2}$$

Thus a decay, measured from emitted photons, that defines the fluorescence lifetime τ_f, is related to the radiative (also called intrinsic) lifetime $\tau_r = 1/k_r$ and other non radiative lifetimes $\tau_{nr} = 1/k_{nr}$ via:

$$\tau_f = \frac{1}{k_r + k_{nr}}. \tag{2.3}$$

Following these definitions the fluorescence quantum yield can be expressed as

$$QY = \frac{k_r}{k_r + k_{nr}} = \frac{\tau_f}{\tau_r}. \tag{2.4}$$

Quenching processes The radiative process in general depends on the local environment its effect on the transition moments of the fluorescent molecule — e.g. dielectric and metallic surfaces in close proximity effect the intrinsic lifetime via influencing the boundary conditions imposed on the radiated field *[Hellen and Axelrod, 1987]*. In addition, there is a wide variety of processes opening non-radiative relaxation paths. The non-radiative processes are usually referred to as quenching and can be divided into two groups: collisional quenching, occuring when the excited state is deactivated upon contact with some other molecule, called quencher, via energy or electron transfer or an enhancement of inter-system crossing to the triplet state, and static quenching, leading to a decrease of the fluorescence intensity by reactions of quenchers with the fluorophore when it is in its ground state, rendering the fluorophore non-fluorescent.

Collisional quenching in general is a diffusion-controlled process and therefore strongly depends on the quencher concentration, as expressed by the Stern-Volmer equation

$$\frac{F_0}{F} = 1 + K[Q] \tag{2.5}$$

with F_0 being the unquenched fluorescence intensity, $[Q]$ the quencher concentration and K the Stern-Volmer quenching constant.

Förster resonance energy transfer (FRET), first described by *Perrin [1932]* and in more detail by *Förster [1948]*, is a non-radiative, distance-dependent energy transfer between a donor and an acceptor molecule. It is not only an efficient quenching process of a donor when approached by an acceptor, but has been used extensively as a molecular ruler for distances from 1–10 nm (as was first suggested by *Stryer and Haugland [1967]*). When absorption and emission spectra from an acceptor and donor, respectively, overlap, the energy of the excited electronic state of the donor can be transferred to the acceptor, resulting in the population of the excited electronic state of the acceptor, by a non-radiative dipole-dipole interaction. The efficiency E of this process depends on the distance r between donor and acceptor:

$$E = (1 + (\frac{r}{R_0})^6)^{-1}. \tag{2.6}$$

The parameters that determine the exact distance dependence are combined in R_0, the Förster radius. R_0 is the distance at which, for a given donor acceptor pair, the FRET efficiency equals 50%:

$$R_0 = \sqrt[6]{0.211\,\kappa^2\,n^{-4}\,QY_D\,J}. \tag{2.7}$$

It involves fluorescence properties of donor and acceptor in form of the following parameters:

- donor quantum yield of the donor QY_D
- spectral overlap $J = \int_0^\infty F_D(\lambda)\epsilon_A(\lambda)\lambda^4 d\lambda$, with emission spectrum F_D, excitation spectrum ϵ_A and wavelength λ
- orientation factor $\kappa^2\kappa^2 = (\cos\theta_T - 3\cos\theta_D\cos\theta_A)^2$, which is calculated from the relative orientation of donor and acceptor dipoles, thus expressing to what extend a dipole-dipole interaction is possible. θ_T is the angle between donor-emission dipole and acceptor-absorption dipole and $\theta_{D/A}$ is the angle between the dipoles and the connecting vector between acceptor and donor. Until today it has been of intense discussion, how to accurately determine κ^2, whenever the assumption of freely rotating dyes (resulting in an average value of $\kappa^2 = 2/3$) breaks down.
- index of refraction n, which is defined by the solution and organic matter that lies between the two fluorophores.

FRET efficiencies can be estimated from either donor and acceptor fluorescence intensities or donor fluorescence lifetimes in presence or absence of the acceptor.

$$E = 1 - \frac{\tau_D^A}{\tau_D} \tag{2.8}$$

Not quite as well characterized in terms of distance dependence, but relevant in the regime of < 1 nm, is photo-induced electron transfer. It not only serves as a quenching path for fluorescent dyes but also provides an efficient way to convert light energy into electrochemical energy, as is utilized in photosynthesis. Upon excitation, the redox-properties of a molecule are altered, so that the molecule is more easily oxidized. Through Coulomb interactions between the resulting radical ion-pairs this reaction becomes strongly distance dependent, but due to a large number of non-defined molecular influences, electron transfer, unlike FRET, cannot easily be employed as a molecular ruler.

Anisotropy Almost all fluorophores consist of a light absorbing and a light emitting molecular unit. The transition moments that represent absorption and emission processes, in general behave like an oscillating dipole and thus have a defined orientation. The dipole orientation, as defined by the molecule, is fixed and allows directly probing the molecule's orientation. Polarized light can be used to selectively excite only those molecules who's absorption dipole is parallel aligned with the electric light vector. In a solution, selective excitation of this supbopulation results in partially polarized emission. The degree of depolarization is determined by the relative angle between absorption and emission dipole and the time scales on which emission (fluorescence lifetime) and rotation of the molecule (rotational diffusion time) occur. Also energy transfer between fluorophores can contribute. Depolarization can be measured from the intensity components parallel $I_\parallel$ and perpendicular $I_\perp$ to the excitation polarization that define the fluorescence anisotropy r and polarization P.

$$r = \frac{I_\parallel - I_\perp}{I_\parallel + 2I_\perp} \qquad P = \frac{I_\parallel - I_\perp}{I_\parallel + I_\perp} \tag{2.9}$$

Both expressions are equivalent and can be interconverted. Whereas polarization was historically the first to be introduced, anisotropy has the advantage to be additive with respect to anisotropies of individual species in a mixture.

2.1.2 Sophisticated Imaging Techniques

The introductory discussion of the basic principles of fluorescence and its application to microscopy has focused on the main element, that is cycling a fluorophore between its electronic ground and first excited state, and observing the fluorescence intensity. In addition to the overall intensity, other characteristics of fluorescence, such as spectrum, lifetime and polarization, can serve as a reporter in fluorescence experiments. The multitude of observables have been utilized as new techniques in fluorescence microscopy.

Multicolor Imaging

In the same way as fluorescence allows separation excitation and emission wavelengths, it is feasible to label multiple species with differently-colored dyes and simultaneously observe their spectrally-separated fluorescence. This way several experiments can be carried out in parallel, ensuring that they are performed under absolutely identical conditions or simply increasing throughput.

Unfortunately the limitations are given by the spectral properties of the fluorophores themselves. To utilize multicolor (also called multiplexed) imaging, spectral separation has to be large enough to distinguish various fluorophores. Large differences in the emission imply separated absorption spectra demanding the use of several excitation sources simultaneously, a technically demanding procedure. In addition, the emission spectrum of most organic dyes tails off towards the red spectrum, thus minimizing the number of separate probes which can be used in a given observation.

Nevertheless, a number of methods have been implemented in recent years to recover the contributions from several spectrally distinct fluorophores *[Zimmermann et al., 2003]*. The development of new probes with either narrower or red-shifted emission spectra helped to increase the number and distinction of simultaneously observed probes. The ideal probe would emit in a tunable, narrow spectrum and be excited at one fixed wavelength. Such performance, limited again by other undesirable properties, was demonstrated with semiconductor NCs *[Michalet et al., 2001]*.

Lifetime Imaging

Methods to explore lifetime — fluorescence lifetime imaging microscopy (FLIM) — have been around for some time. Lifetime can help to map the presence of different fluorophores or the environment of a fluorophore with known lifetime. Each FLIM methodology has its own drawbacks and advantages, making it more or less suitable to a given experimental situation *[Periasamy, 2001]*. Measurements can be performed in the frequency or time domain. Frequency domain measurements rely on radio-frequency modulation of the excitation intensity and successive recording of several images to determine an apparent lifetime from the phase shift between excitation and emission modulation *[Gadella et al., 1993; Lakowicz and Berndt, 1991; Lakowicz et al., 1992]*. The major drawback lies in the time of several minutes, that is required for a reliable determination of lifetimes. Measurements in the time domain always require a pulsed excitation and a time-resolved measurement of the emission following such excitation. Two implementations are possible: either a time-gated ICCD-camera is used to acquire a fluorescence signal in two different time windows and estimate lifetime differences between various species according to the intensity ratio of both images *[Wang et al., 1991]*; or time-correlated single photon counting (TCSPS) is used to measure the time delay of each photon relative to the excitation pulse. The latter method allows a precise determination of lifetimes pixel by pixel in a raster scanning confocal detection scheme. Recent developments of integrated electronics make the combination of TCSPC and confocal scanning microscopy even more attractive *[Becker et al., 2001]*. FLIM has been applied to investigate fluorophores at the single-molecule level *[Tinnefeld et al., 2000]*.

Lifetime Measurements by TCSPC: In fact TCSPC technology is the method of choice when dealing with low photon statistics as is frequently the case in single-molecule detection. Since this method has been used in the context of this work, some more details about lifetime measurements via TCSPC shall be mentioned. The principle is to measure time delays between the detection of single photons and the excitation by a pulsed laser with picosecond accuracy. These microscopic times are binned into finite periods and combined in a single histogram. After the accumulation of a sufficient number of events, the data can be analysed by fitting an exponential decay function. The crucial point in TCSPC measurements is to make sure that the detection probability between two successive laser pulses is much less

than 1 (rule of thumb: $< 5\%$) to avoid so-called pile-up effects. If more than one photon per laser pulse arrive at the detector, it will always be the first one that is detected, the second one not being registered due to the unavoidable dead-time of any detector (on the order of 100 ns), and thus skewing the lifetime histogram to shorter times. On the other hand it is important to keep the distance between laser pulses large enough so that no photons are detected in one time window that follow excitation in the previous time window (rule of thumb: pulse periode$> 5 \cdot \tau_f$). Due to a large number of laser periods in which no photon is detected, TCSPC has to be implemented in a reversed-stop configuration, meaning that the photon-event serves as a start signal and the following laser pulse as the corresponding stop signal. This way a time-measurement by the TAC is only performed when a photon is present and the overall TAC dead-time is limited.

Time-Gated Imaging

The ability to perform fluorescence measurements with a time-gated detection by either using time-gating ICCD-cameras or confocal microscopy in combination with TCSPC electronics, brings another advantage for imaging of biological systems. Since autofluorescence in a biological environment originates from naturally fluorescent proteins and has in general a short lifetime compared to most fluorophores, time gating can reduce background and thus increase sensitivity. The technique works best with fluorophores that exhibit lifetimes much longer than a few ns. It has for instance been exploited for lanthanide chelates *[Vereb et al., 1998]*, metal ligand complexes *[Terpetschnig et al., 1995]* and semiconductor NCs *[Dahan et al., 2001]*.

FRET Imaging

The combination of FRET and imaging techniques has been explored via fluorescence donor/acceptor photobleaching and observation of donor/acceptor fluorescence on two spectrally separated channels *[Damjanovich et al., 1995; Gadella and Jovin, 1995; Jürgens et al., 1996]*. The technique allows identifying background contributions which are needed for a quantitative analysis of FRET. Fluorescence lifetime data make concentration independent FRET measurements possible via Equation 2.8, and in addition, circumvent extensive illumination *[Gadella et al., 1999]*. A combination of intensity and lifetime observation allows even better as-

sessment of FRET processes *[Hanley et al., 2002]*.

Two-Photon Microscopy

Imaging biological samples and observing processes in vivo requires high signal intensity and low impact on the biological system, both conflicting each other. An improvement of the excitation scheme was achieved by implementation of two-photon excitation *[Denk et al., 1990]*. Sufficient absorption of two photons, carrying half the energy of the transition (usually near IR-wavelengths), requires extremely high spatial and temporal light densities. These conditions can only be provided in a confocal excitation scheme using ultra-fast laser excitation. In this configuration photodestruction outside the observation volume is reduced due to a quadratic dependence on the excitation intensity and due to the use of less damaging near IR wavelengths. A greater penetration depth of such wavelengths also allows observations being performed deeper inside biological tissue. And because of the redundant pinhole, fluorescence signal can be collected even when it is scattered on its way out of the biological sample. Some drawbacks became visible through a comparative study of photobleaching under one- and two-photon excitation *[Sanchez et al., 1997; Patterson and Piston, 2000; Dittrich and Schwille, 2001; Hopt and Neher, 2001]*. For most fluorophores, two-photon excitation turns out to significantly increase photobleaching rates, but the technique has found impressive applications in neuroimaging and deep-tissue imaging and details are covered in a number of reviews *[So et al., 2000]*. The advantages of two-photon microscopy apply also to the field of FLIM and have been explored for frequency domain FLIM *[Piston et al., 1992; So et al., 1995]*, time-gated FLIM *[Sytsma et al., 1998]* and TCSPC FLIM *[Becker et al., 2001]*.

2.1.3 Pushing the Sensitivity to the Single-Molecule Limit

Fluorescence emission can be well separated from excitation light illuminating all components of a sample. This leaves fluorescent objects as the only visible ones, thus increasing contrast between fluorescent (of interest) and non-fluorescent (of no interest) objects tremendously. In fact, fluorescence is better suited than all other optical methods to reach the ultimate level of sensitivity, being able to observe single molecules.

The ultimate challenge in the detection of single fluorophores is reducing background contributions at the same time as optimizing the detected signal. This

becomes plausible from a discussion of signal-to-background (SBR) and signal-to-noise (SNR) ratios. What really counts is to detect a molecule with the best possible SNR. Let s be a signal rate that is detected in an optical setup after excitation of a fluorophore with a rate $P/h\nu$ (P being the excitation power at a frequency ν and $h\nu$ the photon energy) and let b be a background rate per unit-volume and unit-excitation power. This background definition is reasonable since background contributions like Rayleigh and Raman scattering as well as fluorescence of the medium or substrate are excitation power and volume (V) dependent. With additional detector background, a dark count rate d, and negligible readout noise (readout noise from detector and electronics is independent of the integration time), the SNR for a measurement of duration τ yields:

$$SNR = \frac{s\tau}{\sqrt{(s + bVP + d)\tau}}. \tag{2.10}$$

The noise (denominator) is given by the root-mean-square of all signal contributions that are influenced only by shot noise. Shot noise means that the signal is Poisson-distributed, such that the variance equals the mean. Including the cross-section of the excitation beam A, a detection efficiency E, and the parameters that describe a fluorophore, absorption cross section σ and quantum yield Q, such that $s = EQ\sigma P/Ah\nu$, the SBR can be written in the following form:

$$SBR = \frac{s\tau}{bVP} = \frac{EQ\sigma}{bVAh\nu}. \tag{2.11}$$

Formulating the relationship between SNR and SBR,

$$SNR = \sqrt{s\tau}(1 + SBR^{-1})^{-1/2}, \tag{2.12}$$

one can see how to influence SNR on the experimental side: an increase in collection efficiency improves SNR, as does reduction of the excitation volume; longer integration time or larger excitation power also improve SNR even though they do not influence SBR.

Another main reason why reduction of background contributions is essential and therefore as small excitation volumes as possible need be used, is the fact that fluorescence from most fluorophores is limited by irreversible photo-destruction to something on the order of 10^6 photons. This makes it impossible to reach sufficient SNR by just increasing excitation power or integration time.

The quest for optical detection of a single molecule can be traced back to *Hirschfeld [1976]*, who succeeded in detecting single antibodies that were labeled with 80 to 100 fluorophores. He already realized the need for efficient background suppression and demonstrated techniques like: reduced excitation volume, time-gated detection and pre-photobleaching of impurities. Depending on the application, several groups focused on slightly different approaches to single-molecule detection. *Moerner and Kador [1989] [Moerner, 1994]* demonstrated the real first detection of a single fluorophore by measuring fluorescence excitation spectra of pentacene in p-terphenyl at liquid helium temperature. Since Keller and colleagues were very much motivated by the quest for rapid DNA sequencing methods, they steadily increased the detection sensitivity in a hydrodynamically focused flow and succeeded in detecting the first single fluorophore in solution at room temperature *[Shera et al., 1990]*. This approach is now widely used in a confocal version *[Nie et al., 1994]*. The first image of a single molecule was obtained using near-field methods *[Betzig and Chichester, 1993]*, but very soon followed by far-field confocal microscopy *[Macklin et al., 1996]* and total-internal-reflection microscopy *[Funatsu et al., 1995]*.

Each one of these experimental methods represent a different approach to increase specificity for single molecules or reduce the excitation volume. Absorption spectroscopy at low temperature makes use of the fact that the zero-phonon-absorption line, the transition from the ground state to the first excited state, is extremely narrow and slightly shifted depending on the local environment. Thus the number of fluorophores that absorb at a given time is limited by the position in laser-frequency space. All emission spectroscopy approaches, on the other hand, make use of the Stokes-shift as described above. Hirschfeld used a total-internal-reflection (TIR) scheme to reduce the excitation volume to a layer of ~ 100 nm in close proximity of an interface. Axelrod and coworkers further developed various geometries of TIR microscopy *[Axelrod, 2001]*. All of them make use of an evanescent field that is penetrating into an optical thin medium, but decaying exponentially, when a light wave coming from an optical denser medium is totally reflected. Total internal reflection takes place when the incidence angle is smaller than a critical angle, determined by the indices of refraction (for a more detailed account see page 53). TIR microscopy has become a widely used wide-field approach to study a large number of immobilized molecules simultaneously, thus improving statistics, or even monitor diffusion trajectories of single molecules in live cells *[Schütz et al., 2000b; Sako et al., 2000]*.

The alternative to wide-field approaches is a point-detection scheme, in which the

excitation of fluorophores is limited to extremely small volumes. Point-detection schemes encompass confocal and near-field scanning optical microscopy (NSOM). In confocal microscopy diffraction by optical elements limits the excitation volume to a radius on the order of the excitation wavelength. In NSOM, where a tapered fiber core determines the dimension and sets a limit around 100 nm, slightly better resolution is achieved. Since NSOM has not been used in this work, the reader is referred to *Betzig and Chichester [1993]; Dunn [1999]; Enderle et al. [1998]* for further details.

The invention of confocal microscopy first expanded the capabilities of fluorescence microscopy to 3D-imaging and later became essential to many single-molecule applications. Confocal microscopy is a point-detection scheme in which a laser, focused to a diffraction limited spot in the sample, is raster scanned through the sample and the emission is collected for each individual pixel. The great advantage is that a pinhole with a diameter of 50–200 nm in the imaging plane rejects all light which originates from outside the focal plane. Implemented as a confocal laser scanning microscope (CLSM), where the laser beam is scanned by fast galvanometers, the method allows acquiring images in three dimensions at video rate. The detection of single molecules requires longer integration times per pixel and therefore employs a scanning stage geometry. The fact that the laserbeam is stationary on the optical axis and the sample is moved relative to it, also reduces optical aberrations and increases the collection efficiency. But single-molecule detection, as first demonstrated by *Rigler et al. [1993]*, profits even more from the fact that the excitation volume can be reduced to the size of a laser focus. The dimensions of this spot, typically on the order of femtoliter, are determined by diffraction in the optical system and are closely related to the dimension of the detection point-spread-function (PSF). Diffraction causes the intensity distribution of a point-source to spread out when transferred through optical elements, resulting in a PSF that can approximately be described (in 2D) for a circular lens with radius a by an Airy-disc (J_1 being the first Bessel function, k the wave vector and r the radial coordinate):

$$I(r) = I_0 \left[\frac{2J_1(kar)}{kar}\right]^2 \tag{2.13}$$

The position of the first minimum r_{Airy} depends on the wavelength and the numerical aperture (NA) of the lens system and determines the resolution limit of an optical microscope. Following the established Rayleigh criterion, two points can be

resolved if their distance is equal or larger than r_{Airy},

$$R = r_{Airy} = 0.61\frac{\lambda}{NA}. \tag{2.14}$$

It was stated that this resolution limit can be improved in confocal microscopy, due to the point-detection scheme, by a factor of 1.41 *[Pawley, 1995]*. This results in an overall resolution limit for confocal detection of $R = 0.8\lambda/2NA$ lateral and $R = 1.4\lambda n/NA^2$ axial. This means that two single molecules, fluorescing at 600 nm and being detected with an oil-immersion objective of NA=1.4, can be separately identified if they are spaced more than $\sim$ 200 nm laterally and $\sim$ 700 nm axially.

With an increase of sensitivity to the single molecule level, the stochastic nature of photophysical parameters appears and becomes accessible for statistical investigation. The probability distribution function of an experimental parameter allows determining the width of a distribution or even subsets that can give evidence for heterogeneity in the sample or the involved physical mechanisms. In addition, dynamic processes that are extremely difficult to synchronize on an ensemble level can be recorded molecule by molecule. This way it becomes feasible to record time trajectories and unravel dynamics on a molecular level in non-equilibrated systems. Intermediate states in chemical reactions can be identified and their time-dependent pathways back to equilibrium can be observed. Figure 2.2 illustrates the capability of single-molecule detection to unravel subpopulations that are hidden in an ensemble due to the inherent averaging.

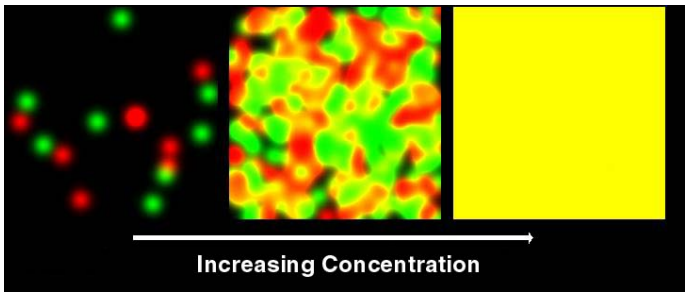

Figure 2.2: Two subpopulations that are characterized by the colors red and green can only be resolved at low concentration. At ensemble level the average value, yellow in this case, will be observed.

These advantages have been extensively demonstrated over the past 10 years

[Tamarat et al., 2000; Moerner, 2002; Xie and Trautman, 1998]. For instance *Ambrose and Moerner [1991]* could show that the ensemble excitation spectrum is the result of inhomogeneous broadening, a superposition of spectra from single molecules with a much narrower homogeneous line width. Dynamic phenomena at low temperature, such as sudden changes in the resonance frequency, called spectral diffusion *[Orrit and Bernard, 1990]*, or intermittency in the fluorescence signal, attributed to population of a long lived triplet state *[Basche et al., 1995]*, were observed. And similar characteristics were found at room temperature: spectral jumps in the emission spectra *[Trautman et al., 1994; Xie and Dunn, 1994; Lu and Xie, 1997]*, and on-off fluctuations on the timescale of ms due to triplet state kinetics *[Ha et al., 1997]* or on the timescale of seconds due to conformational changes *[Dickson et al., 1997]*. So overall, phenomena of fluorescence intermittency are observed in almost any molecular system, and, even though they can be attributed to different mechanisms, they seem to be rather characteristic for single-molecule detection in general, independent of the individual fluorophore or environmental conditions. Another general characteristic is a stringent limit in the total number of emitted photons. After the emission of several million photons most fluorophores are irreversibly photobleached. Several mechanisms have been identified that lead to sudden photodestruction of fluorophores. Most prominent is the influence of reactive oxygen species that are present in any biological environment *[Dittrich and Schwille, 2001]*. This phenomenon is very disturbing for the investigation of biologically relevant dynamics on second to minute timescales and studies are performed to reduce photobleaching by choosing the right fluorophore or the right excitation method. It was found that photobleaching poses an even larger problem under two-photon excitation.

The Signature of a Single Fluorophore

Since the described phenomena appear to be quite ubiquitous they were soon taken as experimental evidence to really look at single fluorophores. Especially one-step-photobleaching is often named to prove the observation of single molecules. Since the beginning of single-molecule spectroscopy, the question of singleness has been under debate and up to now it remains a challenge to really prove that no second, or third, molecule is part of the observation. *Betzig and Chichester [1993]*, later extended by *Nie and Zare [1997]*, were the first to propose a set of indicators that can be used to argue for the detection of single particles. The suggested criteria are

the following :

- The observed density of emitters is compatible and scales with the known bulk concentration.
- The observed fluorescence is consistent with that of a single emitter.
- Each detected emitter has a well-defined absorption and emission dipole, both of them are most often linear but can also be planar (e.g. for NCs).
- Fluorescence intermittency results in two distinct levels (on and off) as long as no changes in the environment are involved.
- If more than two levels are observed, other photophysical property changes are correlated.
- Irreversible photobleaching results in a sudden and digital extinction of fluorescence.
- The correlation between emitted photons exhibits the signature of antibunching.

Most of these arguments can give some evidence for singleness. Unfortunately, some fluorophores have very unique optical properties that can interfere with the proposed criteria. Spherical NCs, for example, have two degenerated emission dipoles *[Empedocles et al., 1999]* making it more complicated to prove singleness by polarization measurements. Intensity fluctuations can appear as on-off switching even when two molecules, exhibiting very long off-times, are observed *[Kuno et al., 2000]*; one-step-photobleaching, discrete intensity fluctuations and spectral jumps have also been observed in multi-chromophore systems such as light harvesting complexes *[Bopp et al., 1997; van Oijen et al., 2000]*, conjugated polymers *[Vanden Bout et al., 1997; Yip et al., 1998; Huser et al., 2000]* or polyphenylene dendrimers *[Hofkens et al., 2000]*. Light-harvesting complexes, an essential component enabling the energy-providing mechanism of photosynthesis, have actually been found to be comprised of several fluorophores, which act effectively as one quantum emitter *[Wu et al., 1996]*.

One unambiguous signature of the emitted light that proves fluorescence to be caused by a single quantum emitter is photon antibunching. Due to the limited lifetime of the excited state, it is impossible for a fluorophore to emit more than

one photon at a time. This fact is reflected in the autocorrelation function of the fluorescence emission at a timescale of the same order of magnitude as the fluorescence lifetime. Photon antibunching, first measured in resonant fluorescence from sodium atoms by *Kimble et al. [1977]*, has been observed in the emission of single dye molecules trapped in a solid *[Basché et al., 1992; Fleury et al., 2000]*, on a glass surface *[Ambrose et al., 1997]*, or in solution *[Mets et al., 1997]*, and of semiconductor NCs *[Michler et al., 2000]*. In combination with pulsed excitation this quantum-mechanical effect has been utilized in the development of a single photon source *[Brunel et al., 1999; Lounis and Moerner, 2000]* or in the investigation of multi-chromophoric units *[Tinnefeld et al., 2002]*.

Multi-Parameter Analysis

Any combination of imaging techniques focusing on different observables, e.g. spectral and temporal information, can help to increase the capability to resolve different species or increase specificity for a given process. As mentioned above, a combination of lifetime and intensity information can improve the quantitative analysis of FRET processes. It is possible to simultaneously collect spectral, lifetime and polarization information. For instance the groups of Keller and Seidel have pioneered multi-dimensional analysis methods for the detection of single molecules, mainly in order to maximize the classification confidence in single-molecule DNA sequencing *[Fries et al., 1998; Van Orden et al., 1998]*. The group of Sauer has used spectrally-resolved FLIM in a comparative study of three dye families,oxazines, carbocyanines and rhodamines, emitting in the red spectrum *[Tinnefeld et al., 2001]*.

Single Molecules in Living Cells

The next challenge for fluorescence microscopy is to perform the observation of biological processes at the ultimate limit of sensitivity but in vivo. The non-invasiveness of fluorescence observations makes the technique advantageous over other high-sensitivity, high-resolution techniques such as electron microscopy or atomic force microscopy. On the other hand single-molecule studies in live cells are challenging due to background and accessibility issues. First experiments have been carried out to demonstrate the tracing of fluorescently labeled lipid molecules *[Schütz et al., 2000a]*, their diffusion *[Schwille et al., 1999a]* and ion channel distributions in the cell membrane *[Schütz et al., 2000b]*. Diffusion of the ion transport protein transferrin

and synthetic oligonucleotides in cytoplasm and nucleus was investigated *[Byassee et al., 2000; Knemeyer et al., 2003]* and single viruses were traced before and after cell uptake *[Seisenberger et al., 2001; Lakadamyali et al., 2003]*. *Sako et al. [2000]* combined imaging of epidermal growth factor receptors (EGFR) with single pair fluorescence resonance energy transfer to investigate the formation of EGF-EGFR complexes on the cell surface and oligomerization of E-cadherin was investigated in mouse fibroplast L cells through imaging of single GFP molecules *[Iino et al., 2001]*. Due to the extremely rapid progress in this field, many more observations are to be expected.

2.1.4 Commonly used Fluorophores

A large variety of dyes have been used as staining materials to increase contrast or select specific components in microscopy. Fluorophores, have been developed and used in fluorescence microscopy to further increase specificity and thus unravel biological processes. And, as Lacowicz writes: "The probe is everything!" *[Lakowicz, 1999]*: the fluorophore determines how many photons can be detected, what spectral ranges can be addressed and how these molecules can be turned into specific labels to report on e.g. conformational changes of biological macromolecules.

Fluorophores come in form of very different molecules. There are naturally fluorescent biomolecules, which serve as probes, on one hand and small organic dyes on the other. Proteins with aromatic amino-acids like tryptophan, tyrosine, phenylalanine emit without further modifications at UV wavelength. Enzymes using NADH or flavins as cofactors are fluorescent, dependent on oxidation state, and can be observed in the blue spectrum *[Lu et al., 1998]*. All these intrinsic fluorophores are the cause of mostly unwanted background fluorescence in biological media and especially live cells. This so-called autofluorescence is of great concern in many experiments, and it is an unsolved problem how to reduce its contribution.

Since the advent of molecular biology a number of techniques became available for specific labeling of proteins, DNA or lipids (both the latter are essentially devoid of fluorescence) with organic fluorophores. The number of fluorophores has increased dramatically over the last two decades and a large variety of requests can be met by commercial products *[Haugland, 2003]*. Fluorescein, rhodamines and the newly developed family of Alexa-dyes, to just name a few, are widely used fluorophores in site-specific labeling schemes. Good dyes in terms of brightness, photostability and

large Stokes-shift are needed in demanding single-molecule applications *[Kapanidis and Weiss, 2002]*. Fluorophores that emit in the red or even near-IR spectral range are essential in biological experiments. Since spectral separation provides one way to remove unwanted autofluorescence, dye families like oxazines, carbocyanines and red emitting rhodamines are further modified and investigated with special interest *[Sauer et al., 1996; Tinnefeld, 2002; Buschmann et al., 2003]*.

A different strategy in site-specific labeling is to genetically encode fluorescent proteins, such as the green fluorescent protein (GFP) from the jellyfish *Aequorea victoria*. By placing the DNA sequence coding for GFP adjacent to the DNA sequence of a protein of interest, the hybrid protein, with GFP fused to the protein of interest, can be expressed and observed in the cell. Variants, that differ in their spectral properties, like blue, cyan, green, yellow and even red fluorescent proteins, have been identified and used in a number of experiments *[Tsien, 1998; Heikal et al., 2000]*.

2.2 Quantum Dots: a Novel Class of Fluorescent Labels

Crystalline structures of semiconductor materials constitute another family of fluorescent material that has become of great interest to the photonics community. Especially nanometer-sized crystals, so called quantum dots (QDs) or nanocrystals (NC), have been investigated with growing interest in recent years.

Fluorescence in quantum dots is due to the radiative recombination of an excited electron-hole pair, or exciton. As excitonic energy levels are influenced by quantum confinement and exciton-phonon interactions in the crystal, resulting optical spectra are unique. QDs are one example of fluorescing objects that combine a broad excitation spectrum with a narrow emission spectrum. In addition, the fluorescence lifetimes are larger or on the order of 10s of nanoseconds, long enough to allow time-gated detection but short enough to not limit the signal by low turn over rates (as is the case for lanthanides or metal ligand complexes with ms lifetimes). And most fascinating, fluorescence from single QDs has been observed longer than from most other individual fluorophores, enabling to collect many billions of photons.

With potential applications ranging from quantum dot lasers *[Fafard et al., 1996; Klimov et al., 2000]*, LED designs *[Colvin et al., 1994]*, solar cells *[Hagfeldt and*

Grätzel, 1995] and other optoelectronic components *[?]*, single-photon sources *[Michler et al., 2000]* to biological labeling *[Michalet et al., 2001]*, the optical performance of QDs is constantly enhanced. Preparation and chemical modifications are further developed with an increasing commercial motivation.

2.2.1 Quantum Dots in a Historical Perspective

Since the beginning of the 70's materials science has provided experimental methods to manipulate matter on a nanometer scale. Molecular beam epitaxy allows growth of heterostructures made up of layers of various semiconductors. With increasing precision, the dimensions of charge carrying structures were reduced from 3 to 0 dimensions, yielding quantum wells (2 dimensional object), quantum wires (1D) and quantum dots (0D). As length scales approach nanometer scales, fundamentally new material properties arise. One of them is the discretization of electronic energy levels due to quantum confinement, observable for example through optical spectra.

The first systematic studies of NC's size dependent optical properties was performed almost two decades ago in two different materials. *Ekimov and Onuschenko [1982]* investigated semiconductor-doped glasses, the same material that has been used since the Middle-Age to stain glass windows and decorate churches with multicolor ornaments. *Henglein [1982]* and *Brus [1983]* looked at chemically synthesized NCs in the form of colloidal solutions. Both of them showed absorption and emission spectra to follow a $1/r^2$ dependence, with r being the particle radius. These observations could be recovered with good accuracy from a theoretical treatment of quantum confinement *[Efros and Efros, 1982]*.

Colloidal suspensions of NCs from different materials or their compounds have been explored by an ever increasing number of groups due to their potential in applications ranging from biological labeling to solar cells *[Hagfeldt and Grätzel, 1995]* and tunable lasers *[Alivisatos, 1996; Eychmüller, 2000]*. Different synthesis routes have been developed and the overall quality of colloidal NCs has been much improved. A major advance in terms of fluorescence brightness was accomplished by applying a technique following band gap engineering developed for molecular beam epitaxial growth of 2 dimensional heterostructures. By growing a shell of a lattice-matched, higher band gap material on the NC core, the chemical potential for electrons and holes jumps abruptly at the interface of the two materials, confining the excitation to the core. At the same time the crystal lattice is extended with as little

lattice mismatch between the two materials as possible, reducing surface defects. Surface strain that builds up from missing atoms and incomplete coordination in the crystal structure leads to surface states that might act as traps for electrons and holes. Passivation of the NC surface which reduces trap states causing non-radiative relaxation therefore increases the quantum yield. One of the first core-shell syntheses were performed in aqueous solution *[Spanhel et al., 1987]*. Major improvements leading to highly fluorescent particles were accomplished in the mid 90's *[Hines and Guyot-Sionnest, 1996; Dabbousi et al., 1997; Peng et al., 1997]*.

2.2.2 More Atom than Crystal — Photophysical Properties of QDs

When the dimensions of crystalline solids are reduced to below a characteristic length scale, which usually is on the order of 10 nm, the well known electrical and optical properties change dramatically due to 2 effects. First, quantum effects due to confinement become increasingly important. Second, the surface to volume ratio increases to a level where surface atoms constitute the larger part of all atoms that make up the crystal.

Quantum confinement Quantum confinement arises when the spatial dimension of a semiconductor crystal is reduced below a characteristic length scale. As light in semiconductors is absorbed by delocalization of electrons and holes with respect to each other, excited states of electron-hole pairs, called excitons, are created. The amount of delocalization is limited by Coulomb interaction and depends on the effective masses of the semiconductor electron and hole and the dielectric constant of the material. The characteristic length of bulk excitons is given by the exciton Bohr-radius:

$$a_B = \frac{\kappa \hbar^2}{\mu e^2}, \tag{2.15}$$

with μ being the reduced exciton mass, κ the dielectric constant of the semiconductor and e the electron charge.

As one shrinks the semiconductor crystal to length scales on the order of the Bohr radius, physical properties begin to strongly depend on the size. This fact can be qualitatively explained by the quantum mechanics textbook example of a particle in a box. For a particle that is confined in a three dimensional box constrained by

walls of infinitely high potential energy, the allowed energy states for the particle are discrete with a nonzero ground state energy. As the length of the box r — which corresponds to the radius of the quantum dot — is changed, the energy gap between the ground and the first excited state varies proportional to $1/r^2$. For a real NC this means that the smaller the particle radius the larger the energy gap to the first electronically excited state becomes. In case of an optically-allowed transition this relates to a blue shift in absorption and emission as has been observed in all kinds of NCs.

Solving the effective hamiltonian for a spherical nanocrystal surrounded by an infinite potential barrier, the electron and hole energy levels can be written in the simplest approximation as

$$E_{l,n}^{e,h} = \frac{\hbar^2 \phi_{l,n}^2}{2 m_{e,h} a^2} \tag{2.16}$$

where $m_{e,h}$ is the electron and hole effective mass, a is the crystal radius and $\phi_{l,n}$ is the nth root of the spherical Bessel function of order l ($\phi_{0,0} = \pi$, $\phi_{1,0} = 4.49$, $\phi_{2,0} = 5.76$, $\phi_{0,1} = 2\pi$) *[Efros and Rosen, 2000]*. For instance for CdSe, the energy gap can be calculated to increase from 1.8 eV (the bulk value) to 3 eV by a decrease in radius, thus passing through almost the whole visual spectrum. This approximation though is not sufficient when Coulomb interactions between electron and hole become significant. As the Coulomb energy is on the order of $e^2/\kappa a$ it is only a small correction in small crystals but becomes more important than the quantization energies in large crystals. Depending on the relative importance of Coulomb and quantization energies, three regimes are considered: the weak confinement regime ($a >> a_B$), the intermediate confinement regime ($a \sim a_B$) and the strong confinement regime ($a << a_B$), which is the most important regime for all NCs used in this work.

More thorough treatments of the exact structure of conduction- and valence-band (due to the various atomic orbitals contributing in a CdSe crystal structure and due to the non-spherical shape of a nanocrystal) result in a non-parabolic relation between energy E and wave vector $\vec{k}$. This leads to a fine structure in the accessible exciton states and a number of transitions, which can be observed at low-temperature. Some of these transitions are only allowed through phonon-interactions and relax much slower than allowed transitions. The existence of dark excitons *[Nirmal et al., 1995]* can therefore explain the prolonged exciton lifetimes that are observed in NCs (at low temperature: μs in NCs compared to ns in bulk semiconductor) *[Norris et*

al., 1997].

Material dependence Material constants, most importantly the bulk band gap and the effective electron/hole mass, determine the electronic and photophysical properties for nanocrystals just as much as they do for bulk materials. NCs have been explored from a large variety of materials and their compounds. The prototypes of colloidal NCs are II-VI compounds with CdSe being one of the most studied NCs. Depending on the band gap of the materials, colloidal NCs can emit at the lower end of the visual spectrum (ZnS, ZnSe), in the visual wavelength range (CdS, CdSe, CdTe) or in the near infrared (InP, InAs, HgTe).

The choice of material also determines how sensitive optical properties are to size. Through the effective mass of electrons and holes, sensitivity is influenced as can be seen in Equation 2.16. For example, a material with very light electrons (InAs: $m_e = 0.02$) is very sensitive *[Banin et al., 1998]* whereas a material with heavier electrons is less sensitive (CdSe: $m_e = 0.1$; CdS: $m_e = 0.2$) to size in the strong confinement regime *[Nirmal et al., 1995]*.

Surface effects Nevertheless, a quantum dot is neither an atom nor a molecule. The solid structure enables extremely stable optical properties. NCs, which are grown on a substrate, can emit for many days before they deteriorate. The large surface to volume ratio (around 20–50 % of all atoms are on the surface) on the other hand can have significant effects on the emission *[Kuno et al., 1997]*. Since electrons and holes sample the surface much more often than they do in bulk material, surface defects, e.g. non-coordinated atoms, will lead to trap states, that result in a broad emission of lower energy and with an order of magnitude longer lifetimes than band edge fluorescence. Trap states can also result in photochemical oxidation on the surface, which is irreversible and further increases the number of defects leading in the extreme case to complete quenching of band-edge fluorescence *[Bowen Katari et al., 1994]*. Colloidal NCs are more exposed to (photo-)chemical modifications on the surface if not passivated chemically (shield from reactive molecules) and electronically (reducing local potential minima that trap free charges). The passivation quality is very different depending on the organic ligand. E.g. phosphines, phosphine oxides and amines are very good at electronically passivating the surface, enabling high quantum yields in colloidal particles.

2.2.3 Semiconductor Nanocrystals in the Form of Colloidal Particles

Synthesis The different synthesis routes that are explored today are all based on similar principles. In a mixture of precursors, the nucleation process is initialized. Nucleation is then stopped rapidly minimizing the size distribution of NCs. This is achieved by a rapid change of growth conditions, either by changes of temperature or pH and coverage by organic ligands. Ligands also ensure to keep NCs in a monodisperse state at later times, influence the solubility and are critical to further chemical treatment. As mentioned before they also influence electronic properties by passivating the surface.

Synthesis was initially performed by precipitation from a solution that contains metal ions (Ag, Hg, Pb, Zn, Cd, In) and a hydride of S, Se, Te or P. Colloid stabilizers, such as thioglycerol, polyphosphate or citrate, were added and growth was terminated by a sudden drop in pH *[Duonghong et al., 1982; Rossetti and Brus, 1982; Vossmeyer et al., 1994]*. Synthesis was further progressed involving inverse micelle synthesis *[Kortan et al., 1990]* and high temperature, hot-soap synthesis *[Murray et al., 1993]*. In this approach a dimethyl-cadmium precursor is injected into a solution of trioctylphospineoxide (TOPO) and trioctylphosphine selenide (TOPSE) and heated to approximately 360°C. The diffusion-controlled growth is often progressing slow enough to monitor the NC's size by removing aliquots from time to time and measuring the absorption spectrum. The growth is then stopped by reducing the temperature, a condition under which TOPO molecules form an organic monolayer, yielding stable NCs. The size distribution is further improved by size-selectively precipitating the particles and redissolving them in either butanol, toluene or other non-polar solvents and can be on the order of a few percent.

The major advantage of the water-based synthesis is, that particles are readily dissolved in aqueous solution. The hot-soap synthesis on the other hand yields colloidal solutions of higher quality particles. NCs are highly crystalline and exhibit very narrow size variations. In many cases limitation are given by low quantum yields of a few percent.

To increase quantum yields both methods can be extended to yield core-shell systems. Materials with different band gap energies have been combined in core-shell or graded structures. Core particles, synthesized as described, are capped by a layer of semiconductor material with a higher band gap energy. E.g. CdSe ($E_{BG} =$

1.8eV) can be capped with either CdS (E_{BG} = 2.49eV) or ZnS (E_{BG} = 3.8eV). If addition of e.g. Zn-S precursors to a CdSe-TOPO solution is done slowly at reduced temperature, ZnS nucleation can be prevented and few monolayers of ZnS can form on already stable CdSe particles. The core-shell NCs then are stabilized by the same organic ligands as were already stabilizing the cores. Quantum yields can be increased by a factor of 10–100 compared to core NCs *[Eychmüller et al., 1993; Hines and Guyot-Sionnest, 1996; Dabbousi et al., 1997; Peng et al., 1997]*.

Solubilization and Bioconjugation To render NCs usable for biological applications, they need to become water-soluble and accessible for further chemical modifications to provide binding sites. For TOPO-NCs various approaches have been presented, where the hydrophobic TOPO ligands are exchanged with a linker that is hydrophobic on one end and hydrophilic on the other. The first demonstrations of biological NC-labeling used either silanized NCs or mercapto-ligated NCs to functionalize crystals *Bruchez et al. [1998]; Chan and Nie [1998]*. In the first approach thiol derivatized silane was used to form a first layer, which then can be modified with other silane reagent, like aminopropyl-silanes (APS) or phospho-silanes, via well-established silane chemistry. The resulting particles have mercapto (SH) and phosphate groups (PO_{4^-}) or amino (NH_2) groups facing the solution, which then can be used for further functionalization *[Bruchez, 1998; Gerion et al., 2001]*. This scheme was used by Bruchez and coworkers to specifically label F-actin filaments in fixed cells. After the cytoskeleton filaments were covered with biotinylated phalloidin binding to streptavidin, they could be recognized by biotinilated NCs (silanized NCs, conjugated to biotin) through the strong biotin-streptavidin interaction.

Chan and coworkers developed solubilization protocols using mercapto-ligands, such as mercapto propionic acid (MPA), mercapto succinic acid (MSA) or dithiothreitol (DDT), to react on the surface of CdSe/ZnS NCs. Through carboxyl or hydroxyl groups Chan and coworkers were able to label the protein transferrin and immunoglobulin G to recognize specific antibodies.

Recent developments encompass the encapsulation of NCs in the hydrophobic core of phospholipid micelles *[Dubertret et al., 2002]*. The micelles were conjugated to DNA and used in hybridization assays or injected into frog embryo cells to trace cell-lineage over long times. *Jaiswal et al. [2003]* used CdSe/ZnS ligated with dihydrolipoic acid (DHLA) and bound to avidin or a synthetically engineered two-domain protein via electrostatic interactions *[Goldman et al., 2002; Mattoussi et al., 2000]*,

to conjugate antibodies. Cell surface proteins were selectively labeled allowing cell imaging and tracking. And *Wu et al. [2003]* targeted cancer marker Her2 on the surface of fixed and live cells using NC-immunoglobulin and NC-streptavidin conjugates. CdSe/ZnS core-shell particles were coated with an amphiphilic polymer, bound by lysine and further coupled to streptavidin or antibodies.

Since activity in the field of functionalization and bioconjugation is quite intense, new developments are evolving at rapid speed and more examples can soon be expected.

2.2.4 Single Particle Characteristics of CdSe Nanocrystals

Single-molecule methods helped to get additional insight in the luminescence of NCs, revealing some characteristics that are very similar to already established fluorophores, namely: inhomogeneous broadening, spectral fluctuations, and fluorescence intermittency. Some of these characteristics, most important the blinking, pose severe limitations to applications in fluorescence microscopy. Others, such as extraordinary photostability also on the single-molecule level, make NCs superior over all other fluorophores for a number of applications.

Spectral diffusion Observations of the spectrum at low and room-temperature, revealed two factors that influence the width of the ensemble emission spectrum. Due to the atomic-like energy structure, one can observe very narrow emission spectra at low temperature with a width of few hundred μeV. Monitoring these spectra over several minutes, spectral jumps of up to several nanometers were discovered *[Empedocles et al., 1996; Empedocles and Bawendi, 1999; Neuhauser et al., 2000]*. Raising the temperature to room-temperature, these spectral jumps cannot be resolved in time, but contribute to a broadening of the emission spectrum from a single NC compared to low temperature spectra (called homogeneous broadening). Slight variations in the position of the spectra between individual NCs, mainly due to size differences, constitute the spectral width observed from an ensemble (called inhomogeneous broadening).

Blinking The first observation of fluorescence time traces from single NCs by *Nirmal et al. [1996]* uncovered intermittency, or blinking, in the fluorescence signal similar to what had been observed for other fluorophores. Further investigations

though revealed a major difference in the blinking statistics *[Kuno et al., 2000, 2001; Shimizu et al., 2001]*. Whereas switching between a fluorescent and non-fluorescent state at a certain rate, results in on- and off-time distribution that follows an exponential decay, NC's on/off-time distributions are described by a power law $P(\tau)$. It is expressed in the following form

$$P(\tau) = C\tau^{-m}. \tag{2.17}$$

One peculiarity of this distribution is that the integral over time diverges towards small times. Since the integral over all possible events for any probability distribution has to converge towards 1, a cut-off time $\tau_0 > 0$ has to be specified, such that

$$\int_{\tau_0}^{\infty} P(\tau)d\tau = \int_{\tau_0}^{\infty} C\tau^{-m}d\tau = 1. \tag{2.18}$$

The most important property of a power law distribution is that there is no single characteristic time scale for the observed fluctuations. Contrary to exponential distributions, where observations averaged over a time much larger than the characteristic decay time, eliminate effects from blinking, such averaging is not possible for power law distributions. No matter how long the observation time is, there is always a significant probability to observe on- and off-times on the order of that observation time. Or in other words the average on/off-time $< \tau >$ depends on the binning τ_{min} and observation time τ_{max} *[Kuno et al., 2001]*:

$$< \tau >= \frac{\int_{\tau_{min}}^{\tau_{max}} \tau P(\tau)d\tau}{\int_{\tau_{min}}^{\tau_{max}} P(\tau)d\tau} = \frac{(m-1)}{(m-2)} \frac{(\tau_{max}^{2-m} - \tau_{min}^{2-m})}{(\tau_{max}^{1-m} - \tau_{min}^{1-m})}. \tag{2.19}$$

Power law exponents were measured to be around 1.6 for off-times and 1.8 for on-times over more than 9 orders of magnitude in CdSe/ZnS and CdTe particles. Variations due to temperature or excitation intensity have only been reported for on-time distributions *[Banin et al., 1999; Kuno et al., 2000, 2001]*. *Shimizu et al. [2001]* recently observed a slight deviation from power law distributions for large on-times.

The mechanism causing fluorescence intermittencies is not known at this time. *Nirmal et al. [1996]* first suggested that under simultaneous excitation of two excitons, pair annihilation can eject either electron or hole from the NC interior, a mechanism called Auger ionization, leaving an ionized NC core. Ionization might also result from thermal effects. The free charge inside the NC leads to nonradiative Auger recombination of any exciton that is excited before the trapped charge

thermally returns. This three-body quenching process is extremely efficient, and thus renders the NC dark. But such a three-level system with a single trap (dark) state, as modeled by *Efros and Rosen [1997]*, can only predict exponential decays of probability densities for on- and off-states. To result in a power law, multiple pathways from a distribution of dark states have to be assumed. It can be shown analytically, that a distribution of trap states, e.g. an Arrhenius energy distribution $\rho(\epsilon) = \beta \exp(-\beta\epsilon))$ or a constant distribution $\rho = const$, with recovery rates depending on the individual state (and describing an exponential probability that a carrier remains in that particular state), leads to a power law.

Spectral shift and photobleaching In addition to spectral diffusion, continuous shifts in the emission (up to 30 nm) towards the blue have been observed for individual NCs under air atmosphere *[van Sark et al., 2001]*. This observation differs from experiments done under nitrogen where only minimal shifts (up to 5 nm) were observed. Photo-oxidation has been reported that can account for some blue shift due to an effective reduction of the particle radius *[Nirmal et al., 1996]*.

In the same experiments bleaching times, meaning the extinction of fluorescence, of 2.5 (air) and 3.5 (nitrogen) min were observed. This photobleaching was explained by irreversible photo-destruction. Even though photo-oxidation processes have been reported that may lead to photobleaching, the appearance of long off-states due to power law blinking cannot be excluded. In fact the statistical influence on an observed fluorescence signal over time was recently described in some detail by *Brokmann et al. [2003]*. Whenever the off-time exponent is smaller than the on-time exponent, the probability for a NC to switch on decreases with time of illumination. This effect results in a decrease of observed fluorescence in a NC ensemble and for apparent bleaching events in the case of single particles, that can be entirely explained by blinking.

2.3 Fluorescence Correlation Spectroscopy

Fluorescence correlation spectroscopy (FCS) is a method to decipher dynamics on the molecular level by statistical analysis of a fluorescence signal. Fluctuations in the detection of fluorescence from an observation volume are caused by changes in the number or properties of fluorescent particles. These changes can be due to diffusion, binding or switching between on/off-states. By calculation of an autocorrelation

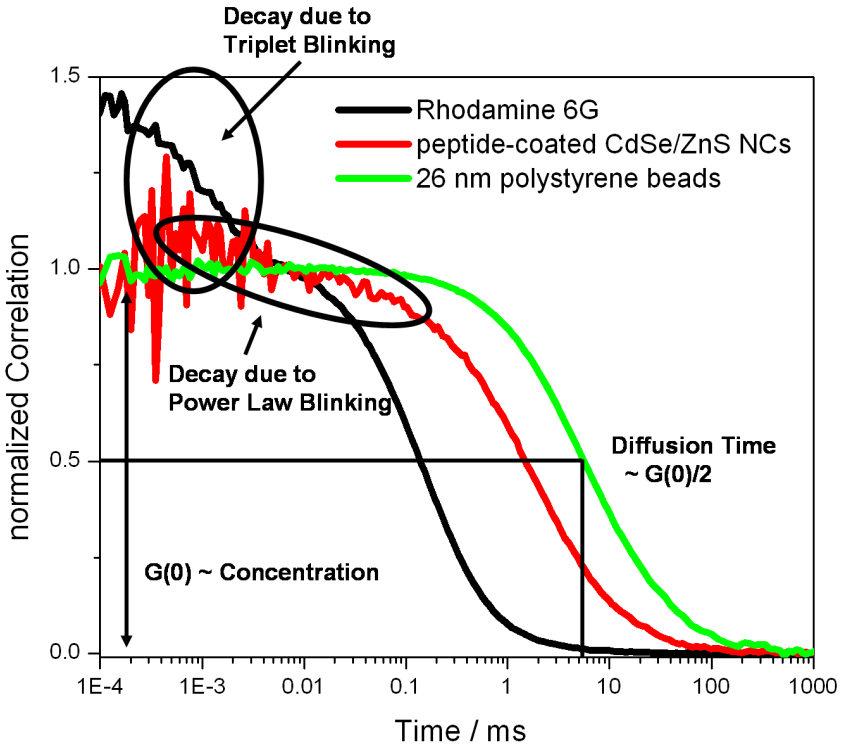

Figure 2.3: Fluorescence correlation curves calculated for purely diffusing particles (polystyrene beads), fluorophores which exhibit blinking following exponential (R6G) or power-law statistics (NCs). Typical features are highlighted.

function of the observed fluorescence intensity, time constants of the involved dynamical processes can be determined. Depending on the involved fluctuation causing processes, an analytical or numerical model can be derived and fitted to the data to extract parameters like diffusion and rate constants and concentrations. With the implementation of confocal microscopy sensitivity in the detection of fluorescence from molecules diffusing in solution was increased to the single-molecule level and FCS became a method to investigate photophysical processes (blinking, antibunching, photobleaching) in addition to the above mentioned parameters *[Rigler and Elson, 2001; Krichevsky and Bonnet, 2002]*.

Autocorrelation analysis has been used extensively in analog signal processing. In principle the autocorrelation function provides a measure of the self-similarity of a time series $F(t)$. The second order autocorrelation function is defined as:

$$g^2(\tau) = \frac{\langle F(t)F(t+\tau)\rangle}{\langle F(t)\rangle^2} = \frac{\langle \delta F(t)\delta F(t+\tau)\rangle}{\langle F(t)\rangle^2}, \tag{2.20}$$

with $\delta F(t) = \langle F(t)\rangle - F(t)$ being the deviation from the temporal average of the signal. It is obvious that the autocorrelation amplitude $g^2(0)$ equals the normalized variance of the fluctuating fluorescence signal $\delta F(t)$. To interpret the temporal fluctuations as being representative for the state of the total system, ergodicity has to be assumed. This means that the averaging process $\langle\rangle$ is equivalent if performed as a time or ensemble average.

Even though FCS is averaging fluctuation properties from a large number of molecules, it actually is probing these fluctuations with single-molecule sensitivity and thus allows distinguishing sub-populations. Two molecular species can be distinguished and their relative concentrations estimated, if their corresponding fluctuation time constants are separated well enough, e.g. the diffusion time ($\sim 1/$diffusion constant) has to differ by a factor of approximately 2 *[Meseth et al., 1999]*.

2.3.1 Historical Development

At its first introduction in 1972 FCS was used by *Magde et al. [1974]* to determine diffusion coefficient and binding constant for ethidium bromide onto double-stranded DNA. The method was soon applied to a number of biochemical problems where concentration, mobility or kinetic rate constants were of interest. The major limitations during these first years were due to low sensitivity and insufficient background suppression resulting in low signal to noise ratios.

The development of optical techniques with single-molecule sensitivity started a new era in FCS experiments. With the introduction of confocal microscopy to FCS by *Rigler et al. [1993]* the sensitivity was dramatically increased. At the same time background contributions could be further reduced resulting in much better signal to noise ratios and a renaissance of FCS altogether. In addition to measuring diffusion and binding constants of biological macromolecules, it became feasible to monitor conformational fluctuations of biomolecules and photophysical processes of the fluorophores itself *[Eigen and Rigler, 1994; Widengren et al., 1995; Haupts et al., 1998; Widengren and Schwille, 2000; Rigler and Elson, 2001]*.

A second major improvement came with the increase in calculation power of new computers and the development of ever faster hardware. Since a correlation function has to be calculated from a time trace of a fluorescence signal, efficient algorithms are a necessity for FCS to become a routine technique. The calculation can be performed either post-acquisition using software algorithms or in real time with the help of efficient hardware correlators. A straightforward calculation following Equation 2.20 has the major disadvantage that it is extremely slow. Imagine an experiment of duration T with $N = \frac{T}{\Delta t}$ data points. In that case the number of calculations, that are required to perform the time averaging for each time-lag τ, is on the order of $O(N^2)$. In FCS experiments dynamic processes can be covered that extend easily over 10 orders of magnitude (10^{10}). The calculation of such correlation function is not possible in a reasonable amount of time using a linear correlator. To be able to handle large dynamic ranges the Multiple Tau Correlation Technique was developed *[Schätzel, 1985]* and implemented in a hardware device by ALV *[Peters, 2000]*. The basic idea is to rebin the data with twice the sampling time, after every 8 time lag calculations. In other words, whereas the first 8 time lags are calculated with maximum time resolution, the next 8 time lags are calculated with half the time resolution and so on. From considering the rebinning, it follows that the required number of operations for the calculation of a correlation function scales with $O(N)$, meaning that real-time calculation is feasible if the calculation time for one operation is below the time required to record one data point.

FCS is one example how a data set made up of intensity values (or, for the best possible resolution, photon arrival-times) can be reduced in such a way that useful characteristics about fluorescent species can be extracted. One drawback is that during the process of calculating a correlation function from the intensity signal, any brightness information is lost. Alternative methods to analyze fluorescence sig-

nals from single-molecules or low-concentrated ensembles have been developed that focus on the brightness more than on temporal fluctuations. A technique investigating the first three moments of an intensity distribution (mean, variance and skewness) was first proposed *Qian and Elson [1990]* and further generalized under the name Moment Analysis of Fluorescence Intensity Distribution (MAFID) *[Chen, 1999]*. It allows monitoring macromolecular interactions of two fluorescent species, even when the change in diffusion time is not detectable with FCS. Also the Photon Counting Histogram (PCH) method *[Chen et al., 1999; Muller et al., 2000]*, as well as Fluorescence Intensity Distribution Analysis (FIDA) *[Kask et al., 1999, 2000]*, analyzes the frequency distribution rather than the time-dependent decay of fluorescence fluctuations. It allows identifying subpopulations with different brightness and concentration. In principle FCS can be performed together with PCH or FIDA on the same data set to extract temporal and brightness information. However there is no direct way to relate both parameters to each other when multiple species are present. Fluorescence Intensity Multiple Distribution Analysis (FIMDA) *[Palo et al., 2000]* and the recently developed Photon Arrival-Time Distribution (PAID) *[Laurence, 2002]* tackle the problem to obtain the maximum amount of information for each individual species in a multi-component mixture in one analysis procedure. This is helpful for high-throughput assays where the heterogeneous composition of a sample has to be deciphered.

Nowadays FCS and related methods are widely used in the field of physical chemistry, molecular biology and cell biology. Since much new information is expected to be gained from observations of molecular interactions in the live cell environment, a number of groups has started to perform in vivo FCS measurements *[Bacia and Schwille, 2003]*. But fluorescence fluctuation methods have also found their place outside fundamental research in areas like high-throughput drug screening due to its capability of combining very short acquisition times with a straightforward data analysis.

2.3.2 The Theory of FCS

Deriving Analytical Expressions of the Autocorrelation Function

FCS obtains information about molecular dynamics from fluorescence intensity fluctuations. As opposed to its precursors, techniques investigating temperature-jumps or fluorescence recovery after photobleaching, it monitors the relaxation of fluc-

tuations around an equilibrium state in a non-invasive fashion. The samples are maintained at thermal equilibrium during the whole measurement.

Any process causing signal fluctuations, can be described by one or more rate equations with characteristic kinetic coefficients. The coefficients determine the dynamics and thereby contribute to the shape of the autocorrelation curve $G(\tau)$. In principle all these coefficients can be determined from $G(\tau)$. In practice, however, the situation becomes often very complex, with additional noise making it impossible to extract more than a few parameters unless their timescales are very well separated.

In the following section the general formalism of FCS theory is presented as it is used in most experiments that involve a confocal observation volume[1].

In order to extract quantitative information about parameters like diffusion constant D or kinetic rates k a model for the correlation function has to be derived. If an analytical model with a finite (and rather small) number of parameters is available, this can be used to fit an experimental correlation curve and extract numerical values. If the model can only be derived on the basis of numerical approximations or Monte-Carlo Simulations one has to hope for the validity of a simple scaling law involving the parameter of interest. If e.g. it can be shown that $G_{sim}(\tau) = f(D, \tau)$ and $f(a \cdot D, \tau) = f(D, a^n \cdot \tau)$ or $f(a \cdot D, \tau) = a^n \cdot f(D, \tau)$, then a can be used as a free parameter to fit $G_{sim}(\tau)$ to $G_{exp}(\tau)$. If no such dependence exists, a fitting algorithm cannot be applied. In that case it is only possible to make a comparison between experimental data and a finite amount of calculated or simulated curves in a database.

Analytical models have been derived for a number of systems involving single- and multi-component diffusion and switching between fluorescent and non-fluorescent states. All of these derivations are built on the assumption of an ideal chemical solution, meaning that the positions of all involved molecules are uncorrelated. To calculate an analytical expression of $G(\tau)$ one has to derive expressions for the fluctuations δF that are caused by diffusion or chemical changes. A general expression

[1]The following definitions are used throughout this document: a confocal observation volume is the three dimensional space, in which excitation of fluorophores takes place and emitted photons are collected. This volume is described by a 3D probability distribution, the observation profile (OP). The OP is derived from a probability distribution to excite a fluorophore, the excitation profile (EP), and a probability distribution to detect the emitted photon, the detection profile (DP). The EP is equivalent to the PSF of an optical system. The DP is often mentioned under the term collection-efficiency-function. The OP is the product of EP and DP.

for the number of detected photons in a confocal setup during an infinitely small time interval δt is given by:

$$F(\tau) = \delta t \int_V d\mathbf{r} I(\mathbf{r}) \sum_{k=i}^{m} Q_k C_k(\mathbf{r}, \tau), \tag{2.21}$$

where $I(\mathbf{r})$ describes the observation profile that is determined by the laser profile and the optics, Q_k the quantum yield and the detection efficiency for component k, $C_k(\mathbf{r}, t)$ the local concentration of component k and m the number of different components in the solution.

In most cases the fluctuations can be explained by molecules populating various states emitting with different fluorescent intensities. Under this assumption the only variable parameter in Equation 2.21 is the local concentration and Equation 2.22 holds:

$$\delta F(\tau) = \delta t \int_V d\mathbf{r} I(\mathbf{r}) \sum_{k=i}^{m} Q_k \delta C_k(\mathbf{r}, \tau). \tag{2.22}$$

To find an expression for the variation of the local concentrations we need to look at the differential equations that describe the fundamental physical and chemical processes that take place. Diffusion is described by the well known diffusion equation:

$$\frac{\partial}{\partial t} \delta C_j(\mathbf{r}, t) = D_j \nabla^2 \delta C_j(\mathbf{r}, t). \tag{2.23}$$

The chemical processes can usually be described by a set of linear rate equations, that connect the available states with kinetic processes quantified by rate constants:

$$\frac{\partial}{\partial t} \delta C_j(\mathbf{r}, t) = \sum_{j,k} K_{jk} \delta C_j(\mathbf{r}, t). \tag{2.24}$$

Going back to the definition of the autocorrelation function 2.20 and substituting Equation 2.22 in it, we obtain:

$$G(\tau) = \frac{(\delta t)^2}{F^2} \int \int d\mathbf{r} d\mathbf{r\prime} I(\mathbf{r}) I(\mathbf{r\prime}) \sum_{j,l} Q_j Q_l \langle \delta C_j(\mathbf{r}, 0) \delta C_l(\mathbf{r}, \tau) \rangle. \tag{2.25}$$

This formula says that the autocorrelation function of intensity fluctuations is a convolution of the correlation functions of the concentration fluctuations with the observation profile.

The concentration term $\langle \delta C_j(\mathbf{r}, 0) \delta C_l(\mathbf{r}, \tau) \rangle$ has to be evaluated and the convolution integral evaluated, using standard mathematical techniques. Essentially the

concentration term can be evaluated in Fourier space, solving an Eigenvalue problem stated by the diffusion-rate equations. The convolution with the observation profile turns into a multiplication in Fourier space and for certain observation profiles the integration can be performed. The details of the general mathematical treatment are very well described in *[Krichevsky and Bonnet, 2002]*. An analytical solution is not always straightforward or might not be obtainable at all. Especially the explicit form of the observation volume can make it impossible to solve the integral in Equation 2.25. Therefore in most cases where a confocal optical setup is used, the observation profile is assumed to be very close to a Gaussian observation profile:

$$I(\mathbf{r}) = I_0 exp(-\frac{2(x^2+y^2)}{\omega_{xy}^2} - \frac{2z^2}{\omega_z^2}). \tag{2.26}$$

Single-Component Diffusion Model

In the simplest possible case where a single chemical species is diffusing in a dilute solution and a Gaussian observation profile can be assumed, the final solution to the above stated problem yields:

$$G(\tau) = \frac{1}{\bar{N}}(1+\frac{\tau}{\tau_D})^{-1}(1+\frac{\tau}{\omega^2\tau_D})^{-1/2}, \tag{2.27}$$

with:

$$\bar{N} = V_{eff}\bar{C},\ V_{eff} = \pi^{3/2}\omega_{xy}^2\omega_z,\ \tau_D = \frac{\omega_{xy}^2}{4D},\ \omega = \frac{\omega_z}{\omega_{xy}}. \tag{2.28}$$

As was expected from Poisson statistics describing the number fluctuations of molecules inside a given volume, the correlation amplitude $G(0)$ is inversely proportional to the average number of molecules in the sampling volume. In Equation 2.27 one can see that each spatial dimension brings in an additional term of the form $(1+\tau/\tau_D)^{-1/2}$. Whenever $\omega_{xy} \ll \omega_z$, the 2D diffusion equation:

$$G(\tau) = \frac{1}{\bar{N}}(1+\frac{\tau}{\tau_D})^{-1}, \tag{2.29}$$

serves as a good approximation, since the relaxation of number fluctuations is determined by the rate of diffusion in the smaller dimension.

This formula states that the concentration and the diffusion coefficient of a fluorescent species in a dilute solution can be evaluated from the FCS measurement of $G(\tau)$, provided that the dimensions of the observation volume are determined in a separate experiment.

Multi-component Diffusion Model

In the case of solutions which contain more than one species, which diffuse independently from each other, Equation 2.27 can be extended into a sum of terms, each describing one component. Also the various quantum yields have to be taken into account. A general expression for many diffusing and non-interacting components is:

$$G(\tau) = \frac{1}{(\sum_k Q_k \bar{N}_k)^2} \sum_j Q_j^2 \bar{N}_j (1 + \frac{\tau}{\tau_{D_j}})^{-1} (1 + \frac{\tau}{\omega^2 \tau_{D_j}})^{-1/2}. \tag{2.30}$$

Exponential On-Off Blinking Coupled with Simple Diffusion

If in addition to diffusion, a chemical reaction takes place, in which molecules can go from a fluorescent to a non-fluorescent state, the following set of rate equations become important. For a reaction between states A and B, that can be described by exponential kinetics:

$$A \longleftrightarrow B, \tag{2.31}$$

with rate coefficients k_{AB} and k_{BA} the rate equations take the form:

$$\frac{\partial}{\partial t} \begin{pmatrix} C_A \\ C_B \end{pmatrix} = \begin{pmatrix} -k_{AB} & k_{BA} \\ k_{AB} & -k_{BA} \end{pmatrix} \begin{pmatrix} C_A \\ C_B \end{pmatrix}. \tag{2.32}$$

Following the above mentioned steps the following expression for $G(\tau)$ is derived

$$G(\tau) = G_D(\tau)(1 + K \exp(-\frac{\tau}{\tau_k})), \tag{2.33}$$

with

- $G_D(\tau)$ being the diffusion term 2.27,
- $K = \frac{k_{AB}}{k_{BA}} = \frac{\bar{C}_B}{\bar{C}_A}$ the equilibrium constant,
- $\tau_k = \frac{1}{(k_{AB}+k_{BA})}$ the relaxation time of the chemical reaction, and
- $\bar{N} = (\bar{C}_A + \bar{C}_B)V_{eff}$.

A special case of on-off blinking is given when fluorescent molecules can relax from an excited state to long-lasting triplet states by inter-system-crossing. The transition from a triplet state to the ground state is quantum mechanically forbidden due to symmetry rules. Therefore the triplet state has a lifetime on the order of μs to ms

and resembles a non-fluorescent state. Since the rate equations involve three levels with four rate constants the derivation of $G(\tau)$ is more complex than for the two level system, described in the previous paragraph. The details are given in *Widengren et al. [1995]*. The final result is equivalent to Equation 2.33:

$$G(\tau) = G_D(\tau)(1 + \frac{S}{1-S}\exp(-\frac{\tau}{\tau_T})) \tag{2.34}$$

where

- S is the fraction of molecules in the triplet state, and
- $1/\tau_T = k_{20} + \frac{k_{12}k_{01}}{k_{01}+k_{10}}$ involves the rate constants between the ground (0), excited (1) and triplet (2) states.

Other Analytical Expressions

There are a number of other analytical models that have been used to fit experimental data and thereby gather evidence that a certain physical model might be applicable. *Mets et al. [1997]* have used FCS to measure anti-bunching in the fluorescence of Rhodamine 6G in water applying the simplified expression:

$$G(\tau) = \frac{1}{\bar{N}}(1 - exp(-(k_{10} + k_{01})\tau) \tag{2.35}$$

for the fast timescale (timescale on the order of the fluorescence lifetime).

Another parameter that can be investigated in the fast time regime is rotational diffusion. The rotational diffusion time depends on the cube of the radius of the molecule $\tau_{rot} = \pi\eta r^3/(k_B T)$, and therefore allows addressing the molecule's size independent from translational diffusion which might be limited by obstacles, e.g. a lipid membrane in a cell environment. A detailed discussion can be found in *Rigler and Elson [2001]*.

One of two widely used extensions to the diffusion of a single component is the case where a directed flow overlays brownian motion. Active transport with velocity ν will show up as an exponential decay in the autocorrelation function

$$G_{flow}(\tau) = exp(-(\frac{\tau\nu}{\omega})^2). \tag{2.36}$$

It has been used in the application of capillary electrophoresis and the characterization of microfluidic devices *[Gösch et al., 2000]*.

The other case has its origin in the investigation of diffusion within membranes, where the 3D diffusion is hindered in various ways. The experimental observation is that the mean square displacement is no longer directly proportional to time as it is for regular diffusion, but rather depends on t^α. This results in a correlation term of the form:

$$G_{anomalous}(\tau) = \frac{1}{\bar{N}}(1 + (\frac{\tau}{\tau_D})^\alpha)^{-1}, \tag{2.37}$$

which has been applied to a number of biological systems *[Schwille et al., 1999b; Schwille, 2001]*.

Photobleaching of dyes has been studied via FCS by *Widengren and Rigler [1996]; Eggeling et al. [1998]; Dittrich and Schwille [2001]*. These authors use a FCS model in which photobleaching is described by an additional exponential decay:

$$G_{Bleach}(\tau) = 1 - B + B \cdot \exp(-k_{Bleach}\tau). \tag{2.38}$$

Enderlein [1996] has derived a more accurate analytical expression via a path integral approach.

Fitting Expressions to Data

A given analytical expression $f(P_i, t_j)$ with p free parameters P_i can be fitted to an acquired data set $g(t_j)$ with n points using non-linear fitting routines. The most widely used algorithm is the Levenberg-Marquardt algorithm *[Press, 1993]*, which has been implemented in a number of programs for data-analysis (such as Origin and LabView). By adjusting the parameters such that a goodness of fit parameter is minimized, the best possible fit for a noisy data set is determined. Various expressions can be used as quality parameter for the fit. In most implemented algorithms the χ^2 value is used:

$$\chi^2 = \sum_{t_j} \omega_j \frac{[g(t_j) - f(t_j)]^2}{n - p}, \tag{2.39}$$

where ω_j is a weighting factor to account for an expected error at time t_j.

The difference between fit and data, called residuals res, can also be used to visualize systematic deviations. In this work normalized deviations of fitted FCS data will often be used to illustrate how well a chosen model accounts for the experimental situation. To be able to compare FCS residuals independent of the actual correlation amplitude $g^2(0)$, normalized residuals will often be shown:

$$res(t) = \omega(t)\frac{[g^2(t) - f(t)]}{g^2(0)}. \tag{2.40}$$

Statistical errors can be included through $\omega(t)$ which usually is the inverse of the standard deviation of the measurement at time t.

The Signal-to-Noise Ratio in FCS

Quantitative evaluation of FCS data is done by fitting a model function and extracting numerical values for free varying parameters or by comparing different models to validate the physical assumptions that contribute to the derived model. In both cases knowledge of the noise inherent to the FCS measurement increases the accuracy of the results when less weight is put on noisy data. Fitting becomes more reliable, when the noise is taken into account as a weight factor in the determination of the goodness of the fit (usually a Chi^2 value serves as fitting criteria and can be significantly changed using standard deviations of data points as weight factors). Noise, or equivalently SNR, depends on the mean count rate per particle, the mean number of particles per observation volume, the time characteristics of the correlation function, the observation profile, the data collection time and the bin time. The number and nature of these parameters already tell that an analytical expression of the SNR is not available for arbitrary experimental conditions. Following the first fundamental publication by *Koppel [1974]* a number of authors looked at SNR under certain conditions and present SNR for the correlation amplitude $g^2(\tau = 0)$ *[Qian, 1990; Wohland et al., 2001]*. Using a multiple tau correlator, the SNR was estimated empirically at all time delays by *Saffarian and Elson [2003]*.

Considering that photon statistics improve with increasing signal and thus higher particle concentrations (lower shot noise contributions) but the correlation amplitude is inversely proportional to the concentration, the question for an optimal range arises. It turns out that under certain conditions, both effects cancel out such that SNR is independent of the particle concentration. For too high concentrations the relative fluctuations become so small that correlated laser noise contributes to $g^2(\tau)$. At the lower end, when no molecule is detected for significant times, background takes over and reduces the correlation amplitude and SNR. It can also be shown that SNR depends on the count rate per molecule ν and the total acquisition time T as $SNR \propto \nu\sqrt{T}$ *[Krichevsky and Bonnet, 2002]*. In other words a 10-fold loss in the detection efficiency has to be compensated for by a 100-fold increase in acquisition time.

3

Experimental Concepts

This chapter will present the experimental concepts and methods of fluorescence spectroscopy and microscopy that were used to investigate photophysical properties of semiconductor nanocrystals. The focus will be on fluorescence acquisition geometries that allow detecting fluorophores with single-molecule sensitivity, such as total-internal-reflection (TIR) microscopy and confocal microscopy.

3.1 Ensemble Fluorescence Measurements

The characterization of nanocrystals in solution at high concentrations was done with either a UV/VIS absorption spectrometer or a spectrofluorometer looking at the fluorescence emission.

For the absorption measurements a Lambda 25 (PerkinElmer Inc.; Wellesley, MA) was used. In this instrument light from a deuterium or halogen lamp is spectrally selected by a monochromator made from holographic gratings. The bandwidth is determined by a fixed slit width to be 1 nm. Over a range of 190 to 1100 nm the transmission through a cuvette holding the sample solution can be measured using a photodiode detector. The decrease of signal, $I(\lambda)$, is related to the extinction coefficient ϵ of the sample via Lambert-Beers law (concentration c, path length d):

$$log\frac{I_0}{I(\lambda)} = \epsilon(\lambda)cd. \tag{3.1}$$

Cuvettes are made from quartz glass holding between 10 and several 1000 μl of solution and providing a path length of 10 mm.

Fluorescence was investigated in a L-201M spectrofluorometer (PTI Inc.; Lawrenceville, NJ). A sample solution of 50 μl (or more) is excited inside a quartz cuvette with light from a Xenon-lamp. The light is spectrally selected by either a monochromator or fluorescence filters. Photomultiplier tubes (PMTs) are used to record the emission two channels, oriented perpendicular to the excitation path. PMTs can be driven in an analog or digital mode, in which single photon detection provides the highest sensitivity. Optionally, polarization optics (motorized excitation polarizer; two perpendicular emission polarizers) can be installed to perform steady state anisotropy measurements. The cuvette holder is temperature controlled (water cooling or heating cycle) so that long time measurements are performed under constant temperature conditions. The software $FeliX^{TM}$ can be programmed in a macro language to perform consecutive emission or excitation wavelength scans. It also allows recording fluorescence emission over long time periods, while at the same time the excitation intensity is recorded through a reference detector. This way the recorded emission can be corrected for long term intensity fluctuations of the lamp, which are always present on a minute to hour time scale.

3.2 The Microscope

In the experiments that are discussed in this work, mostly inverted research microscopes were used (Axiovert 100; Carl Zeiss, Jena, Germany. IX70; Olympus, Tokyo, Japan). The microscope's architecture allows a combination of excitation and detection through different ports on the back, the front or below the microscope. Modern microscopes are equipped with up to 5 ports so that an optical setup allows including more than one of the described techniques, e.g. lamp wide-field-detection can be carried out on the same microscope that is used for confocal-scanning-microscopy with only a few modifications. One has to be aware of a few major differences between the brands in order to not use incompatible components: 1) The focal length of the tube lens is either 160 mm (Zeiss), 180 mm (Olympus) or 200 mm (Nikon); 2) Corrections to reduce chromatic aberrations are carried out in both objective and

tube lens (Zeiss) or only in the objective (Olympus); 3) Immersion oils differ in its composition, exhibiting various degrees of background fluorescence.

Objectives

Since the aim in high-sensitivity microscopy is to collect as many photons as possible, objectives with extremely large numerical apertures have been constructed. The numerical aperture $\mathrm{NA} = n_i \sin\theta_{max}$ (n_i: refractive index of the immersion medium, θ_{max}: opening half-angle of the objective) is a measure of the opening angle under which photons can enter the objective. The highest NA can be achieved with oil-immersion objectives, since $n_{oil} = 1.52 > n_{water} = 1.33$. Various models are designed to minimize optical aberrations and perform optimally at specific wavelength ranges. Seidel aberrations, which are due to the spherical shape of most optical lenses, and chromatic aberrations, which result from variations of the index of refraction dependent on the wavelength, are present in any optical system but can be minimized by the right combination of optical components. Also depolarization effects can be minimized in specialized objectives to a certain extent. In general all high-NA objectives show some influence on the polarization state of the detected light *[Bahlmann and Hell, 2000]*.

Optical corrections to minimize the effect of aberrations on the image depend on variations in the medium through which the detected light travels before it enters the objective. Even though the index of refraction in the coverslip is very close to the index of refraction in immersion-oil, high-performance objectives are designed for a specific coverslip thickness and imaging on the surface of the glass. With the development of confocal microscopy the influence of a variation in the refraction index between immersion medium and sample becomes important since areas at different depths are imaged. These depths variations influence the optical path that light needs to travel from the object to the objective. Since it is impossible to correct for influences at arbitrary depth in oil-immersion objectives one has to be aware of effects when focusing deep into a sample.

The development and increased utilization of optical tweezers *Svoboda and Block [1994]* have also increased the need for high-quality objectives, that can provide a tight laser focus at various distances inside an aqueous solution. To satisfy this need various microscope companies designed water-immersion objectives. Since the coverslip is enclosed by the same medium (essentially water) on both sides, the

optics can be corrected for a specified coverslip thickness independently of how far away from the surface the focal plane is shifted. These objectives, even though they constitute the highest price range of all objectives, have proven to be very valuable for FCS. An experimental comparison is presented on page 91.

3.3 Wide-Field Microscopy

Following the criteria for single-molecule experiments (page 24) the most straightforward way to perform single-molecule experiments is to decrease the concentration of particles until emission from individual particles can be detected. For this instrumentation is necessary that fulfills the requirement of extremely high sensitivity; in other words maximum detection efficiency and minimal background contributions have to be assured. Fluorescence microscopy is one technique that has been pushed in performance over the years and can be used in a number of modifications to observe single molecules.

Excitation

The simplest and mostly widely used configuration in fluorescence microscopy is the epi-configuration. In this geometry, excitation light, provided by a high-pressure lamp at the back-port of the microscope, enters the objective through a cube containing excitation filter, dichroic beamsplitter and emission filter. The light hits the sample in the field of view, an area with a few hundred μm radius. Fluorescence then is collected by the same objective passing through the dichroic beamsplitter and an emission filter, where residual excitation light is rejected, and exiting the microscope via the tube lens either at the bottom, side or top port, depending on the detector that is used.

High-Pressure Lamps: Most common broadband excitation sources are high-pressure xenon (Xe) or mercury (Hg) lamps. Whereas Hg-lamps in general provide higher intensities, the spectrum of Xe-lamps is more uniform. Their relatively continuous light output ranges from 250 nm to 800 nm so that specific wavelength ranges can be conveniently chosen by an appropriate excitation filter. A more detailed discussion of lamp characteristics can be found in *Lakowicz [1999]*. A note to the user of any high-pressure lamp either on spectrofluorometers or on fluorescence microscopes:

These lamps need high-voltage pulses to be started (20–40 kV). Any high-voltage device causes severe voltage fluctuations in any electronic device that is connected to the same circuit, when switched on or off. To not damage, e.g. computers, make sure to have every other electronic device turned off when switching a lamp on or off.

Defocused Laser Excitation Scheme: If excitation at a specific wavelength is required (monochromatic excitation) one can either use a monochromator as a very precise excitation filter or make use of lasers. Usually laser are the light source of choice due to intensity stability and a high degree of monochromaticity, among other advantages (page 61).

The simplest scheme in which lasers can substitute lamps is that of defocused laser excitation. A collimated laser beam is focused onto the backfocal plane of the objective, resulting in a nearly collimated beam at the exit of the objective. This excitation scheme provides an illumination area that can fill out the complete field of view, when the focusing angle on the back aperture is large enough. A drawback can be given by the fact, that the intensity distribution reflects the incoming laser profile, which is usually very close to a Gaussian distribution, and can display speckles and interferences due to reflections from optical surfaces.

TIR Excitation Scheme: The essential task to push fluorescence microscopy to single-molecule sensitivity is the reduction of background light. In all excitation schemes discussed so far, molecules are excited all over the sample volume. When a certain area in the focal plane of the objective is imaged, light from out of focus areas is still collected, causing diffuse background.

One way to reduce out of focus light is to prevent molecules in those areas from being excited in the first place *[Axelrod, 2001]*. When a light wave travels from an optically denser medium into a medium with a smaller index of refraction, it is refracted at the interface according to Snell-Descartes, law $n_1 \sin\theta_1 = n_2 \sin\theta_2$, with n_i being the refractive index and θ_i the angle of incidence. When the angle of incidence becomes smaller than a critical angle, $\theta_{critical} = \sin^{-1}(\frac{n_{glass}}{n_{medium}})$, no refraction takes place but the entire light wave is reflected back into the optically denser medium. To be consistent with Maxwell's equations, an evanescent light field, meaning an electromagnetic field that decays exponentially, has to built up in the optically lighter medium. The energy stored in the evanescent field can be used

to excite fluorophores that are as close as 100 nm from the surface. A peculiarity of the TIR scheme lies in the fact that the excitation intensity in close proximity to the surface increases with the inset of total-internal-reflection. This is especially helpful for exact alignment of the laser beam.

The concept has been exploited in various geometries, using either objective-type or prism-type TIR *[Ambrose et al., 1999]*. In objective-type TIR a laser beam is focus on the backfocal plane of an ojective, resulting in a collimated light beam entering the immersion oil. By parallel shifting the beam away from the optical axis of the objective, the angle under which the laser beam exits the objective can be controlled up to a maximum angle that is determined by the objectives NA. In prism-type TIR the laser is introduced from the opposite side of the objective through a prism in a geometry to allow internal reflection. Prism-type TIR provides a larger field of view and suffers less from residual epi-illumination, thus it reduces background light even further. Recent (unpublished) investigations found, that prism-type TIR also is the better choice when FRET processes are to be observed, because considerable background in the red spectrum can be caused by the objective itself under objective-type TIR.

Detection

Wide-field microscopy requires wide-field detection schemes. The silicon age has turned the charge-coupled devise (CCD) into the most versatile detector. In fact today it is almost exclusively used in wide-field detection. Steady progress in materials design and processing techniques has increased resolution, sensitivity and readout rates. Depending on the exact requirements of an application one can choose between a large variety of CCD detectors. The most sensitive detectors include back-thinned CCDs with quantum efficiencies up to 90% but a readout rate that is limited by readout noise. One way to overcome these noise limitations is by amplifying the signal prior to readout. This is accomplished with either image-intensified CCD or electron-multiplying CCD cameras.

A representative selection of CCD devices that allow single-molecule detection in wide-field microscopy is given by the image-intensified CCD Pentamax, the recently introduced electron-multiplier CCD Cascade and the CCD Coolsnap *HQ*, all manufactured and distributed by Roper Scientific. Whereas all three cameras are specified as low-light level devices, they rely on fundamentally different techniques.

The Coolsnap *HQ* is based on an interline CCD chip (Sony), allowing the fastest readout rates of the three. It employs no further amplification mechanism, but reaches quantum efficiencies of over 60% at 500–600 nm.

The EMCCD Cascade utilizes on-chip amplification of collected photo-electrons. After illumination, the charges are first shifted row by row into a horizontal register. From there they are accelerated horizontally through a series of registers, and multiplied by impact ionization. The multiplication process allows increasing the signal above the readout-noise level before the actual read-out is performed.

The ICCD Pentamax uses a micro-channel plate to amplify photo-electrons, which are created when photons are detected by a photo-cathode. MCPs multiply electrons through acceleration caused by a large electric field in an array of conductive glass channels. Electrons are convert back into photons on a phosphor screen and detected on a CCD chip. A high-voltage is specified by the user (gain) to built up the electric field in the MCP. It can be used to control the camera with ns time-resolution, making it the only camera in time-gated detection schemes.

A comparison of the detailed parameters given by camera specifications is presented in Figure 3.1.

Camera Model	Pixels	Pixel Size	Field of View
Pentamax ICCD	512 x 521	15 x15 µm	7.68 x 7.68 mm
CoolSNAP HQ	1392 x 1040	6.45 x 6.45 µm	8.77 x 6.6 mm
Cascade EMCD	653 x 492	7.4 x 7.4 µm	4.9 x 3.7 mm
Camera Model	Readout Rate	Frame Rate (FF / 256x256)	
Pentamax ICCD	5 MHz	15 fps	
CoolSNAP HQ	10 / 20 MHz	10 fps / 30 fps @ 20 MHz	
Cascade EMCD	5 / 10 MHz	25 fps / 48 fps @ 10 MHz	
Camera Model	Well Capacity	Read Noise	Dark Current
Pentamax ICCD	120,000 e	32 e rms @ 5 MHz	30 e/sec @ -20 C
CoolSNAP HQ	15,000 e	6 (8) e rms @ 10 (20) MHz	0.05 e/sec @ -30 C
Cascade EMCD	27,000 e	25 e rms @ 10 and 5 MHz (1e with amplification)	1 e/sec @ -35 C

Figure 3.1: Specification for high-sensitivity CCD devices (Roper Scientific).

The simplest way to install a camera is to connect it directly to one of many ports on the microscope. The top port is preferable for larger cameras because no further support is needed, the weight just rests on the port. The connection is generally

standardized by C-connectors. In order to observe two channels simultaneously, e.g. two different colors or two different polarization components, the so-called double-view geometry can be used. In this geometry, the light is collimated after the image plane using plan-concave lenses ($f = 250$ mm), then split into two separate channels by either a dichroic mirror or a polarizing beam-splitter, individually focused on the camera using the same lens as before (to cancel out aberrations introduced by the lens), and combined by another dichroic mirror. Emission filters can be added in each path as required. By limiting the field of view with an aperture in the image plane, the two channels can be placed separate but next to each other on the camera. After a calibration measurement, software can be used to overlay both channels and extract the corresponding values for the whole image.

3.4 Confocal Microscopy

Another way to limit the excitation volume, and thus reduce background contributions from Rayleigh- or Raman-scattering, is to use a confocal geometry. The term confocal describes the fact, that light is only collected from a region limited to the focal excitation volume by the use of a pinhole. Each excitation focus thus corresponds to a "confocal" detection volume. To construct images from a point-wise detected signal, the excitation volume or the sample itself is raster scanned relative to each other. In the experiments presented in this work, a confocal scanning scheme is used, in which the sample is scanned relative to the laser beam. This allows working with slower scanning speeds (increased acquisition time per pixel) to increase signal collection from rather dim light sources, such as single molecules. At the same time, the position of each pixel can be recorded with nm precision and the laser focus can afterwards be positioned at a chosen spot of the acquired image. This parking procedure allows observing the fluorescence emission of single molecules over several minutes, limited by long term drift of the stage. Contrary to a few scanning-beam confocal microscopes that are commercially available, scanning-stage confocal microscopes are only used in a limited number of research laboratories in the form of homemade setups.

The scanning stage used in this work (Physik Instrumente, Germany) is piezo-controlled and offers sub-nm precision over a range of (100 x 100 x 20) μm. The practical limitation on the positioning precision is given by digitization (usually

with 16 bit). A second stage was used alternatively (Mad City Labs). It is currently being integrated into a larger micro-positioning stage to allow nanometer-precision scanning over (200 x 200 x 100) μm, while at the same time being able to choose an area of interest in a total range of (40 x 40) mm. Either stage is fixed to a non-inverted microscope and controlled through analog or digital signals from a computer board (6052E multifunction board, National Instruments).

The software used to control stage movement and data acquisition was also developed in the laboratory and will be described further down.

Excitation

To achieve diffraction-limited focusing (the smallest excitation spot possible in a light microscope), the incoming light beam has to be perfectly collimated. This can only be achieved using lasers. In this work different lasers have been used that are further described in Chapter 3.6. To provide a focus as tight as possible and thus reduce the PSF of a point-emitter, the laser beam has to be expanded to overfill the back aperture of the objective. This can be done using a simple telescope (e.g. $f_1 = 75$ mm, $f_2 = 30$ mm). The laser beam is then coupled into the microscope from the side, using a dichroic mirror to reflect the beam into the objective. Careful alignment has to be performed to center the beam on the optical axis of the microscope, in order to achieve the best possible focus. The polarization state is adjusted using a half- and a quarter-wave plate to be either linearly or circularly polarized after the dichroic mirror.

In some applications, like FCS, the exact shape of the laser focus is of great importance. To get a PSF that resembles the described Airy pattern as close as possible, the laser beam profile has to be perfectly Gaussian when entering the objective. In other words, the laser light should oscillate in only the first translational mode, the TEM_{00} mode. Since most lasers provide an output that has components from other modes, the beam profile has to be "cleaned". This spatial filtering process can be done in two ways: transferring the light through a single-mode fiber; or filtering it using a spatial filter that is comprised of two lenses and a pinhole. Most homemade confocal microscopes employ a single-mode fiber to provide gaussian laser profiles. In these experiments a 532 nm single-mode fiber with a commercial coupling system (OZ Optics, Canada) was used. The intensity after the fiber was stable to at least 0.1%. A simple 10x objective (Edmund Industrial Optics) was used to collimate the

light at the fiber exit. Alternatively a spatial filter comprised by a 10x objective, to transform the laser beam into Fourier space, and a 50 μm pinhole, to perform the filter operation in Fourier space, was used.

Detection

As mentioned before, the confocal microscope works in epi-configuration, meaning that the emitted light is collected through the same objective that was used to focus the illumination light onto the sample. After passing through the dichroic mirror, the emitted light is focused by the microscope's tube lens into image space, from there focused by a second lens onto a pinhole and by a third lens on the APDs. The pinhole assembly is built using a filter wheel (Oriel) to hold various pinholes (50–500 μm, National Aperture), and an xyz-stage (New Focus). After the light has passed through the pinhole, it can be split in up to four channels. Using either dichroic mirrors or polarizing beam-splitters, four spectral or polarization components can be detected. Filters were optimized depending on the fluorophore (Omega Optical; Chroma Technology).

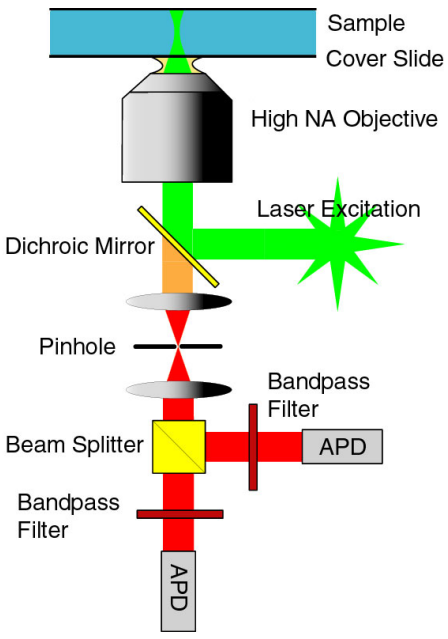

Figure 3.2: Solution-based FCS measurements are performed on confocal setups using two detection channels for cross-correlation analysis.

Even though most confocal microscopes use PMTs as detectors, these devices have QEs that are not sufficient for the detection of single molecules. For that reason avalanche photodiodes (AQR-13, EG&G Perkin Elmer) are used throughout this work. APDs have QEs of up to 70% in the visual wavelength range and are single-photon sensitive with a temporal resolution of 300 ps. The active area has a radius of 180 μm, which is sufficiently larger than the opening of the pinhole. Due to thermoelectric temperature control, the dark count rate can be as low as 25 Hz (100 Hz for the most models used in this work). The count rate is limited to a few thousand kilohertz; above this rate the detector might be irreversibly damaged. After a detected photon the avalanche process leaves the APD insensitive for a dead time of $\sim$ 50 ns.

The FCS-Setup

Since FCS is a solution based measurement that does not require any movement of the sample relative to the laser beam, all FCS measurements were performed with a confocal microscope as described, only without the scanning device. Most experiments required cross-correlation analysis of two channels, separated by a non-polarizing beamsplitter cube, so that correlation due to afterpulses from the APDs is avoided. In Figure 3.2 a typical confocal FCS-setup is depicted. Correlation was performed with either home-developed software algorithms or using a hardware correlator.

3.5 Electronics

Time-resolved photon counting: All of the described setups in this work are equipped with data acquisition electronics from National Instruments (NI). Readout of APD detectors is performed using counter-timer boards (6602 counter/timer, NI) that can time single TTL pulses by use of a 80 MHz clock (temporal resolution: 12.5 ns). Analog signals to control the scanning stage or monitor laser power are recorded and supplied by an analog input/output board (6052E Multifunction, NI). All NI electronic boards are either connected to the computer via a PCI interface or bundled in a PXI system, which then is connected to the computer via a single PCI interface. The PXI system has the advantage, that only single-slot PCs are needed. This makes regular PC updates cost-effective, since multi-slot PCs are much more

expensive. NI electronics can be controlled using program packages that are part of the LabView programming code.

In order to achieve the time resolution that is necessary to determine fluorescence lifetimes or probe the signature of antibunching using the TCSPC approach (required time resolution: 100s of ps), time-to-amplitude converters (TAC, EG&G Ortec 567) in combination with constant fraction discriminators and an analog-to-digital converter board (NI 6111E) were used. These electronic components are designed following the NIM standard, which was initially developed in the field of particle physics, and can easily be integrated in standardized 16" racks.

Alternatively recent developments of integrated electronic boards made it possible to perform similar measurements using a single commercial board for the entire process (TimeHarp 100, PicoQuant; SPC-630, Becker & Hickl). These devices can perform a macroscopic timing of single photons using a 20 MHz clock (temporal resolution: 50 ns) and a microscopic time delay measurement between two pulses, e.g. photon and laser pulses in lifetime measurements or photon and photon pulses in antibunching measurements (100 ps time resolution). The Becker & Hickl SPC-630 allows recording up to 8 channels simultaneously, using a special signal router.

Real-time correlation functions: Fluorescence correlation spectroscopy measurements can either be carried out by recording single photon arrival times and performing a post-acquisition calculation of the correlation function or by using real-time correlation hardware. Several correlator boards, to be used via a PCI or parallel interface with a personal computer, are commercially available. In this work a multiple-tau digital real-time correlator (ALV-6010/160, ALV-Laser Vertriebs-GmbH, Germany) was used to perform FCS experiments. The correlator can compute two correlation functions simultaneously from two detectors, either auto- or cross-correlation, with a minimal time resolution of 125 ns, or one cross-correlation function with a time resolution of 6.25 ns. The multiple-tau lag times (as described on page 40) are fixed and cover a range from 6.25 ns (in the fastest mode) to several hours (in 328 channels). The input count rate can be as high as 80 MHz (31.25 MHz in the fast mode), and is therefore practically limited by the single photon detector (APD works linear up to 1 MHz). The device is controlled by ALV software and allows recording and saving correlation functions, together with low resolution time traces, to monitor average count rates throughout the measurement.

3.6 Lasers

Without the invention of the LASER in the 1960s almost none of the above described techniques would have been possible. The laser provides electro-magnetic radiation, which is coherent (exhibits a fixed phase relation), collimated (divergence on the order of mrad), monochromatic (bandwidth depends on the active medium but can be as low as) and can reach extremely high and stable intensities in a single spatial mode (e.g. TEM_{00}). For a long time the Argon-Ion laser (Ar) was the most popular in biology-oriented research, because it provided several wavelengths (457 nm, 477 nm, 488 nm, 514 nm besides others at low intensity) to excite the most common fluorescent dyes at reasonable cost. Since the active medium in an Ar-laser consists of a gas tube, in which Argon ions are pumped into an excited state via high-voltage discharges, the tube is deteriorating over time and dies after approximately 3000 h. For that reason many laboratories try to increase the number of solid-state lasers, which have become available at an increasing number of wavelength. The cheapest lasers available are diode lasers due to their good performance in the near infra-red spectrum where a large demand in communication technology drives research and development. By now further progress is made to make diode lasers available that emit visual light and thereby become of interest to fluorescence spectroscopy.

The development of pulsed lasers helped to let time-resolved techniques become more fruitful. With the invention of femto-second lasers whole new areas of research opened up. For time-resolved measurements of fluorescent probes with lifetimes on the order of ns, pulse width of tens of ps are sufficient. However two-photon applications require an extremely high energy density in space and time, which can only be provided by femto-second lasers. New developments also make pulsed diode-lasers available as comparably cheap pulsed laser sources.

In this work a Ti:Sapphire femtosecond laser and a Nd:YAG ps-laser besides various cw lasers were used. The Ti:Sapphire laser (Mira, Coherent) provides femtosecond pulses between 700 and 980 nm with a repetition rate of 76 MHz. It was pumped with a high intensity Ar-Ion laser (Sabre, Coherent). The repetition rate was reduced to 5 MHz using a pulse picker (Coherent) and the wavelength was doubled in a non-linear crystal for single-photon applications. Alternatively a frequency doubled Nd:YAG with picosecond pulses at 532 nm and a repetition rate of 68 MHz was used. For cw applications (most FCS measurements) the following lasers providing various wavelengths were used: diode-pumped Nd:YAG laser (532

nm; Crysta Laser), violet diode laser (405 nm; Radius, Coherent), Ar-Ion laser (488 nm, 514 nm; Midwest Laser Products).

3.7 Samples

Various NCs were routinely synthesized in our laboratory. During this work a number of synthesis routes and surface treatments have been explored. NCs, that were made using the TOP/TOPO-synthesis, include CdSe core particles in 5 different sizes. All of these particles were coated with a higher-band gap shell to yield CdSe/ZnS NCs. Radii and emission wavelength were estimated via TEM, AFM and ensemble luminescence measurements in a spectrofluorometer. Observed values were around: 1.5 nm (505 nm), 2.5 nm (530 nm), 3.5 nm (570 nm), 5 nm (610 nm), 6 nm (620 nm) (synthesis by Fabien Pinaud). Various bioconjugation schemes were applied. A peptide coating technique was developed using various peptide sequences to cover the NC surface, obtain water soluble particles and perform further bioconjugation (Fabien Pinaud). In a different approach, the core-shell particles were covered with lipids (in the following called micelle) to provide water-solubility and enable further labeling (Laurent Bentolila). A water-based synthesis was used to prepare CdTe and CdHgTe particles with either mercaptoacetic acid, cysteamine, mercaptoethanol or thioglycerol as stabilizing ligands (Malte Pflughoefft, James Tsay). The only commercially available biocompatible NC used in this work, is a CdSe/ZnS core-shell particle that is covered with an amphiphilic polymer layer (40 % octylamine-modified polyacrylic acid, 2,000 units per NC, QDot Inc.). This polymer protects the surface from environmental effects and provides water-solubility. The polymer layer then is modified to conjugate the NC to streptavidin. Particles were available with 525 nm, 565 nm, 605 nm and 655 nm emission wavelength and specified to be 10–15 nm in diameter. QDot NCs were stored in QDot buffer at high concentrations, but for experiments diluted in distilled water (18.2 MΩ) or phosphor buffer, since QDot buffer showed contamination from fluorescent impurities.

For calibration and alignment purposes different commercial dyes were used. Carboxylate-modified FluoSpheres (Molecular Probes), 26 nm polystyrene beads emitting at 575 nm, were used as FCS standards. The beads were dissolved in distilled water and sonicated for 5 minutes to prevent aggregation. Rhodamine 6G

(Exciton), dissolved in distilled water was used for alignment purposes. Various DNA-dye constructs were used as FCS controls: 32 base pair DNA was synthesized on a DNA synthesizer and labeled with either TMR, Cy3, Alexa488 or Alexa532 (Achilles Kapanidis, Nam-Ki Lee; all dyes from Molecular Probes). DNA-dye constructs were dissolved in buffer (10 mM Hepes buffer (pH7), 1 mM MEA, 50 mM NaCl, 5% glycerol).

3.8 Sample Preparation

The preparation of samples can be divided according to either surface- or solution-based measurements. For confocal-scanning-microscopy or wide-field observations of NCs on a glass surface, highly diluted samples were prepared on No. 1 coverslips (130-160 μm thickness). The coverslips were thoroughly rinsed with acetone, methanol, ethanol and distilled water, sonicated for 15 minutes in 1 M potassium hydroxide and again repeatedly rinsed with distilled water. 20 μl of a NC solution with a concentration less than 10^{-10} M was spin-coated on a nitrogen dried coverslips (30 sec at approx. 2000 rpm; Specialty Coating Systems Inc.).

In some experiments the NCs were dispersed in a polymer matrix to shield the particles from the atmospheric environment, especially reactive oxygen. Depending on the solubility of the NCs they were dissolved into solutions of either poly(vinyl alcohol) PVA (water-soluble) or poly(methyl methacrylate) PMMA (soluble in e.g. toluene). The mixture was spin-coated as described above to yield a thin, homogeneous layer (10s of nm) of polymer with particles uniformly distributed throughout.

FCS experiments were carried out on samples containing as little as 5 μl solution. The chamber to hold the solution was prepared by cutting out holes with a diameter of approximately 5 mm in a silicon gasket (Grace Bio-Labs). The silicon gasket was place on a cleaned coverslip and — after pipetting the solution into the hole — covered with a second cleaned coverslip. By self-adherence the chamber is sealed so that no loss from evaporation can occur. The whole assembly was either put into metal holders or attached to larger microscope slides, so that they can be placed on the microscope stage and put into contact with immersion-oil without drifting during the measurement.

3.9 Software

Even though the field of single-molecule research has recently had its 10 year anniversary, most high-sensitivity fluorescence microscopy experiments are still performed on home-built setups. Since all optical setups described in this work are non-commercial and home-built, so are the software packages to control data acquisition and analysis. Most programs are written in LabView, a graphical programming language provided by National Instruments, that is adapted to easily control and monitor National Instruments data acquisition interfaces. With the dramatic increase in computer speed and memory capacities over recent years, LabView has evolved into a powerful language to develop almost any application that is needed to acquire and analyze data in spectroscopy and microscopy applications.

Confocal scanning microscopy was performed using a LabView package including ScanX and TimeX, developed by Xavier Michalet. ScanX allows acquiring 2D-images, while constantly controlling the 3rd dimension, using a closed-loop scanning table, and up to four APD-channels. After the acquisition of an image, the laser beam can be parked at a specified position (by moving the stage to that particular position) and single-photon arrival times can be recorded. In combination with fast electronics and pulsed laser excitation the time delay between excitation and emission or between successive photons can be recorded. TimeX allows binning arrival times into time traces. Histograms from time delays between laser and photon and photon and photon can be calculated and further analyzed to determine fluorescence lifetime simultaneously with monitoring the signature of antibunching.

Another LabView package, developed by Ted Laurence, was used to record single-photon arrival times on a confocal setup with up to 4 detection channels and NI electronics. The program is divided into an acquisition and an analysis part and can interpret time resolved data acquired with the Becker & Hickl SPC630 computer card. Photon arrival times can be chosen according to detection channel and other conditions. Analysis allows binning photons into time traces, perform multiple-tau-correlation (page 40) or histogram the data into PAID histograms.

Wide-field CCD acquisition was controlled by two commercial programs: WinView (Roper Scientific) and V++ (Digital Optics, New Zealand). Digital image analysis on these movies was performed using LabView.

Additional software was developed to perform quality controls and non-linear fitting on FCS data, and analyze burst characteristics of single-molecule data.

3.10 Monte-Carlo Simulations of Diffusion and Fluorescence Emission in a Confocal Volume

Monte-Carlo simulations were performed on desktop computers using LabView (NI). The simulation program was developed in several steps, each addressing an additional aspect of the complete picture. First a code was developed to simulate the diffusion of a single particle through a confocal volume. Second the photophysics of absorption and emission was incorporated. A single photon was randomly absorbed and emitted with an exponential distribution, characterized by an excitation rate and a lifetime. This scheme already allowed studying the effect of saturation in FCS and will be discussed later. In a third step the population of a triplet state was addressed. The program was modified to simulate photophysical aspects with and without simultaneous diffusion. That way time traces of immobilized molecules could be simulated to test simulations of photophysics without being skewed by the influence of diffusion. In a next step fluorescence intermittency following power-law statistics for the occupancy of on- and off-states was developed and substituted for the triplet-state photophysics. In this first approach the occupancy of on- and off-states was assumed to be completely independent from the absorption-emission cycles. This is not consistent with the experimental results, which show a power dependency and thus a photo-induced process, but serves as a first approximation, since it truly reflects the on-off kinetics under a constant excitation power.

The basic outline for the simulation of translational diffusion on molecules and photon emission and detection follows *Wohland et al. [2001]*. A confocal volume, with either a Gaussian or differently specified shape, is placed at the center of a three-dimensional rectangular box with dimensions ~ 10 times the confocal volume. A molecule is placed at a random starting point inside the box and diffusion is simulated by a series of steps, short enough so that variations of the excitation intensity during one step are negligible. This is guarantied if the diffusion time step Δt is around one hundredths of the diffusion time τ_D (the time it takes the molecule to diffuse through the confocal volume). The actual step size in each direction $d(x, y, z,)$ is determined by a pseudorandom number, that is generated from a Gaussian distribution with mean $\mu = 0$ and standard deviation $\sigma = \sqrt{2D\Delta t}$, where D is the diffusion constant *[Einstein, 1905]*. After the molecule has progressed in the estimated direction, a time for the next absorption event is generated according to an

exponential decay characterized by the local excitation rate (which again is derived from local excitation power and the absorption cross section of the molecule). Excitation is followed by emission, timed by a pseudorandom number according to the fluorescence (exponential) lifetime. The excitation-emission cycle is repeated until enough time has passed for the next diffusion time step Δt. As competing processes intersystem crossing, photobleaching or nonradiative relaxation — all of them specified by an exponential time constant — might be taken into consideration during the cycles. One pseudorandom number, drawn from a uniform distribution that is divided according to the quantum yield of each competing process, first specifies the chosen mechanism. Then a second number, drawn from an exponential distribution, provides the time for the process to take place.

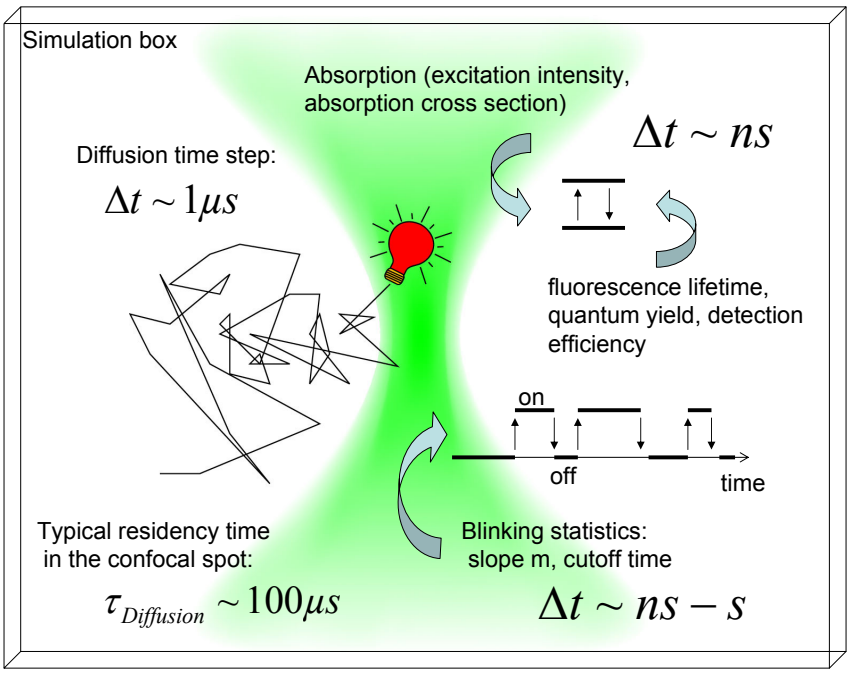

Figure 3.3: Simulations take into account: diffusion of molecules through a confocal observation volume; excitation-emission cylces at specified rates depending on absorption coefficient, laser power and quantum yield; blinking described by various statistics; detection efficiency; observation volume.

To combine diffusion and nanocrystal photophysics a similar scheme was developed, in which the absorption-emission cycles were overlaid with cycles between an

on- and off-state. The kinetics for changes between on- and off-states were simulated by choosing power-law distributed durations with exponents $m_{on/off}$ and a cut-off time t_0 (for more details about power law distributions see 2.2.4).

The individual photon arrival-times are saved. These sequences can be analyzed by any data reduction mechanism, such as binning into time traces or calculating the autocorrelation function. Since most of the data is simulated for comparison with FCS recordings, the autocorrelation function was calculated using a multiple tau correlation algorithm as described in *Peters [2000]*.

4

Results and Discussion

All of the above discussed properties of semiconductor nanocrystals make them suitable as fluorescent probes in a variety of biological applications. Each experiment demands specific chemical modifications of NC surfaces. Due to the fact that surface to volume ratios are extremely large for nanometer-sized objects, these manipulations turn out to have a large impact on the optical performance.

First experiments are presented that prove the unique optical properties of NCs synthesized in various ways. In addition, observations are reported, that are not widely known, but at the same time seem to be characteristic for a number of NC samples. Namely, the effect of photo-induced activation has been investigated under different conditions and turns out to be of great importance for experiments where large temperature changes are required, e.g. in DNA hybridization assays (FISH). In addition to these fundamental observations, the influence of surface modifications is shown. Since every new synthesis or post-synthesis modification turns out to have a huge effect on optical properties, there is need for a technique which allows fast, accurate, and non-invasive characterization in the natural environment of non-polar or aqueous (depending on the kind of NC) solution. This motivated the application of Fluorescence Correlation Spectroscopy (FCS) to semiconductor NCs. Experiments are presented that demonstrate such characterization of NCs, which can

serve as feedback and help to optimize synthesis as well as chemical modifications. In the last part Monte-Carlo-Simulations are presented to unravel the effect of blinking on FCS data and further study effects due to various photophysical properties on FCS data.

4.1 Photophysical Properties of a NC Ensemble

The first characterization to be done on a newly synthesized batch of nanocrystals is a series of ensemble measurements. Absorption and emission spectra allow estimating the quality of particles with respect to size distribution, monodispersity and quantum yield.

Data is presented for CdSe/ZnS particles dissolved in butanol. These nanocrystals are the starting material for the peptide-coated and lipid-covered nanocrystals that were also investigated in the course of this work.

4.1.1 Absorption

The absorption spectra show one of the main photophysical features of NCs: absorption takes place over a broad range of wavelength, reaching far into the UV spectrum (Figure 4.1). At room temperature the available electronic states are broadened by electron-phonon interactions. Therefore, only the resonances of the first and sometimes second exciton are visible as local maxima on the low energy side of the spectrum. The spectral position of the local maximum corresponding to the first exciton excitation is directly related to the average NC size and can be used as an estimate for particle radius *[Norris and Bawendi, 1996]*.

For a monodisperse sample of nanocrystals with a size of less than 10 nm, scattering by the particles is negligible. Only in the case that large aggregates form, light from the incoming beam is scattered out of the optical path. Scattering contributes to the absorption measurement with a $\lambda^{(-4)}$ wavelength dependence. Since this wavelength dependence is significantly different from the real absorption spectra of nanocrystals, presence of large aggregates can be detected.

Since the loss of raw material during the synthesis of nanocrystals is not well characterized and differences between batches cannot be avoided, it is important to determine the concentration of synthesized particles. Optical density measurements provide one way to estimate the concentration. For particles of a given size the

absorption crosssection or extinction coefficient was measured by *Leatherdale et al. [2002]* for CdSe/ZnS particles. Under the assumption that the relation between size and the absorption peak for the first exciton holds *[Norris and Bawendi, 1996]*, these values can be used to calculate a concentration from the position of the first exciton peak and the optical density at 350 nm.

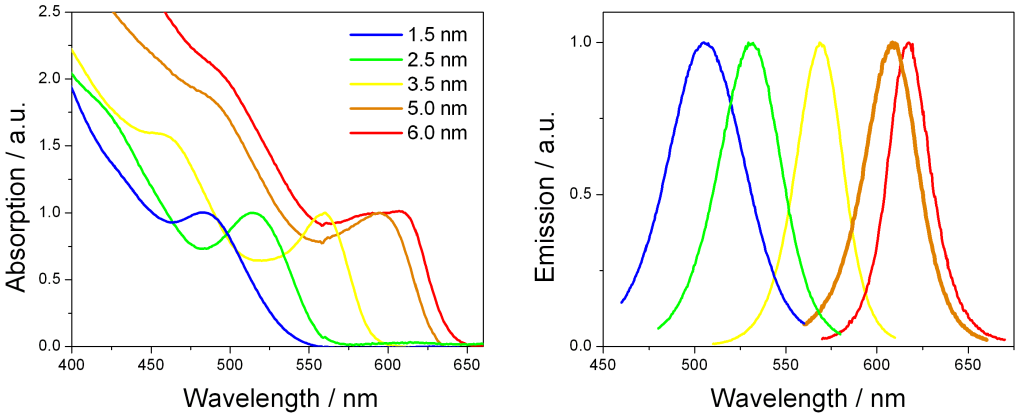

Figure 4.1: Absorption and corresponding emission spectra of CdSe/ZnS:TOPO NCs dissolved in butanol. Particle sizes range from 1.5 to 6 nm, estimated by TEM. Absorption spectra are normalized by the first exciton peak value. Emission spectra are normalized by the maximum value.

4.1.2 Emission

The size-dependent emission illustrates two more typical photophysical properties of NCs. In Figure 4.1 a red-shift of the maximum in the emission spectrum with increasing size is shown. The growth of NCs was stopped during the synthesis at various times resulting in a variation of the average particle radius. The attributed sizes are determined by transmission electron microscopy and atomic force microscopy *[Pinaud, 2002]*. In addition to the size-dependent emission maximum, the narrow spectral width can be observed. Since the line width for a single particle at room temperature was measured to be around one third the width of the ensemble spectrum *[Banin et al., 1999]*, the observed ensemble width of 30–50 nm reflects inhomogeneous broadening caused by a size distribution on the order of 10 %.

4.1.3 Photo-Induced Activation

Whereas emission spectra are an established tool to characterize newly synthesized NCs, the successive recording of spectra over several minutes, has revealed some new information. Depending on the excitation wavelength and intensity, various effects can be observed. The most striking is an increase in the overall emission signal, that may or may not be accompanied by a blue shift in the emission spectrum. This effect is contrary to the expected observation of photobleaching, which is a common phenomenon for almost all fluorophores. Figure 4.2 shows a comparison between fluorescein in water and CdSe/ZnS in butanol as they are illuminated over one hour. The spectrofluorometer in this case is used to observe fluorescence at a specified wavelength (520 nm for fluorescein, 570 nm for NCs with a bandwidth of 5 nm) upon excitation at a specified wavelength (300, 350, 400 with a bandwidth of 20 nm and 400–500 nm broad band) as it develops over time. For all organic dyes this experiment would show an exponential decrease in the emission due to irreversible photobleaching. Even though photobleaching, caused by oxidation processes or the formation of lattice defects on the NC surface, has also been reported for NCs (page 32), here another effect can be observed: whereas fluorescein displays the distinct exponential decrease in fluorescence intensity, CdSe/ZnS NCs in butanol show the opposite behavior, an increase of fluorescence, when illuminated with light at 400–500 nm. The same effect has been observed on a fluorescence microscope, where a high concentration of NCs was illuminated with a wide-field Hg-lamp (data not shown). Illumination at lower wavelength, but also lower absorption due to a smaller bandwidth, resulted in both decrease and increase of fluorescence with strong variations in time constants.

To rule out that an increase at the specified wavelength is caused by a spectral shift, successive emission scans were performed for 10 min with an integration time of 0.05 sec per 0.5 nm step (bandwidth of 0.5 nm), resulting in a 10 sec duration for each scan. The temperature was held constant, using a water-cooling system for the cuvette holder, during the entire measurement and excitation power was surveyed by a reference photodiode. Figure 4.3 reports the results for five different NCs and R6G, representing a variety of different effects. Whereas CdTe cores, synthesized through the water-based route, displayed a significant blue shift of up to 15 nm during illumination, most other samples, that were based on the TOP/TOPO synthesis did not show spectral shifts. In addition, two competing effects were observed that

result in either a fluorescence increase or decrease over time. Comparing CdSe/ZnS NCs in butanol to NC micelles and peptide-coated NC, all made from an identical batch of CdSe/ZnS NCs, an influence of surface modifications can be seen. All modified NCs show a smaller overall emission compared to the original CdSe/ZnS sample. It was confirmed that this difference corresponds to a reduced ensemble QY. Under illumination the photo-induced activation is highest for lipid-covered NCs but also significantly higher for peptide-coated NCs. Even though variations were observed for different colored NCs and their modification, this general trend was confirmed.

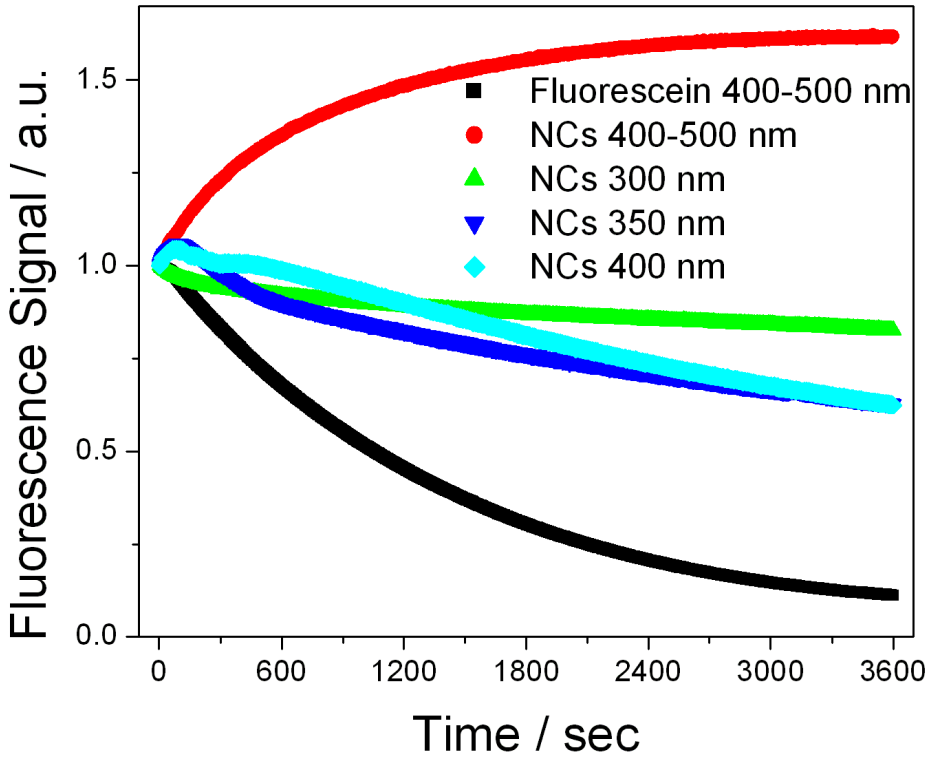

Figure 4.2: Emission of fluorescein in water (at 520 nm) and CdSe/ZnS:TOPO NCs in butanol (at 570 nm) excited at 400–500 nm or at 300, 350, 400 nm (bandwidth of 20 nm) and observed over 1 hour.

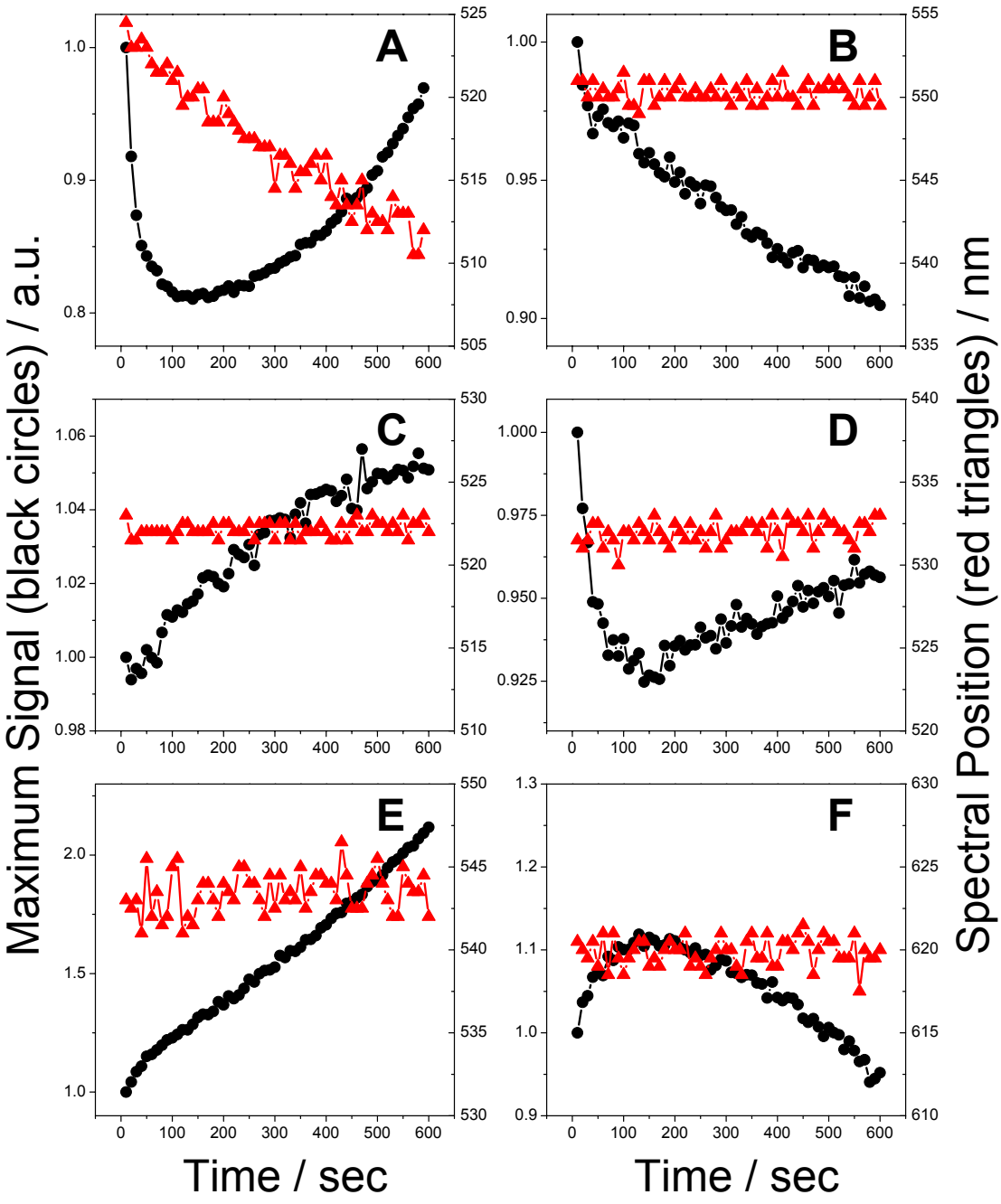

Figure 4.3: Consecutive emission scans from CdTe (A), Rhodamine 6G (B), polymer-coated QDots^{TM} (C), CdSe/ZnS:TOPO (D), CdSe/ZnS micelle (E) and peptide-coated NCs (F) in either water (all but D) or butanol (D). Spectral position of the maximum emission is displayed in red, maximum signal in black.

4.1.4 Discussion

The observation of photo-induced activation resulting in a signal increase is a puzzling event. Figure 4.3 is a clear indication that the effect is significantly influenced by surface modifications, since it appears to be different for differently treated NCs. In fact an overlay of several features can be seen. Whereas photobleaching, meaning a reduction in fluorescence signal over time, has been reported in combination with spectral blue shifts up to 30 nm *[van Sark et al., 2001]* when observed in air, the opposite behavior is a rather new phenomena. In fact the first reports appeared during the course of this work, reporting that photo-induced recovery from long-lasting off states can take place for NCs in films and solution. *Hess et al. [2001]* observed that long-lasting off states can be populated by either heating-cooling or freezing-thawing cycles. Darkened CdSe/ZnS:TOPO NCs remain dark for months unless they are exposed to light. The authors explain the effect with reconstruction of the surface leading to an increased number of surface defects (or trap states) and a transformation reverse under illumination. *Cordero et al. [2000]* reported increases being followed by decreases and accompanied by blue shifts up to 16 nm for CdSe (and CdSe/ZnS) monolayers. They also showed that the photo-induced activation is dependent on the water content in the surrounding atmosphere, since no fluorescence increase was observed under dry nitrogen, and attributed the light-induced activation to surface passivation by water molecules. In all cases the blue shift might be explained by photooxidation of the CdSe surface similar to what has been observed for CdTe NC *[Gaponik et al., 2002]*.

Even though the results shown above have been given some possible explanations by now, they demonstrate that a number of different mechanism contribute to very complex kinetics of NC fluorescence. And just as important, the variety of observations depending on NC, environment and ligands, demonstrate the importance of what is happening on a NC surface. Slight modifications by applying new surface chemistries can dramatically change the photophysical properties.

Since no single-particle observation of photo-induced activation has been reported until today, questions about the exact nature of this signal increase remain. Following $s = EQ\sigma P/Ah\nu$ (s: signal; E: detection efficiency; Q: QY; σ: absorption cross section; $P/Ah\nu$: excitation rate), a change in the brightness of single fluorophores can be attributed to either gradual changes in absorption or QY. Whereas a variation in absorption is rather unlikely and has not been observed, influences

on the overall QY are seen with every chemical modification. But in the case of an ensemble the observed fluorescence signal can also be altered by a variation of the concentration of fluorescent particles. It is possible that surface transitions lead to a complete quenching of fluorescence from single particles, turning them effectively dark. In fact dark subpopulations have recently been reported from combined AFM and fluorescence measurements *[Ebenstein et al., 2002]*. Therefore ensemble measurements as shown in Figure 4.3 cannot distinguish between gradual changes in QY and changes in the number of fluorescent particles, and single-molecule methods will provide more information.

4.2 Photophysical Properties of Single NCs on Surface

The simplest and quite enjoyable way to get a visual impression of the colorful fluorescence from NCs is by placing a drop of NC solution on a coverslip and observing the emission on a standard epi-fluorescence microscope. By lowering the NC concentration it becomes possible to see individual spots as they diffuse around. When the solution evaporates over time, NCs are immobilized on the glass surface. If the concentration is low enough a number of striking observations can already be made by eye. First of all, individual spots are observable for a long time after being immobilized. Second, since they are not moving around any longer, a new phenomenon can be observed. It becomes obvious that the fluorescence is interrupted by off times with various durations resulting in an impression of irregular blinking. And third, the size distribution, causing slightly different emission colors, can be seen by spotting e.g. individual red and green dots in an overall yellow sample. All these observations hint at the fact, that the dots represent individual NCs. The human eye is able to detect single NCs because they can be observed over a longer period of time than most organic dyes.

4.2.1 Confocal Scanning Microscopy of Single NCs

The most sensitive technique that is available today to investigate single fluorescent objects, is confocal scanning-stage microscopy with APDs as photo-detectors (page 56). A simple scan with integration times of 5–50 ms of spin-coated CdSe/ZnS,

diluted around $10^{(-3)}$ times from the stock solution (stock solutions exhibit an optical density on the order of 2 at 350 nm), can already provide additional information to what is observable with the human eye. As can be seen in Figure 4.4 each spot is likely to present the point-spread-function (PSF) from a single NC due to the following reasons: (A) Intermittency is seen inside some spots that represent off-times on the order of the pixel integration times (10 ms) or longer. It can be seen that the blinking behavior changes with increasing excitation power. The higher the excitation power, the more fluorescence intermittency distorts the PSF. (B) Some spots display a sudden stop in emission leaving the PSF far from being round. This off-switching can be due to the beginning of a very long but reversible off-period, that is not unlikely under the power-law statistics for blinking, or it can be due to irreversible photo-destruction of the NC. The fact that fewer spots are visible at higher powers can also be caused by other influences: a higher probability to remain in a long off-state can be attributed to blinking statistics, either by changes in the power law exponents or by the fact that longer off times become more likely when the off-time exponent is smaller than the on-time exponent. The latter effect is called statistical aging and discussed in detail in *Brokmann et al. [2003]*. In addition, irreversible photobleaching by oxidation processes on the NC surface can diminish the apparent concentration. (C) Every now and then a NC, that was not observed in previous scans, seems to be switched on at a later time during the passage through the laser focus. This effect, which has not been observed for organic fluorophores, might be related to photo-induced activation and will be further investigated in the following chapter. (D) The spot size is consistent with the dimensions of a PSF from a single point emitter ($\sim \lambda/2$).

The fact that all these changes in the observed fluorescence occur as discrete and digital events, suggests that individual particles are observed. However, a closer look exposes some features that question this assumption.

Multiple scanning

Even though Betzig's arguments (page 24) were successfully applied to a number of organic fluorophores, the situation turned out to be more complex with semiconductor NCs. A confocal scan as displayed in Figure 4.4 can give a first impression of the concentration of fluorescent particles; but if an identical surface area is scanned several times, it was observed that the number of NCs in that particular area increases

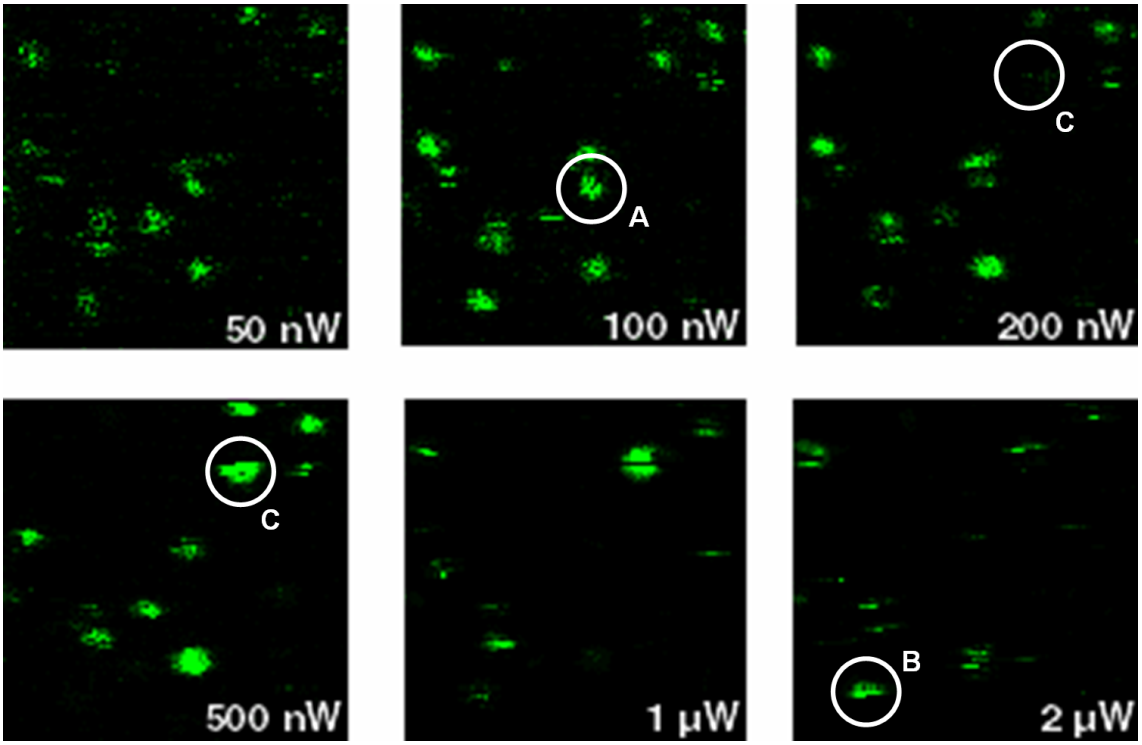

Figure 4.4: Confocal scanning image of CdSe/ZnS NCs, immobilized on a glass surface; 10×10 μm area (100×100 pixel); 15 ms/pixel integration time; 488 nm excitation wavelength; excitation power as displayed. Characteristics of single particles: (A) Intermittency (blinking) with off-times longer than integration times; (B) digital extinction due to irreversible photobleaching or extremely long off-times; (C) light-induced activation.

with each consecutive scan. Figure 4.5 shows five consecutive scans, in which the number of observed NCs increases from 0 to at least 7. The scans were recorded under typical conditions: integration time of 10 ms per pixel, resulting in slightly over a minute total scan-time for a (5 x 5) μm image with (80 x 80) pixel, and laser excitation at 488 nm and 1 μW excitation power. Under these circumstances the apparent concentration during one single scan cannot provide enough evidence to ensure that a particular NC remains single in the later course of an experiment.

The observation of an increase in the apparent concentration of emitting NCs is consistent with photo-induced activation, as has been seen in ensemble fluorescence measurements. Figure 4.5 provides some evidence that NCs do exhibit long-lasting dark states, for which the fluorescence is completely quenched. Under illumination the amount of quenching is reduced and the NC resumes to be fluorescent. Nevertheless the question remains unanswered if the signal increase is due to a gradual increase of individual QYs or to a digital on-switching of individual particles. The consecutive confocal-scan images do not rule out either one of the two possibilities but rather give an impression that either one might contribute. On the other hand they do not provide good statistics concerning the number of investigated particles and therefore cannot convincingly answer the question.

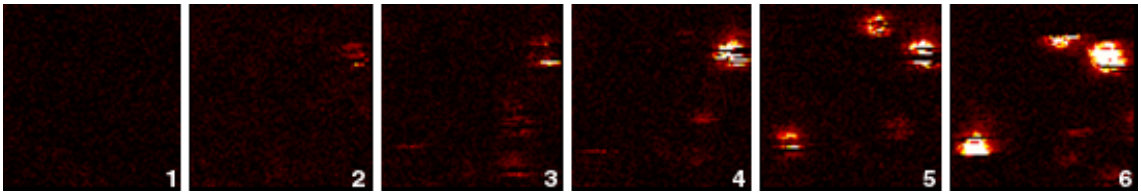

Figure 4.5: Consecutive scans of an identical 5×5 μm area (80×80 pixel) with immobilized Cd/ZnS NCs; 1 μW at 460 nm excitation power; 10 ms/pixel integration time. The image was focused on a neighboring area. The color code represents increasing signal with dark red changing to yellow and white.

On/off Intermittency or Blinking of Single NCs

With the additional capability of parking the laser beam at a specified position inside the scanned area, it is possible to record a fluorescence signal over time and display it as a time series, so called time traces. The use of a confocal microscope with APD

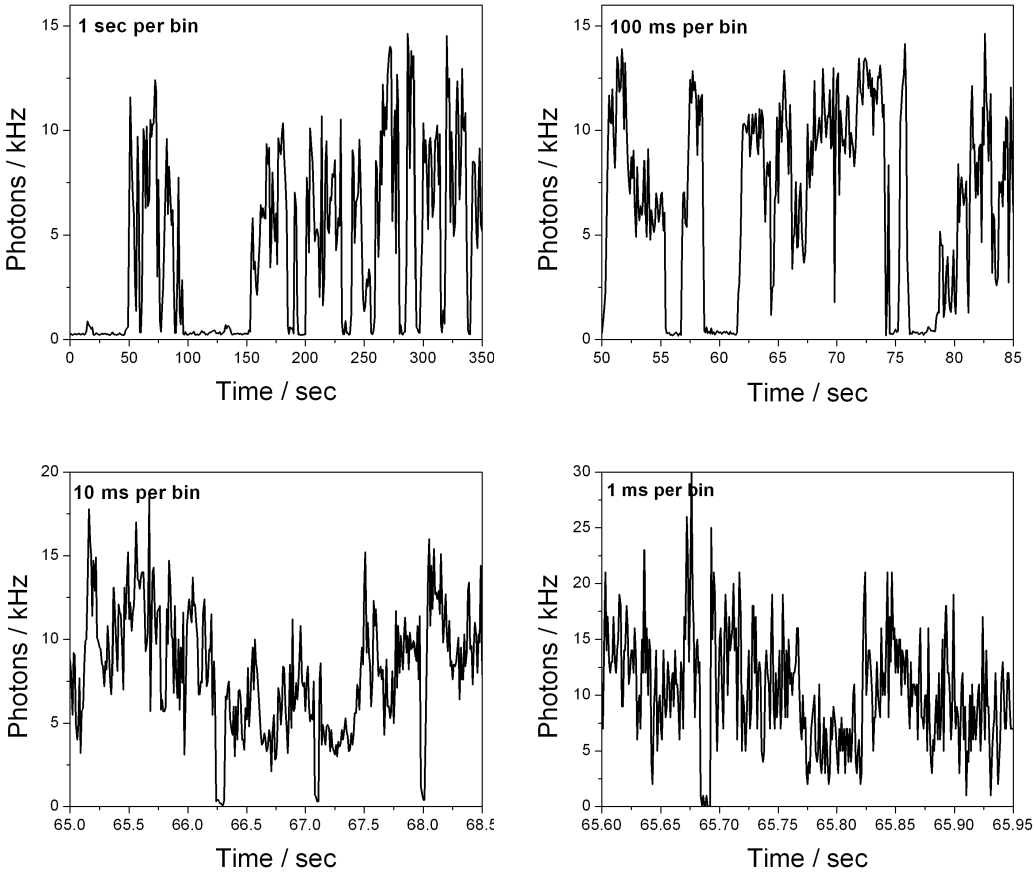

Figure 4.6: Emission from a single CdSe/ZnS immobilized on a glass surface and excited with 1 μW at 488 nm is presented in increasing detail. Bin times vary from 1 sec, 100 ms, 10 ms to 1 ms. Self-similarity in terms of on/off-time distributions reveal the non-exponential blinking behavior.

detectors enables single-photon detection with very high sensitivity (meaning better signal-to-noise ratios due to high quantum yields, negligible readout noise and dark count rates on the order of a few hundred Hz), enabling the exact timing of single photon arrival times (which is impossible with CCD detection). Arrival times of single photons are recorded with a time resolution of 12.5 ns (limited by the NI electronics). In a post-acquisition step the arrival times are binned into certain time slots and displayed as a time trace. Making use of such time traces, one can investigate the fluorescence intermittency of NCs on different timescales.

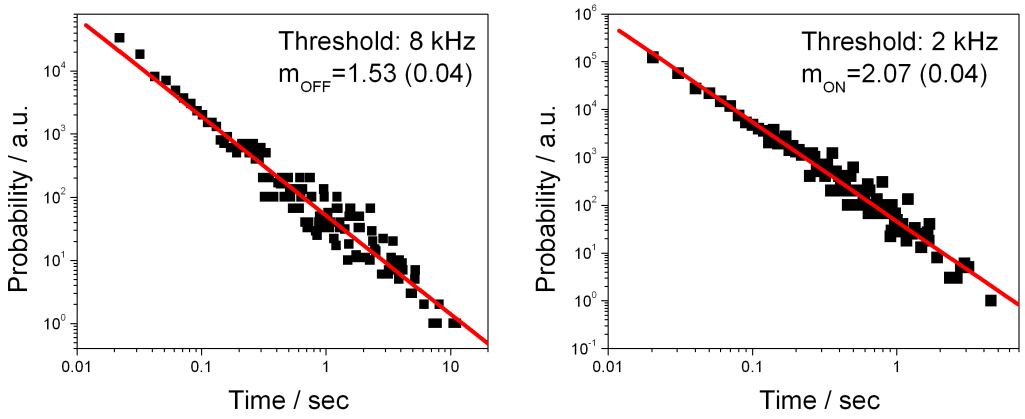

Figure 4.7: On- and off-time distribution in the emission from a single CdSe/ZnS NC, immobilized on a glass surface and excited at 460 nm (pulsed, 5 MHz repetition rate, 200 nW excitation power). The corresponding time trace (10 ms bins) is shown in Figure 4.8 (top, left). The red line represents a power law fit yielding an exponent $m_{on/off}$. On(off)-times are analyzed with a threshold of 8 (2) kHz. Whereas m_{off} did not vary more than 20 % with threshold, m_{on} was increasing from 1.5 to 3.0 with increasing threshold.

Figure 4.6 shows one time trace that is binned at 1 s, 100 ms, 10 ms and 1 ms. A limited area of the time trace is shown in order to keep as many details visible as is allowed by the particular time resolution. By comparing the four panels the most intriguing characteristic of NC blinking becomes recognizable: the distribution of on- and off-times does not exhibit a characteristic timescale, the time trace is self-similar when binned at 1 ms or 1 sec intervals. This behavior was further investigated in a detailed study by *Kuno et al. [2000]*. He determined the probability distribution

for both on- and off-times and found that they follow a power-law distribution, as illustrated for comparison in Figure 4.7. In comparison to the published results, the presented time trace does not display clear switching between an on- and off-state, with two well defined intensity levels. The appearance of multiple intensity levels could be due to fluctuations in the laser intensity or contributions from more than one NC — both possibilities will be ruled out in the following chapter by monitoring the excitation power and observing the signature of antibunching. More likely are environmental influences or imperfections in the NC itself. NC synthesis is still an art rather than a well defined and easily followed protocol. For this reason it has not yet been possible to consistently reproduce two level emission as seen by Kuno and coworkers.

The Signature of Antibunching to Ensure Lifetime Measurements on Single NCs

Since semiconductor NCs have shown fluorescence lifetimes that are significantly longer than those of organic dyes, in principle they make good probes for fluorescence lifetime imaging and time-gated detection. FLIM has been used to identify labeled macromolecules according to their lifetime or monitor environmental changes that have an influence on the lifetime. In order to apply this technique to systems labeled with NCs, one has to know the fluorescence lifetime of NCs under normal (meaning standardized) conditions. A simple lifetime measurement in a time-resolved spectrofluorometer results in a distribution of delay times between excitation pulse and emitted photons, which cannot be described by a single exponential decay *[Dahan et al., 2001]*. To address the question if this multi-exponential distribution originates in (1) a distribution of NCs each with slightly different properties or (2) in a multi-exponential decay for single NCs or (3) in a non-stationary behavior of the fluorescence emission, can only be answered by investigating the emission of truly single NCs in a time-resolved way.

To increase the confidence that single particles are observed, a setup was built that enabled the measurement of time delays between consecutive photons. As was discussed on page 25 a histogram of these time delays displays the signature of antibunching if and only if the detected photons are emitted from a two-level quantum system. Here a pulsed laser source (5 MHz repetition rate), a femtosecond laser (Mira, Coherent) followed by a pulse picker (Coherent) and a doubling

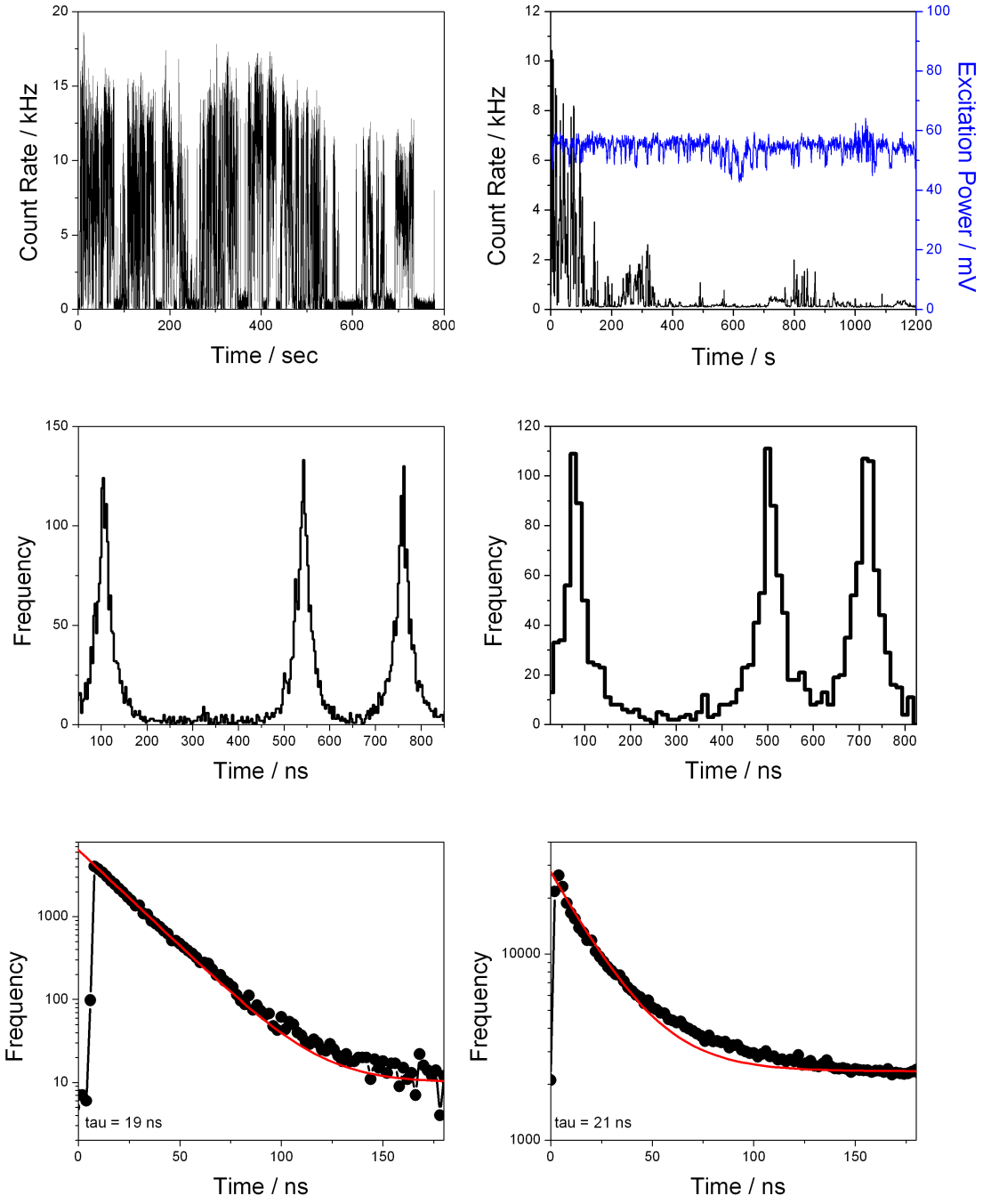

Figure 4.8: Simultaneous measurement of antibunching signature (second row) and fluorescence lifetime (third row) for two CdSe/ZnS NCs immobilized in PMMA on a glass surface and excited by fs-pulses (5 MHz repetition rate, 460 nm wavelength, 200 nW (left) and 1 μW (right) excitation power). The histogram of inter-photon times (second row) is a convolution of the fluorescence decay and pulsed excitation. The missing peak (~120:5 ratio) at 0 delay time (shifted around 300 ns due to an electronic delay) proves the observation of a single two-level quantum emitter. A histogram of delays between photons and laser pulses is fitted by a mono-exponential decay and estimates a lifetime of around 20 ns.

crystal (excitation wavelength 460 nm), was used to excite NCs (CdSe/ZnS stock solution $10^(-6)$ times diluted and spin-coated on a glass coverslip), observe time delays between excitation pulses and emitted photons to determine the fluorescence lifetime and observe inter-photon delays to measure antibunching. The photon delay histogram reflects the excitation pulses convoluted with the fluorescence lifetime. In the case of a light field that originates from a two-level quantum system, the zero time delay peak disappears due to antibunching. This phenomenon was observed with a sufficient signal to noise ratio for a few — single — NCs, embedded in PMMA, as shown in Figure 4.8. The simultaneous lifetime measurement clearly proves that the non-exponential behavior originates from one particle and cannot be explained by a distribution of particles with slightly different properties (right column). In addition, large differences in the deviation from mono-exponential decays exist, as can be seen from the second exemplary NC (left column). This NC could be imaged 5 times for 20 min (almost 1.5 hours altogether) at different excitation powers. The displayed lifetime histogram has a smaller deviation from a mono-exponential decay than the first NC but a comparable antibunching signature (peak to missing peak ratio of around 120:5). The overall lifetime was estimated to be around 20 ns by fitting a mono-exponential decay (red curve). This value is consistent with reports by *Lounis et al. [2000]*. To ensure that fluctuations in the excitation power cannot influence radiative lifetimes and thus contribute to multi-exponential decays, the laser power was recorded simultaneously with photon-arrival times. As displayed for the first NC, no significant power changes were found.

4.2.2 Wide-Field Imaging of Single NCs

To become quantitative in the investigation of single-particle characteristics and at the same time acquire enough data in a reasonable amount of time to be statistically relevant, a setup is used where far-field excitation is combined with detection by a CCD-camera. Excitation can be provided in one of three ways: by use of a fluorescence lamp (Hg or Xe-lamp), a defocused laser beam or a TIR excitation scheme. Here objective-based TIR was utilized to investigate NCs immobilized on a glass surface. A solid state laser emitting at 405 nm (Radius 405, Coherent) provided 1.5 mW (measured before the objective). The resulting field of view has a circular shape with a radius of around 30 μm (Figure 4.9) and allows simultaneous observation of tens to hundreds of single NCs. TIR excitation thus provides the capability

to observe a larger number of single particles over long times, with a drawback in the time resolution, compared to confocal scanning microscopy (typically integration times of 10 to 100 ms are required to overcome readout noise as compared to ns time resolution of APDs).

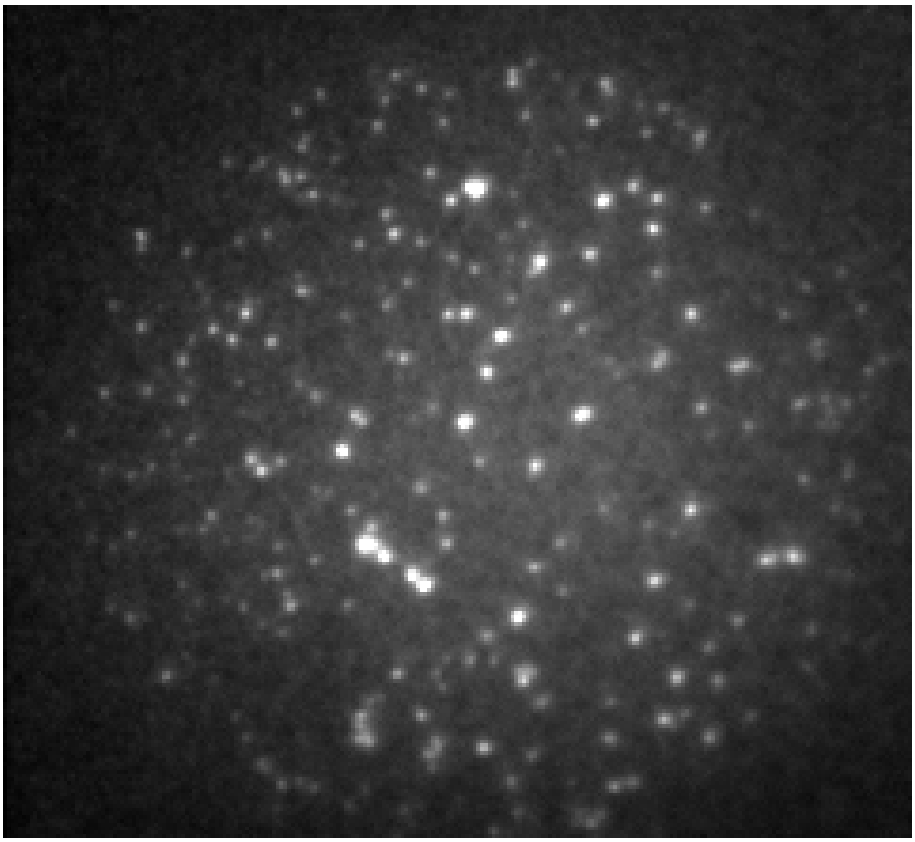

Figure 4.9: CCD-image (100x 1.3NA objective, Zeiss) acquired with a Pentamax ICCD of surface-immobilized CdSe/ZnS NCs ($10^{(} - 3$) times diluted stock solution spin-coated on a glass coverslip) under TIR excitation; (220×240) pixel adjusted to the size of the TIR-illuminated area result in a (33×36) μm field of view; 100 ms integration time; 405 nm (1.5 mW) excitation wavelength.

Photo-induced Activation

Using wide-field single-molecule techniques the effect of photo-induced activation, as first reported from ensemble measurements, was revisited. To address the question of concentration versus gradual QY changes, NCs immobilized on a glass coverslip

were observed at single-particle concentrations ($10^(-3)$ diluted stock solution). Data was recorded on areas that had not been illuminated before the actual measurement (focusing was performed on close-by areas; movement of the stage did not change the focus significantly). Exposure times were adjusted to 100 ms. Several movies of 100 frames each ($\sim$20 seconds) were recorded using a sensitive CCD-camera (Coolsnap *HQ*, Roper Scientific).

The data was analysed using a LabView program that could identify single spots (representing single NCs), determine their center position and calculate the spot intensity (total counts from all pixels inside a circle with fixed size — the circle represents the PSF). In addition, the number of spots per frame was counted and the average spot intensity for each frame was calculated. In Figure 4.10 the number of identified spots and their average intensity per frame is shown. 5 movies were combined to yield better statistics. The overall analysis yields a variation of < 1 % in the average signal per spot ($Mean = 555$ counts, $STD = 5.2$ counts), whereas the number of particles increases as $A - B\exp(-t/\tau)$ with a time constant of 5.5 sec starting from almost zero particles in the first frame and reaching up to 80 particles in the latest frames.

The data clearly states that for NCs on a glass surface exposed to air, photo-induced activation has to be explained by an increase of the concentration of fluorescent particles. At the same time their average intensity remains constant, excluding the influence of any gradual change in QY for all particles.

4.2.3 Discussion

Single-NC observations were presented that provide additional information about photophysical properties, that are not accessible with ensemble methods.

First blinking of the fluorescence signal was shown and revealed the self-similarity at various time-scales, illustrating the fact that no characteristic time exists to describe NC blinking.

Second, the fluorescence lifetime of a single NC was measured to be around 20 ns, fluctuating from NC to NC. It was shown that no mono-exponential function can describe the fluorescence decay and that in addition, the deviation from a mono-exponential function is different from NC to NC. The fact that indeed single particles were investigated, was proven by the simultaneous observation of an antibunching signature. These observations point out two aspects which become important when

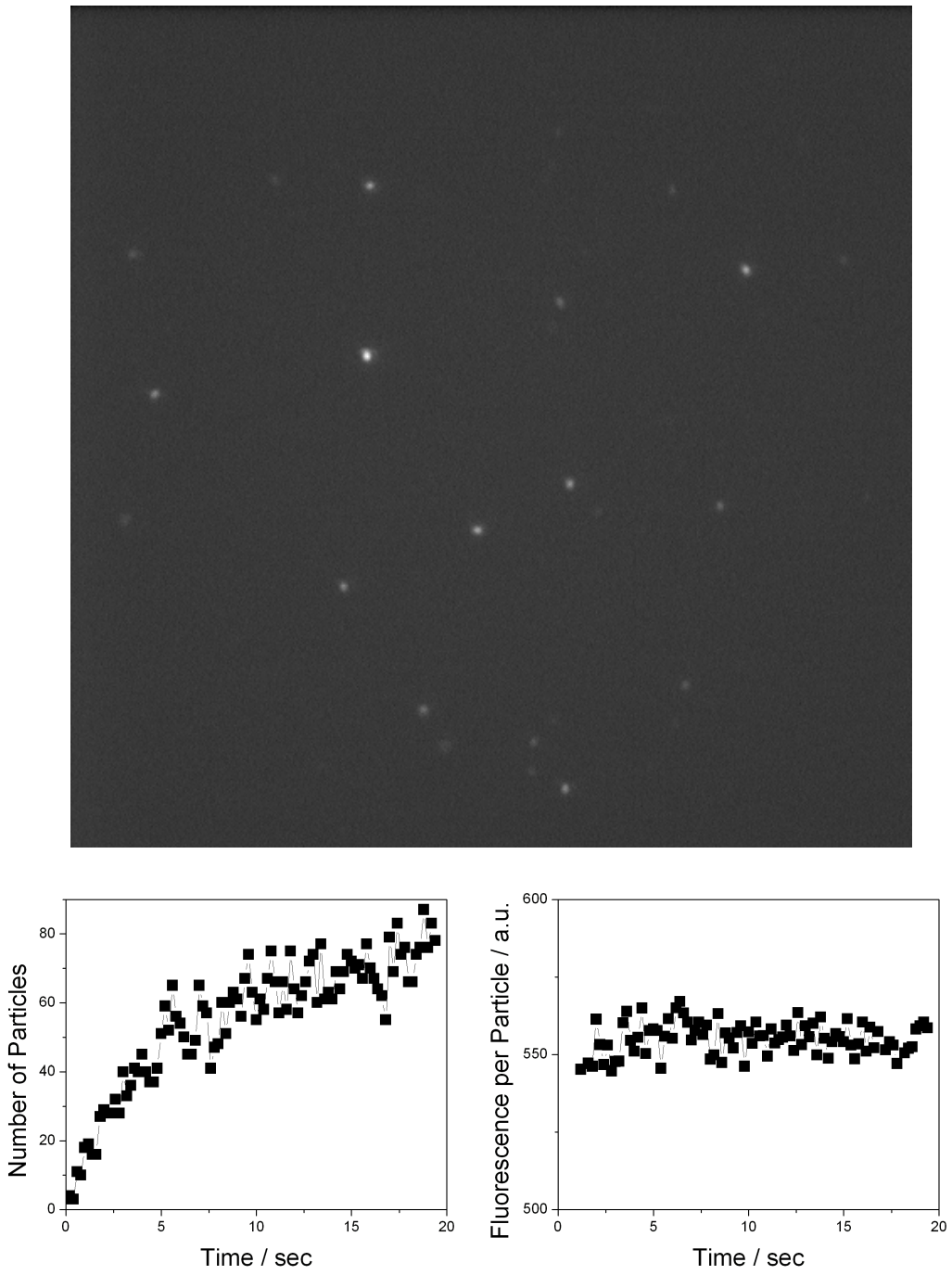

Figure 4.10: Photo-induced activation causes the number of fluorescent particles to increase whereas the average detected count rat per particle stays constant. Immobilized CdSe/ZnS particles were observed using TIR excitation (1.5 mW, 405 nm) and CCD detection ((500× 500) pixel, (32 × 32) μm, 100 ms exposure time).

NCs are to be used as fluorescent reporters. First, the fluorescence lifetime is about one order of magnitude larger than that of most organic dyes and especially than that of autofluorescence from proteins or staining agents in cells. On the other hand the lifetime is not well defined for even a NC which is immobilized in a fixed matrix-environment (PMMA). This makes employment of fluorescence lifetime as a reporter for a changing environment or molecular interactions rather difficult. A quantitative use of FLIM, with NCs as lifetime-probes, thus faces many challenges. Nevertheless, the comparably long lifetimes enable time-gated detection, which does not depend on the exact lifetime value or small variations. *Dahan et al. [2001]* have nicely illustrated the advantages of rejecting photons, that are emitted in the first 35 ns after excitation with a femto-second laser in a confocal microscope. The SNR in a fixed cell could be improved from 3 to 45, as shown in Figure 4.11. This successful utilization of NCs' lifetime will be further extended to solution-based applications in the following chapter.

Third, the effect of photo-induced activation was confirmed for NCs immobilized on glass surfaces. Even though high-resolution confocal scans gave the impression, that changes in brightness and apparent concentration both contribute to the activation effect, TIR measurements revealed a different behavior for NCs immobilized on a glass surface and excited through objective-based TIR. Making use of the TIR wide-field approach to acquire sufficient amounts of data to increase statistical confidence levels (observation of up to 80 particles), it was shown that an increase in apparent concentration of bright particles was not at all influencing the average brightness per particle. Even though the data is very convincing, one should keep in mind, that the way particles are excited, is dissimilar for TIR or confocal excitation. Both the excitation time (continuous for TIR but depending on the scanning procedure in confocal mode) and the exact excitation power (which is not well characterized for objective-based TIR and difficult to compare due to the fundamentally different CCD and APD detectors) can be very different. And these factors might contribute to the fact, that a gradual change in QY per particle is not detected via TIR. The results do not contradict the suggestion by Hess, that surface transformations cause trap states, which then quench the fluorescence. But they point out that these transformations have to be reversed in one step (on the timescale of 100 ms) leading to complete recovery of the emission.

Of course all surface-based measurements suffer from the limitation that influences from the surface or the atmospheric environment cannot be excluded. To rule out

such effects, experiments with single-particle sensitivity have to be performed on freely diffusing particles in a solution environment.

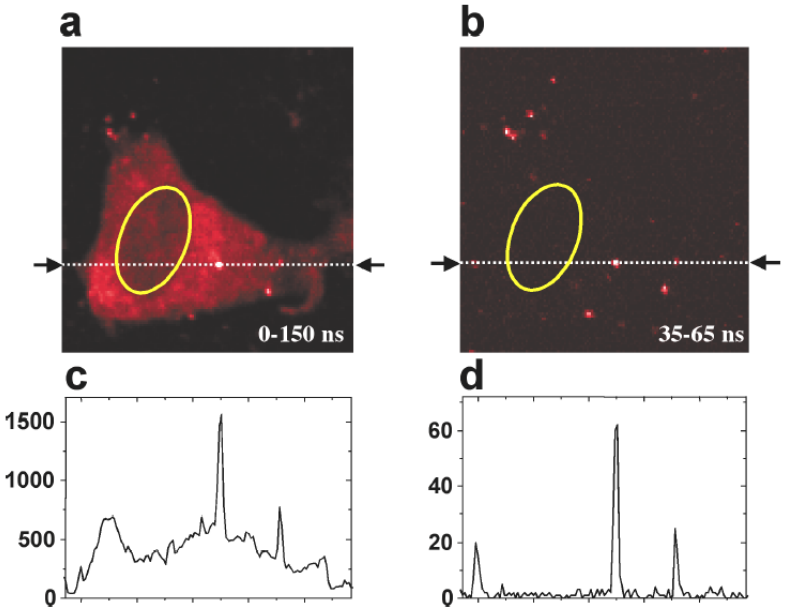

Figure 4.11: Time-gated imaging of fixed mouse 3T3 fibroplasts using femto-second excitation in a confocal microscope. Integration time per pixel is 10 ms, the lifetime window being 0–150 ns (5 MHz repetition rate for the laser pulse). In image (A) all photons are collected leading to a NC signal as displayed in the marked profile (C). In image (B) only photons from inside the time window 35–65 nm are colledted. The SNR can be improved from 3 to 45. Data from *Dahan et al. [2001]*

The notion of quantum yield for single particles

As single-particle observations revealed large variations of the number of fluorescence particles, the notion of QY as defined for an ensemble measurement needs to be discussed.

The fluorescence QY is one of the most important parameters in the characterization of biological probes. It directly refers — together with the extinction coefficient — to the brightness of fluorophores. QY is the ratio of the number of emitted photons to the number of excitations (transitions from the ground state to the excited state upon absorption of a photon). A QY smaller than one is the signature for non-

radiative processes, which allow the fluorophore relaxing from an excited electronic state to its ground state without photon emission.

QY measurements are routinely performed on ensembles of the investigated fluorophore, by comparison of the emission to absorption ratio to a well characterized standard. Rhodamine 6G, for example, has a QY of 0.95 in water and is routinely used in such measurements *[Miller, 1981]*.

The main assumption in these measurements is a static and dynamic homogeneity (between members of the ensemble and over time, respectively) of the molecules' characteristics and environment. As has been shown in the above measurements, this assumption is not valid in the case of fluorescent semiconductor NCs.

Since the concentration of fluorescent particles was observed to first, be lower than the total NC concentration and second, to change over time of illumination, the definition of QY needs to be redefined. An ensemble QY measurement underestimates the QY for fluorescent particles as long as a considerable amount of dark, but still absorbing, particles is present. In addition, given a blinking mechanism that allows long off-states to occur (due to power law statistics), a certain QY, meaning a certain ratio of emitted to absorbed photons, does not specify the brightness during on-periods without taking the duration of all on/off-states into account. Many biological applications are essentially interested in probes with as high levels of emission as possible at times, they can be observed. Therefore the QY of interest, for applications such as particle tracking, is that of a fluorescing (not in a long-lasting dark state residing) NC during its on-time. Since dark subpopulations have been found in many NC samples, a more practical value would be derived from brightness measurements, combined with a simultaneous determination of the concentration of emitting particles and also, in the optimal case, determination of the power law parameters. This brightness per particle value can be estimated by FCS and will be explored in the following chapter.

4.3 Photophysical Properties of NCs in Solution Investigated by FCS

The previous chapters illustrated the need for a method that allows characterizing photophysical properties of NCs in solution with single molecule sensitivity. FCS, as described on page 37, in principle can provide the information that is needed to

obtain a better knowledge and understanding of NCs' optical performance.

First FCS can be used to evaluate brightness and concentration of fluorescent particles at the same time, thus giving a better QY estimation than ensemble measurements can provide in the presence of dark particles. The same parameters can help to estimate saturation intensities and define the limitations that saturation poses on the observable fluorescence signal. Relative concentration changes can be monitored as is important to investigate photo-induced activation.

Second, effects that alter the overall shape of the correlation function can be observed. Most important blinking and photobleaching have an influence on the exact shape. It will be shown that blinking statistics can be monitored for various NC samples and compared with surface-based measurements. In combination with Monte-Carlo simulations some limits can be set for power law parameters. Photobleaching as well will influence the correlation function, but in a different way than blinking does. Therefore it will be shown that both effects can be distinguished and the photobleaching behavior for different NC batches investigated.

And third, colloidal properties such as particle size and monodispersity can be evaluated via a measurement of the diffusion constant. The ability of FCS to detect changes in the diffusion constant has been used to quantify a number of biochemical interactions.

In the following FCS will be established as a characterization technique for NCs in solution. Several aspects that might influence the measured parameters are investigated in more detail and example measurements on various NC samples are presented. Remaining uncertainties due to optical effects which are not well established are discussed.

4.3.1 Setting the Stage for FCS Measurements

Even though FCS is a rather established technique to monitor macromolecular interactions, a number of peculiarities concerning the advanced optics involved have to be taken into account. The application of confocal microscopy to FCS helps to increase the signal to background ratio by minimizing the observation volume. From theory (page 41) it is evident that the particular shape of this observation volume critically influences the experimental results. The use of high-NA objectives in combination with a variable focal depth - the distance between the focal plane inside the solution and the glass surface on which a mismatch occurs for the index of refraction - leads

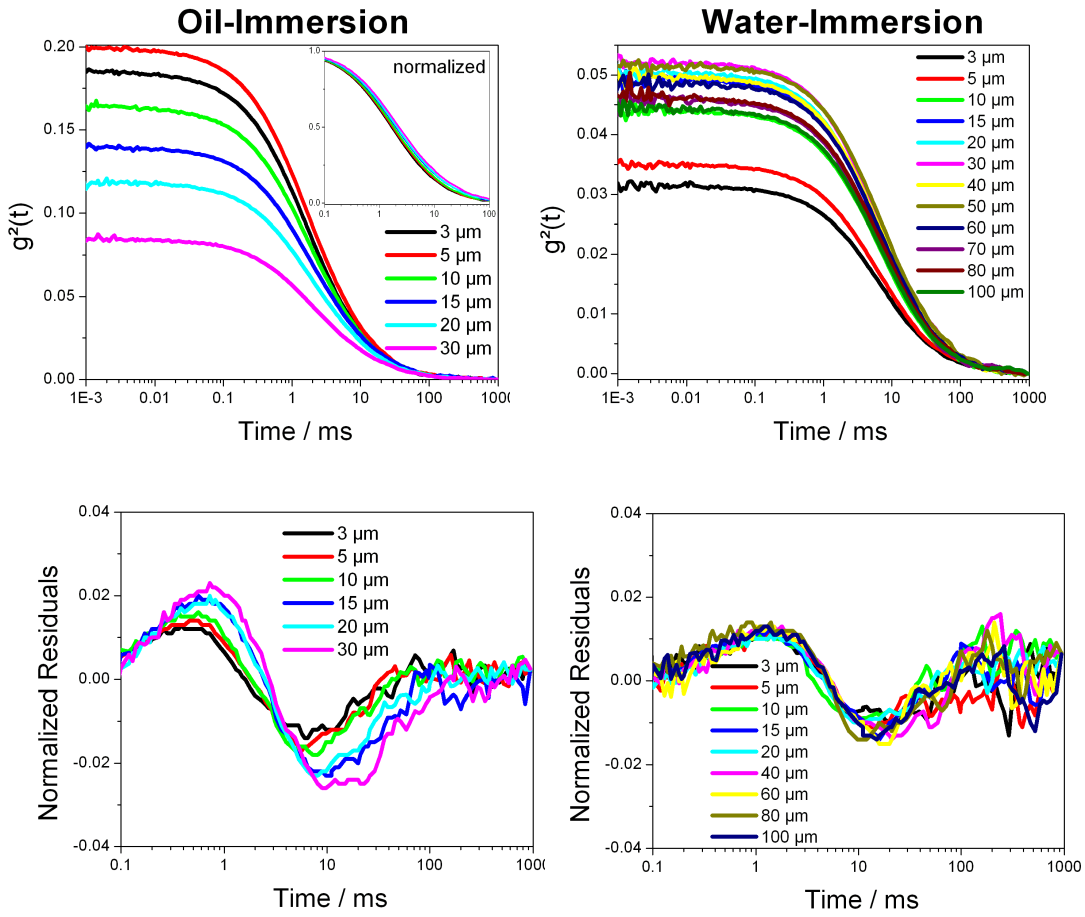

Figure 4.12: FCS data recorded with either a 1.4 NA oil-objective or a 1.2 NA water-objective at various depths (nominal distance between focus and glass surface). Residuals from fits of a 2D-diffusion model are presented. The residuals were normalized by $g^2(0)$. All data was taken on 26 nm polystyrene beads in distilled water (excitation power 20 μW at 532 nm). Significant alteration of the observation volume can be seen for the oil-objective from variations in the residuals. The water-objective on the other hand allowed identical excitation up to at least 100 μm depth. Very close to the surface scattered light contributes to background reducing the correlation amplitude.

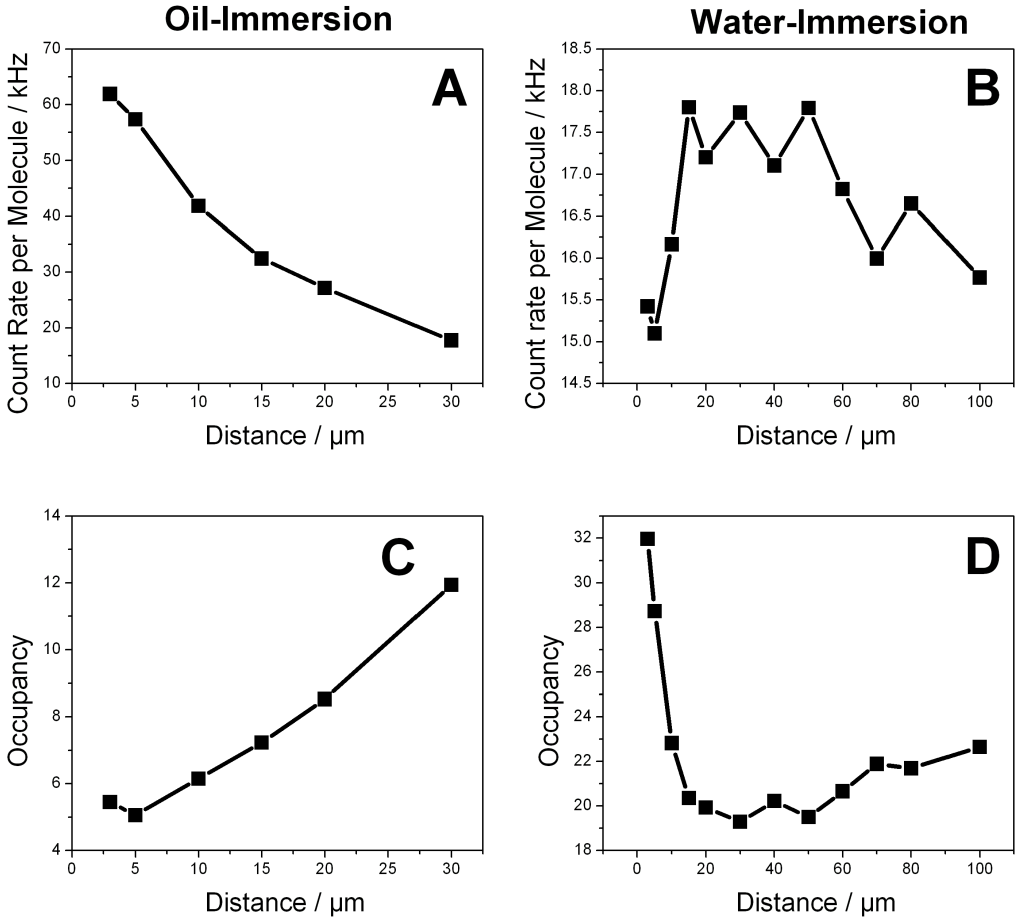

Figure 4.13: Count rate per molecule and occupancy of the observation volume were extracted from the above shown data. Results are shown for oil- (A, B) and water- (C, D) objectives (note the different distance ranges). Water objectives are less sensitive to depth variations inside the solution. In close proximity to the surface (closer than 10 μ m) scattered light contributes to background reducing the correlation amplitude (B, C). The smaller count rate detected with the water-objective is caused by a lower power density due to a larger focal spot (confirmed from diffusion times, see next Figure) and a lower NA.

to variations in the collection efficiency and the size of the observation volume, as has been reported by *Hell et al. [1993]*. The variations can be significantly reduced with the use of water-immersion objectives (page 50).

A comparison between a 1.4 NA oil-immersion (Plan-Apochromat, Zeiss) and a 1.2 NA water-immersion objective (UPlan-Apo/IR, Olympus) clearly show the reduced focal depth dependence for the latter objective. FCS measurements were performed on a solution of 26 nm polystyrene beads in distilled water. A cw Nd:YAG laser was used to excite the beads at 532 nm with 20 μW excitation power. Each data set was collected for 300 sec. Analyzing the data by fitting a standard 2D-diffusion model (Equation 2.29) illustrates how pronounced changes in the shape of the observation volume are for various focal depths (Figure 4.12).

The molecular occupancy N, which is proportional to the size of the observation volume V_{eff} and inversely proportional to the correlation amplitude $g^2(0)$

$$\text{Occupancy} = N = \frac{1}{g^2(0)} \propto V_{eff} \tag{4.1}$$

was determined from the $g^2(0)$ together with the average count rate per particle: count rate, averaged over the whole measurement time, divided by the occupancy. Even though the quality of the fit depends on the depth of the focal plane, fitting provides a good estimate of $g^2(0)$, such that these values clearly reflect the objective's characteristics. For an oil-immersion objective occupancy as well as count rate per particle strongly varies with the focal depth. The variation is much smaller when observed with a water-immersion objective even for depths up to 100 μm.

These results clearly point out how important it is to control the depths of the focal plane very carefully, when experiments with oil-immersion objectives are performed. In many solution-based experiments oil-immersion objectives are preferred because the higher NA allows acquiring data with higher sensitivity.

In FCS not only the overall size but also the particular shape of the observation volume is of interest, when the complete correlation curve is to be analyzed. The shape of the observation volume is also dependent on the focal depth. Figure 4.14 shows the correlation curves for various depths and the residuals after fitting a 2D-diffusion model. The different behavior for water- and oil-immersion objectives can clearly be seen: whereas no changes in the residuals can be detected for the water-objective, the deviation from a Gaussian observation volume increases significantly for the oil-objective.

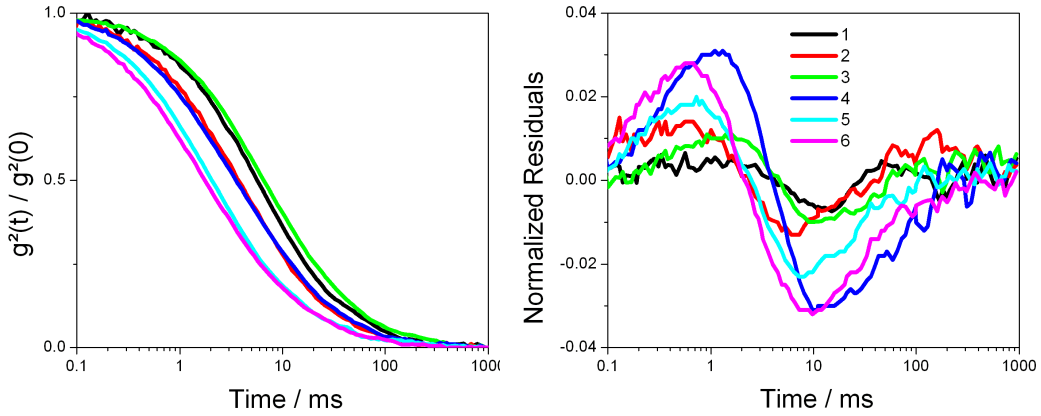

Figure 4.14: FCS data and residuals for 2D-diffusion fits, recorded on 26 nm polystyrene beads with either a 1.2 NA water-immersion (1–4) or 1.4 NA oil-immersion (5,6) objective; the objective's back-aperture was underfilled (1,3,5) or slightly overfilled (2,4,6) and a pinhole of 50 (1,2) or 100 (3–6) μm was used; the excitation power was 20 μW at 532 nm. The shift in the correlation function expresses different observation volume sizes. These are larger for water- than oil-objectives and for underfilled back apertures. Variations in the residuals reflect variations in the overall correlation function and are due to deviations from Gaussian observation volumes. These are largest for high NA oil-immersion objectives, bigger size pinholes and overfilled laser illumination.

Another important factor that influences the observation volume, is the radius of the incoming laser beam in relation to the objective's back-aperture, as shown by *Hess and Webb [2002]*. Using a telescope ($f_1 = 75$ mm, $f_2 = 30$ mm), the beam was expanded to underfill ($\beta = 1.5$ [1]) or slightly overfill the objective ($\beta = 0.5$). FCS data was recorded for both objective types and two different pinhole sizes. The pinhole size d was changed from 50 to 100 μm, which corresponds to 8.3 (11.8) and 16.6 (23.6) optical units for the oil- (water-) immersion objective. An optical unit (OU) is an objective- and wavelength-independent measurement for the detection aperture size, directly related to the objectives Airy-pattern (k: wave vector, M: magnification):

$$OU = \frac{d \cdot k \cdot NA}{M} \tag{4.2}$$

[1] the underfilling fraction $\beta = r_{BA}/r_0$ is defined as the ratio of the back-aperture radius r_{BA} to the $1/e^2$ intensity radius r_0

Residuals clearly reveal that oil-objectives create an observation volume that deviates more from a Gaussian shape than in the case of water-objectives. Despite the fact that the effective pinhole size is smaller in optical units for the oil objective, deviations from a Gaussian excitation profile caused by the objective are still dominant. However, reducing the pinhole size for one objective does reduce the deviation from Gaussian observation volumes, in the same way as underfilling the objective's back-aperture improves the profile. This result is especially important to remember, since in most confocal applications a minimized confocal spot is used. For FCS applications it is important to remember that the smaller the confocal spot the larger the deviation from a Gaussian profile becomes.

4.3.2 Characterization of NCs by FCS

In the following chapter the application of FCS to NCs is demonstrated by presenting typical data for a variety of NCs.

Applying the demonstrated technique of FCS to colloidal NCs dissolved in non-polar solvents such as n-butanol, distilled water or biological buffer, allows monitoring a number of parameters that are of interest in terms of fundamental photophysical properties but at the same time allow testing the quality of NC samples when being used in labeling experiments. Following the theoretical description of FCS the following parameters yield valuable information about a NC sample:

- average count rate S
- occupancy N
- diffusion time τ_D
- overall shape of the correlation curve

Each parameter is by itself describing a valuable characteristic of the NC sample or can be used to derive additional parameters of interest, e.g. the brightness per particle (the ratio of average count rate to occupancy).

Particle Concentration

The amplitude of the correlation function $g^2(\tau = 0)$ provides an estimation of the occupancy of the observation volume. The real concentration of fluorescent particles

in the sample is determined by multiplying this number with the effective observation volume V_{eff}. The direct measurement of the observation volume is more difficult due to a number of reasons. As was discussed above, V_{eff} depends on the exact shape of the confocal volume and can only be calculated from physical parameters, such as diameter of the laser beam and the characteristics of the objective, using diffraction theory. Neither is it possible to directly measure V_{eff} with high accuracy. One way to estimate V_{eff} is by assuming that the observation volume is described by a Gaussian profile. Fitting FCS data from a fluorophore with a known diffusion constant to a 3D diffusion model, the beam waist ω_{xy} and ω_z can be estimated (Equation 2.28). A more direct way to measure particle concentrations is to use a standard sample of known concentration to determine V_{eff}.

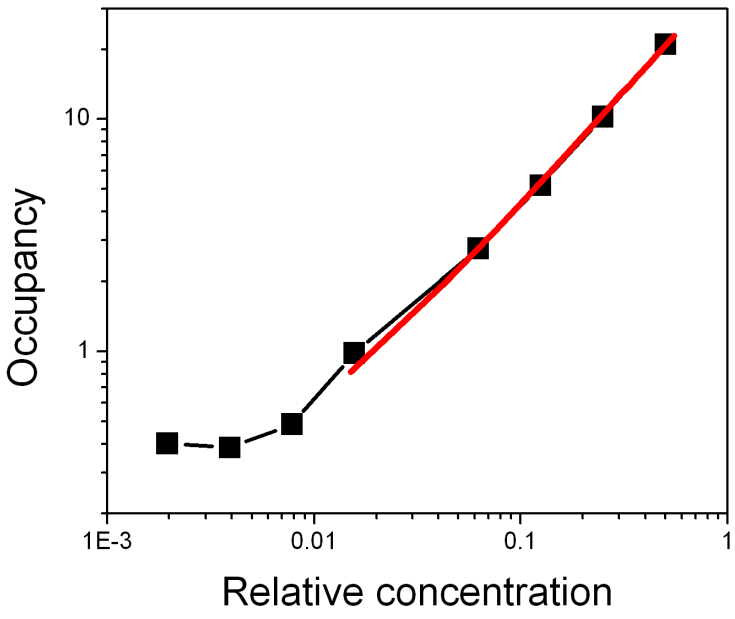

Figure 4.15: The number of particles in the observation volume as a function of relative NC concentration. The red curve is a linear fit to the data points at higher relative concentrations. Good agreement can be seen until single-particle concentrations are reached and SBRs are significantly decreased.

At the rather small concentrations required in FCS measurements to achieve sufficient signal to noise ratios (nM–μM), concentration measurements are always in

danger to be influenced by sample loss from adherence to glass or chamber walls. One way to test if such nonspecific binding of particles to chamber walls occurs, is by taking measurements on a dilution series. Figure 4.15 shows the inverse of the correlation amplitude, approximating the number of particles N in the observation volume, depending on the dilution of the sample. A linear relationship between N and the relative concentration of NC is observed over three orders of magnitude down to 0.4 particles per observation volume (on average). The red curve describes a linear fit to the experimental data. Deviations at large dilutions arise from the decrease in signal to background ratios. Below an occupancy of approximately $N = 1$, individual bursts appear with only background counts in between, meaning that single-particle concentrations are reached. Due to long observation times without fluorescence from a NC, the averaged signal is decreased to a level where the background contribution is high enough to decrease the correlation amplitude.

To extract concentration values for different NC samples a comparison with a sample of synthesized DNA (32 base pairs) labeled with Alexa532 was used. FCS data was recorded for 300 sec. Using a 2D diffusion fit, the following concentrations were determined for various NCs:

Particle	Specified Conc.	FCS Conc.
red QDot^{TM}	2 μM	1.0 μM
orange QDot^{TM}	2 μM	750 nM
yellow QDot^{TM}	2 μM	740 nM
red peptide-coated NC	280 nM	10 nM

Specified concentrations are given for comparison. They are determined by absorption measurements, either as specified by the supplier (QDot Inc.) or estimated via published absorption coefficients *[Leatherdale et al., 2002]*. The fact that a smaller concentration of fluorescent particles, as compared to the concentration from absorption measurements, is measured, can be explained by the above described photo-induced activation. To have photo-induced activation occur, a subpopulation of dark NCs needs to be present. *[Ebenstein et al., 2002]* used combined AFM and confocal microscopy to observe 1 in 5 CdSe/ZnS NCs, immobilized on a glass-surface, to be fluorescent. This ratio of dark to bright particles lies in between the factor of 2 (observed for QDot^{TM}) and 30 (observed for peptide-coated NCs). The high ratio for peptide-coated NCs is reinforced by ensemble measurements which have shown

that peptide-coated NCs show much larger photo-induced activation than QDot^{TM}s do.

Complications can arise from the following effects that influence the amplitude of the correlation function: (1) The signal-to-background ratio has to be sufficiently high. Small SBRs influence the correlation amplitude by a factor

$$N_{cor} = N_0 \frac{S^2}{(S+B)^2} = N_0 \frac{1}{(1+SBR^{-1})^2}. \tag{4.3}$$

This factor was measured to be negligible for the presented measurements. When it does become significant, it will always result in an apparent concentration that is higher than the real concentration. (2) Saturation of the fluorescence signal reduces the correlation amplitude by a factor of ~ 20 % for an excitation power equal to the saturation power, as will be shown by Monte-Carlo simulations (page 125). The presented measurements were taken with excitation powers of 10 μW, which should be lower or just equal to saturation intensities for NCs. Therefore saturation effects should not lead to variations larger than 20 %. (3) Additional effects, which have been attributed to optical trapping, have recently been reported for FCS measurements and will be further discussed on page 108. Even though the effect has not been thoroughly quantified, it can only cause an overestimation of the real concentration which is becoming more severe at higher excitation powers. The same applies to influences from saturation.

Taking all these effects into account, the measured concentrations (measurements performed at low excitation intensities: < 10 μW) should not deviate more than the statistical uncertainty for $g^2(0)$ (< 10 %) from the real concentration towards lower values and not more than 50 %, due to saturation and optical trapping, towards higher values.

Average Brightness per Particle

The average brightness per particle is a parameter that is much easier to extract than accurate concentrations. It can serve as a direct quality control for the NC batch, since brightness is of greatest concern in any labeling application. Under the assumption that the absorption per particle does not change significantly from surface defects and oxidation processes (in other words that it is comparable for fluorescent and non-fluorescent particles), the brightness is a direct measure of the fluorescence quantum yield of the particle (see the discussion on page 75).

The brightness per particle η can be extracted through a multiplication of the correlation amplitude $g^2(0)$ with the average count rate CR over the total acquisition time:

$$\eta = \frac{CR}{N} = CR \cdot g^2(0). \tag{4.4}$$

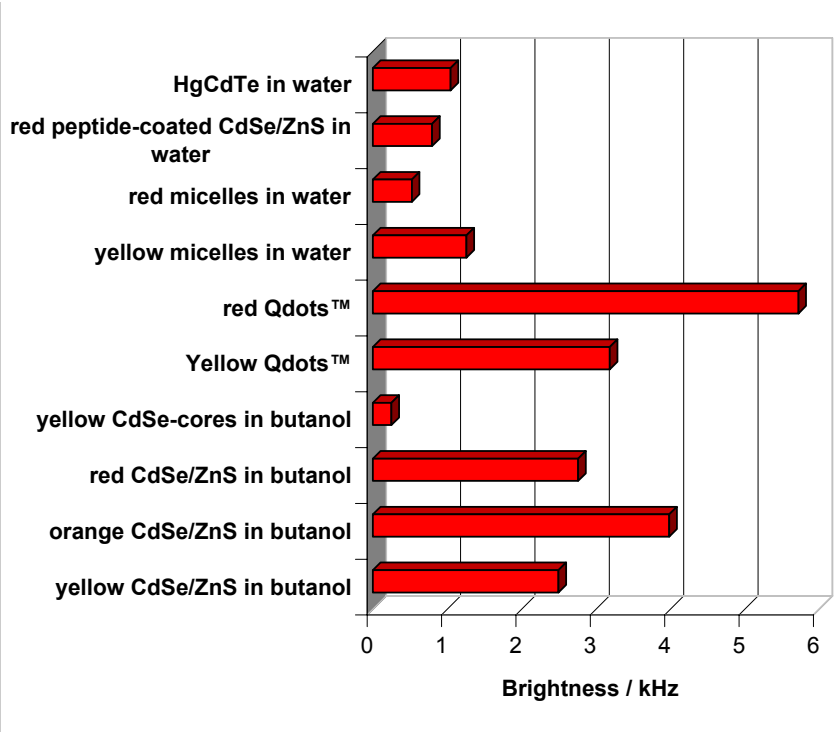

Figure 4.16: Brightness per particle is presented for various NCs. All measurements were taken with ~ 10 μW excitation power at 532 nm and normalized to 1 μW.

As long as the measurement is performed at such low excitation powers that saturation effects can be excluded, but high enough powers to still ensure negligible background contribution ($S^2/(S+B)^2 \approx 1$), all other influences, like the type of objective and the underfilling fraction β, only change the size of the observation volume, or in other words the total number of particles per observation volume at a given time. Multiplication of the average count rate with $g^2(0)$ therefore normalizes the count rate to the observed number of particles, and the exact size of the observation volume is irrelevant. Figure 4.16 gives a comparison between the various NCs investigated in this work. All measurements were taken at the same excitation power (1 μW) and excitation wavelength (532 nm) using a 1.4 NA oil-immersion

objective with an underfilled back aperture.

In this comparison the brightness values are not corrected for differences in the absorption coefficient. Most applications make use of a specific excitation wavelength, so that a direct comparison of used NC excited at this one wavelength is of interest. To interpret the data as a measure of the quantum yield, the increased excitation coefficient for larger (red-shifted) particles at a fixed excitation wavelength has to be taken into account.

A more severe complication can arise from aggregated particles. Small aggregates can easily increase the observed brightness per particle by a factor of 2–10, without necessarily being detected from time trace observations. Very large aggregates would show up as very few but extremely bright bursts, whereas smaller aggregates cannot be distinguished from single particles that diffuse right through the center of the excitation volume. This might explain the large η values for red and yellow QDot^{TM}, since recent surface-based measurements also showed, that no clear antibunching signature could be observed *[Campbell and Michalet, 2003]*.

Saturation Intensities

Having a measure of the average brightness per particle, it is straightforward to perform a series of measurements at different excitation powers and thereby observe fluorescence saturation that occurs in any fluorophore. One has to keep in mind that the correlation amplitude itself is influenced by the saturation of fluorescence emission at higher excitation powers due to the distortion of the observation volume. But as will be shown by Monte-Carlo-Simulations on page 125 this influence causes a 2-fold overestimation of the saturation intensity in the worst case. For that reason the average brightness per particle, as determined from FCS, allows estimation of the order of magnitude of the saturation intensity for various fluorophores. Figure 4.17 shows a comparison between Rhodamine 6G in water and CdSe/ZnS NCs in butanol. The measurements are fitted to a saturation function $\frac{I}{I+I_{Sat}}$ and yield a saturation intensity of 1 mW for R6G and 10 μW for core-shell NCs. This difference of one to two orders of magnitude in the saturation intensity for organic dyes and NCs is consistent with surface-based confocal microscopy measurements that were taken on the same kind of NCs *[Michalet, 2003]*. Also *Lounis et al. [2000]* report a saturation intensity $\sim$80 μW (peak irradiance: $\sim$ 40 kW/cm^2) for CdSe/ZnS measured via antibunching measurements.

A smaller saturation intensity poses limitations on the overall signal that can be collected from NC emission. Depending on the exact excitation wavelength and observation window, organic dyes might provide better SBR in spite of the much larger extinction cross sections of NCs.

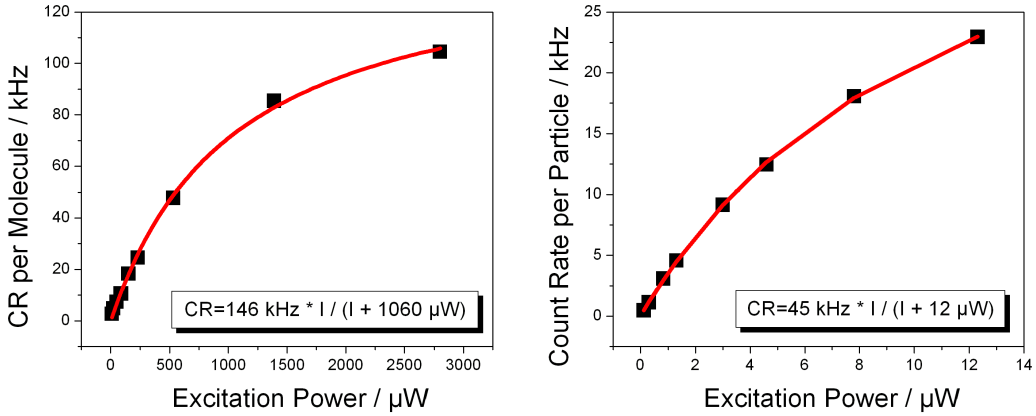

Figure 4.17: Saturation intensity estimated by FCS for Rhodamine 6G in water(left) and CdSe/ZnS in butanol (right). The excitation wavelength was 532 nm. The red line represents a fit resulting in the displayed parameters.

Photobleaching

As was discussed in the introductory parts, NCs are especially advantageous over organic dyes when long term observations are required. In the previous surface-based experiments data from single NCs was shown that had been recorded over 20 min and additional observations were made for more than one hour. Nevertheless, some NCs also show photobleaching. Here the term photobleaching describes any conversion of a fluorescent NC into one that remains dark over the course of the experiment. This condition can in principle be fulfilled by reversible processes, like blinking. But also irreversible oxidation processes of the surface have been reported and might cause real photo-destruction. The degree of photobleaching in NCs depends strongly on synthesis and chemical modifications and is therefore important to be monitored for each new NC batch especially when chemical protocols were changed.

Photobleaching can be seen in FCS measurements, whenever the bleaching rate is high enough to turn off a considerable fraction of NCs during their passage through the confocal spot. Since the diffusion time is on the order of a few milliseconds, this should only be the case if excited at high laser powers. Severe photobleaching was observed for a sample of pure CdTe cores in water. Since it is an intensity dependent process, a series of FCS measurements at various excitation powers was performed (Figure 4.18). Increasing the excitation power first results in an almost parallel shift of the entire correlation curve towards shorter times. At even high powers a shoulder appears that leads to distortion and a very different shape. CdTe NCs were observed under cw excitation at 532 nm with excitation powers ranging from 10 μW to 1 mW.

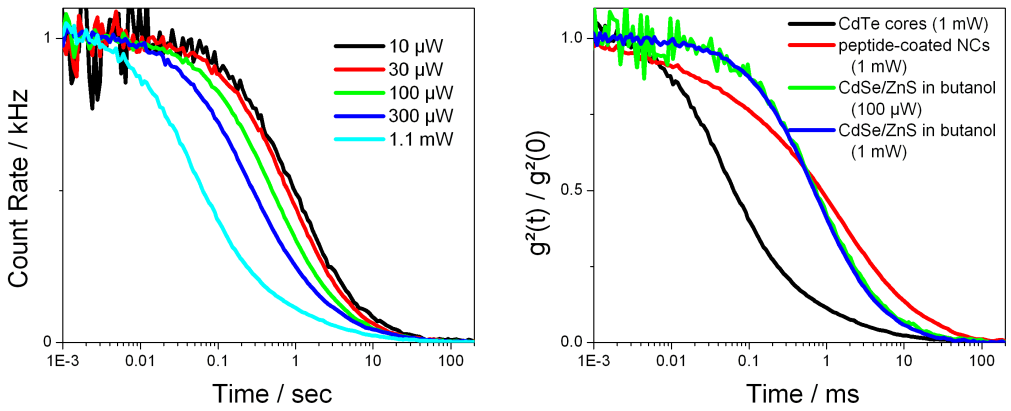

Figure 4.18: Correlation curves recorded at excitation powers between 10 μW and 1 mW (532 nm). (left) CdTe cores dissolved in water showed reduced diffusion times and changes in the $g^2(t)$ shape, which are attributed to photobleaching. (right) CdSe/ZnS core-shell in butanol, peptide-coated CdSe/ZnS and CdTe in water are compared at 1 mW excitation power (CdSe/ZnS also at 100 μW). Whereas no effect is seen for core-shell particles, strong photobleaching is observed for CdTe. The flattening of the curve for peptide-coated NCs is qualitatively different from the effect of photobleaching and can be attributed to fluorescence blinking (discussed in more detail on page 127).

For comparison Figure 4.18 shows three representative NC samples: core-shell NCs in butanol, peptide-coated NCs and CdTe cores in water. All were excited at

1 mW excitation power. In addition, the core-shell particles were excited at 100 μW to prove that no changes were observed at higher powers. All NCs exhibit a different diffusion time and the curves are therefore shifted with respect to each other. The different shapes on the other hand reflect various influences due to blinking and photobleaching. Whereas CdSe/ZnS NCs do not show any alteration in their correlation behavior at high powers, CdTe clearly displays the appearance of a shoulder that can be fitted with an exponential decay. Peptide-coated NCs do also show slight variations in the shape, but not nearly as pronounced. In addition, the variation results more in an increased slope at shorter timescales and a flattening of the overall correlation curve. That the distortions for CdTe and peptide-coated NCs can be attributed to photobleaching and blinking, respectively, will be shown by Monte-Carlo simulations.

Particle Sizes

FCS allows gathering more information about diffusing objects besides photophysical parameters. In the case that single diffusing objects do not exhibit any processes causing additional fluctuations, such as blinking, a simple diffusion model can be used to fit experimental data and extract the diffusion constant from the estimated diffusion time $\tau_D = \frac{\omega_{xy}^2}{4D}$ (assuming a Gaussian observation volume). Following the Stokes-Einstein equation for spherical particles *[Einstein, 1905]*

$$D = \frac{k_B T}{6\pi\eta R} \tag{4.5}$$

one can see that the diffusion time τ_D is directly proportional to the particle radius. For an absolute size measurement a calibration is needed, similar to when absolute concentrations are estimated. Either the size of the observation volume has to be measured directly, or a well characterized sample is required as a calibration standard.

In Figure 4.19 correlation curves for various NCs are compared to the correlation curve of 26 nm large polystyrene beads (diameters are determined by the vendor using TEM). Using a 2D diffusion model (Equation 2.29) to extract diffusion times and comparing these to the diffusion time of 26 nm beads, NC sizes were approximated as listed in the following table:

Particle	Diameter	Diffusion Const.
HgCdTe	5 nm	5.2 E(-8) cm^2/s
red peptide-coated NC	8 nm	3.3 E(-8) cm^2/s
yellow micelle	17 nm	1.5 E(-8) cm^2/s
red micelle	24 nm	1.1 E(-8) cm^2/s
yellow QDot^{TM}	25 nm	1.0 E(-8) cm^2/s
polystyrene beads	26 nm	9.3 E(-8) cm^2/s

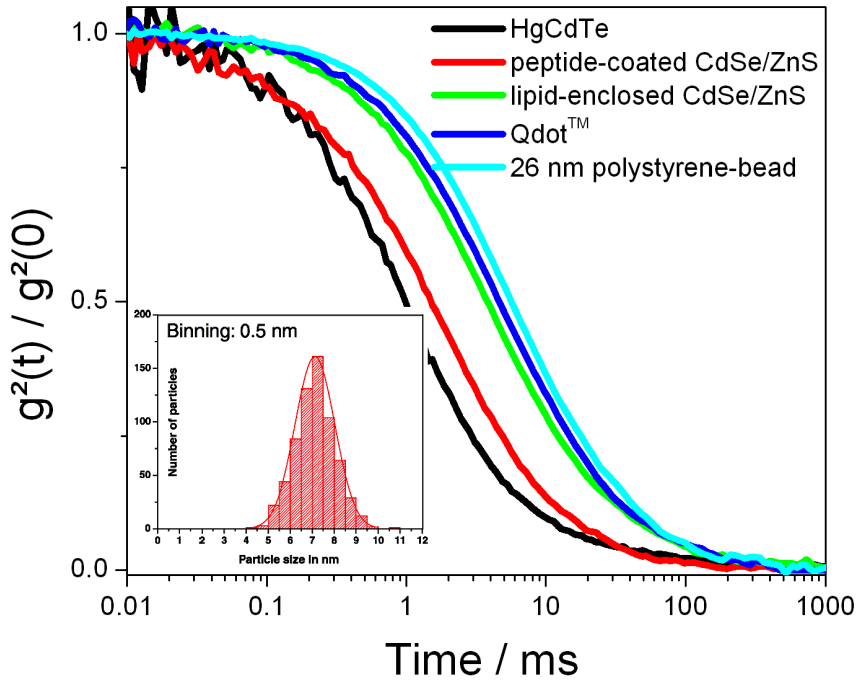

Figure 4.19: (left) Correlation curves for various NCs and 26 nm polystyrene beads. The estimated diffusion time as extracted from 2D fits id directly proportional to the particle diameter. Sizes relative to specified 26 nm for beads and corresponding diffusion constants are displayed in the previous table. (inlet) Size histogram from TEM measurements on the same peptide-coated CdSe/ZnS NCs as used in FCS measurements (courtesy of Fabien Pinaud).

Repeated measurements yield relative errors of 10 % or better. A size histogram

for peptide-coated NCs, that was acquired by transmission electron microscopy, gives good evidence for the validity of this approach. The average size of ~ 7 nm agrees well with FCS measurements and proves that the Stokes-Einstein relation is valid down to the smallest particles investigated in these experiments.

Estimated particle sizes can also be used as evidence for aggregation whenever measured values exceed the expected values. Once a NC batch has been characterized, influences of e.g. various buffers can be monitored or it can be checked if the samples stay in a monodisperse state over long times (months).

Blinking

On page 79 it was shown that NCs exhibit intermittency in their fluorescence emission. This phenomenon, called blinking, has been found in almost every single quantum emitter and is by now considered to be characteristic for single object fluorescence. Depending on the exact mechanism which causes the intermittency, the probability distributions for on/off-interval durations follow various statistics. In the case of semiconductor NCs a power-law distribution has been observed for on as well as off-times.

As was described in detail on page 35 power-law statistics do not show any characteristic timescale. In fact the average on/off-time depends on the observation time of the experiment and increases with longer observation times. For FCS measurements this means that the blinking always overlaps with the characteristic diffusion time and thus the two processes can never be separated. Therefore a second-order correlation function describing blinking, as was derived by *Verberg et al. [2002]; Verberg and Orrit [2003]*, cannot be extended into an analytical expression including diffusion.

But blinking takes place and can be observed in FCS data when the excitation power becomes high enough. Figure 4.20 shows the influence of fluorescence intermittency depending on the excitation power for polymer-coated Qdots^{TM} (A) and peptide-coated CdSe/ZnS (B) in water. The data is normalized by $g^2(\tau = 1\,\mu\text{s})$ and clearly displays a faster decay with increasing power without pointing to a characteristic timescale. Surprisingly the data can be accurately described with a simple diffusion model (Equation 2.27) for excitation powers well below the saturation power. This has also been reported for two-photon FCS on the same kind of NCs *Larson et al. [2003]*. The fact that excitation powers below $\sim 10\ \mu$W do not lead to the obser-

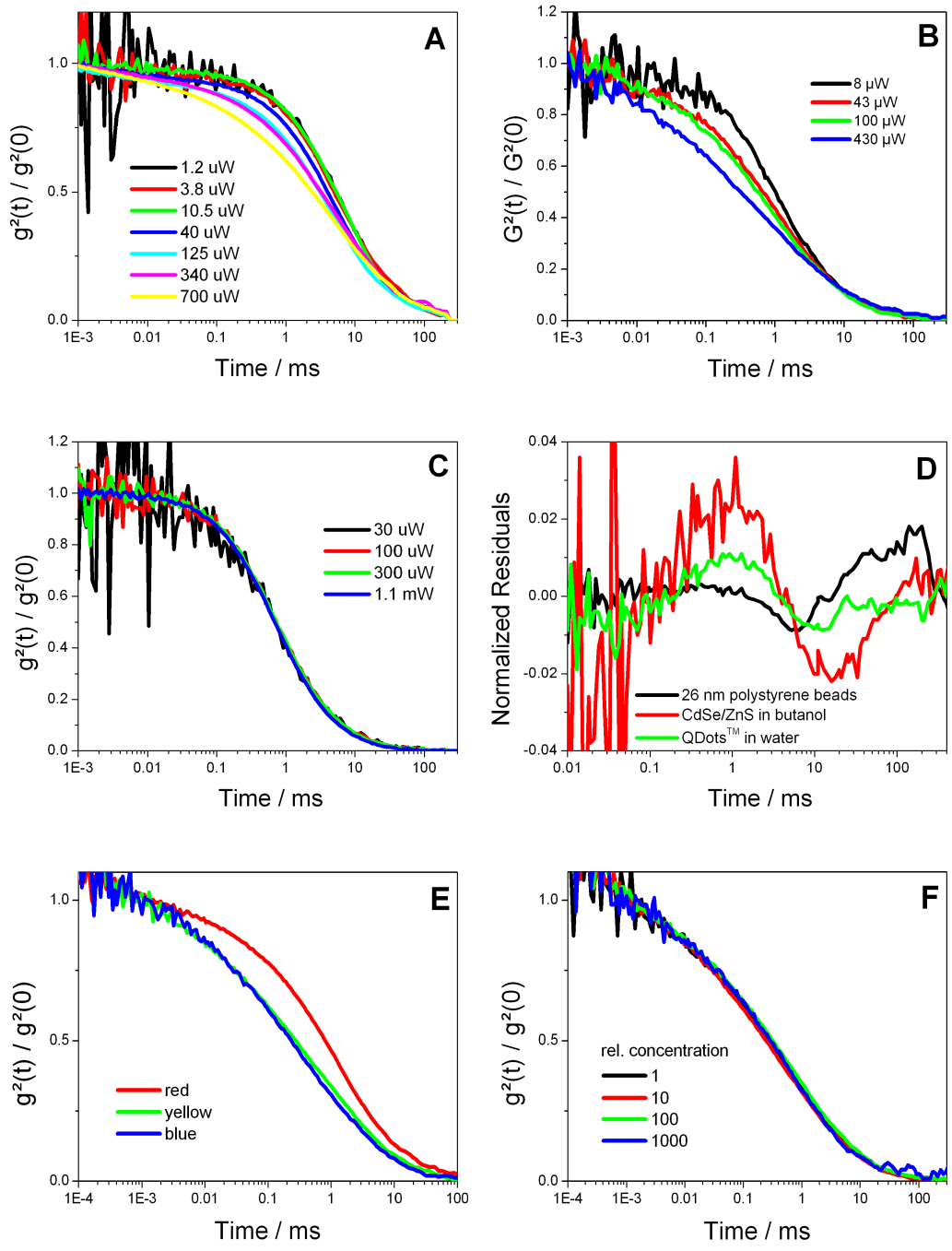

Figure 4.20: (A) Polymer-coated CdSe/ZnS Qdot^{TM} in water and (B) peptide-coated CdSe/ZnS in water exhibit photo-induced blinking behavior. (C) Red CdSe/ZnS core-shell particles without further modifications in butanol, do not display any photo-induced blinking effect. (D) Residuals of 2D fits to FCS data recorded from 26 nm polystyrene beads, polymer-coated QDots^{TM} in water and CdSe/ZnS NCs in butanol (excitation at 532 nm with 5 /muW). (E) CdSe/ZnS NCs of three different sizes (excited at 488 nm with 200 μW). FCS data shows an influence from blinking for yellow and blue particles but not for red particle. (F) Variations of the relative concentration does not change the blinking effect under constant excitation (488 nm with 200 μW, yellow CdSe/ZnS NCs).

vation of blinking appears like another discrepancy in comparison to surface-based confocal microscopy measurements (Figure 4.20). However simulations will show that blinking might for certain parameters occur without having a significant effect on FCS data. For some NCs contributions from blinking cannot be detected even at higher excitation powers. In Figure 4.20 (C) data are presented that were recorded on red CdSe/ZnS NCs in butanol between 10 μW and 1.1 mW. Even at very high powers no blinking effect was observed. Figure 4.20 (D) presents the residuals from a 2D fit to the experimental data from (C) and for comparison to data recorded on polystyrene beads. The residuals clearly underline the non-significant influence of blinking. Figure 4.20 (E) and (F) give comparative measurements for CdSe/ZnS NCs in butanol with different sizes or at various concentrations. It can be seen that for these particular CdSe/ZnS batches, smaller NCs display a larger blinking effect. But since the size dependence study did not show any specific relation between size and blinking effect, it is likely that the quality of either cores or shells, which can differ from batch to batch, are the main cause for such variations. Concentration changes on the other hand do not show any influence, as was expected.

4.3.3 Effects on the Correlation Amplitude

The correlation amplitude in principle is a measure for the concentration of fluorescent particles. Measurements at various excitation powers should not influence $g^2(0)$ as long as background contributions do not become significant and the excitation intensity is below the saturation intensity I_{Sat} for the investigated particle.

However, when looking at a series of FCS measurements on NCs at different excitation powers, a significant decrease of $g^2(\tau = 0)$ was observed. Measured for various NCs the effect is significant even at excitation intensities below the saturation intensity. The data in Figure 4.21 illustrates the behavior for CdSe/ZnS NCs in butanol, investigated with either a 1.4 NA (100x) oil-immersion objective (PlanApochromat, Zeiss) or a 1.2 NA (63x) water-immersion (C-Apochromat, Zeiss) objective. All experiments were performed with 532 nm (cw) excitation on samples with nM concentrations (1000 x diluted from the stock solution). In addition to raw data, the occupancy N, which equals the inverse of the correlation amplitude ($N = 1/g^2(0)$), is shown as a function of excitation intensity (measured before the objective's back aperture).

To decipher the effects that cause intensity dependent variations of the correlation

amplitude, control measurements were performed using doubly-labeled DNA strands (32 base pair double-stranded DNA labeled with Cy3B). As shown in Figure 4.21 an increase of N on the order of 25 % was observed for an intensity change up to 2 times the measured saturation intensity (using a 1.4 NA oil-immersion objective).

It is known that, as saturation effects cause a distortion of the observation profile, the measured occupancy will change for increasing excitation powers *[Widengren et al., 1995]*. To quantitatively evaluate the effect of saturation on $g^2(0)$, Monte-Carlo simulations were performed, in which a fluorophore is excited at excitation intensities ranging from 0.1 to 20 times I_{Sat} (Figure 4.27 on page 126). Occupancy is extracted from simulated FCS data, in which diffusion and excitation-emission cycles contribute to fluctuations. Saturation in this case is due to the finite fluorescence lifetime. A comparison to saturation for an immobilized emitter (no diffusion through an excitation profile) showed that an estimation of I_{Sat} via the brightness per particle (from a FCS measurement) is off by a factor of 2 as compared to saturation intensity determined from the signal of the immobilized emitter. This is caused by the distortion of the excitation profile, which influences the estimated number of particles N and thus changes the brightness per particle in the FCS measurement. Nevertheless, an estimation of I_{Sat} within a factor of 2 can still be used to correct for saturation effects on $g^2(0)$.

From simulations the effect of saturation on $g^2(0)$ for $I_{Sat}^{Cy3B-DNA} = 280\ \mu$W (determined from the experimental FCS data) is calculated to be on the same order ($\pm 10\%$) as the experimentally observed variations. The squares in Figure 4.21 (top, right) show experimentally observed N. The circles show N values corrected for the influence of saturation. The effect of saturation was estimated by simulations to increase the occupancy by a factor of $1 + 1.7(I/(I + 7.3I_{Sat}))$ (I: excitation power). This factor was applied to the first measured value (much below saturation intensity) and subtracted from measured N at higher intensities. The graph shows that simulations seem to overestimate saturation effects (N decreases). This might be due to non-Gaussian observation volumes and poses the largest uncertainty. However the error is not larger than 10 % up to excitation powers of 2 times I_{Sat}.

To evaluate the effect of saturation on $g^2(0)$ when measured for NCs (raw data: squares), the same steps were performed. The saturation intensity was estimated via the brightness per particle, the extracted saturation intensity was divided by 2 and the corrected occupancy values (corrected data: circles) were determined by subtracting the occupancy increase that is expected from saturation. Contrary to

what was observed for Cy3B-labeled DNA, NCs showed an increase in N by 300 % and 100 % (oil- and water-immersion objective, respectively) after correction for saturation effects. One difference between the water- and oil-immersion objective is the size of the focal spot. As was already seen in an objective comparison (page 91), the oil-immersion objective forms a tighter focus, which is reflected in an occupancy twice as large. This is confirmed by an estimation of I_{Sat} of half the size. A reliable estimation of the peak irradiance cannot be given due to the very different excitation profiles, as was also shown by FCS fits (Figure 4.14).

The origin of this significant change in occupancy with excitation power is open for debate. An influence of photo-induced activation is unlikely since no correlation between the degree of photo-induced activation, as measured in ensemble emission scans, and amplitude changes in FCS could be found. In addition, large amplitude changes were also detected with polystyrene beads and conjugated polymers, for which no photo-induced activation effect is observed.

One further possible influence has been suggested by *Chiu and Zare [1996]; Osborne et al. [1998]; Chirico et al. [2002]*. They claim that an interaction between the colloidal particles and the excitation light field can lead to optical trapping effects. Dipole moments can be induced in a dielectric material by the oscillating electromagnetic field. These induced dipoles then interact with E, giving rise to scattering and gradient forces, which have been extensively explored in optical traps. So-called optical tweezers have been used to optically trap cells, organelles inside cells and small beads *[Svoboda and Block, 1994]*. The same principles have been utilized in the development of atom traps *[Chu et al., 1986]*.

The important physical parameter is the material's polarizability α, which is defined as the proportionality factor between the dipole moment that an electric field can induce (higher orders like hyperpolarizability β will not play a role in this work):

$$\vec{\mu} = \alpha \vec{E}. \tag{4.6}$$

The SI unit for polarizability is $[\alpha] = (\mathrm{Cm})^2/\mathrm{J}$. A modification is often used to express α in terms of a polarizability volume, $\alpha' = \frac{\alpha}{4\pi\epsilon_0}$, which in general is similar in magnitude to molecular volumes and has the unit $[\alpha'] = m^3$. Since polarizability depends strongly on the frequency of the driving electric field, there are different regimes. As these experiments deal with optical frequencies, the regime of interest is that of electronic polarizability, meaning that induced dipole moments are due to

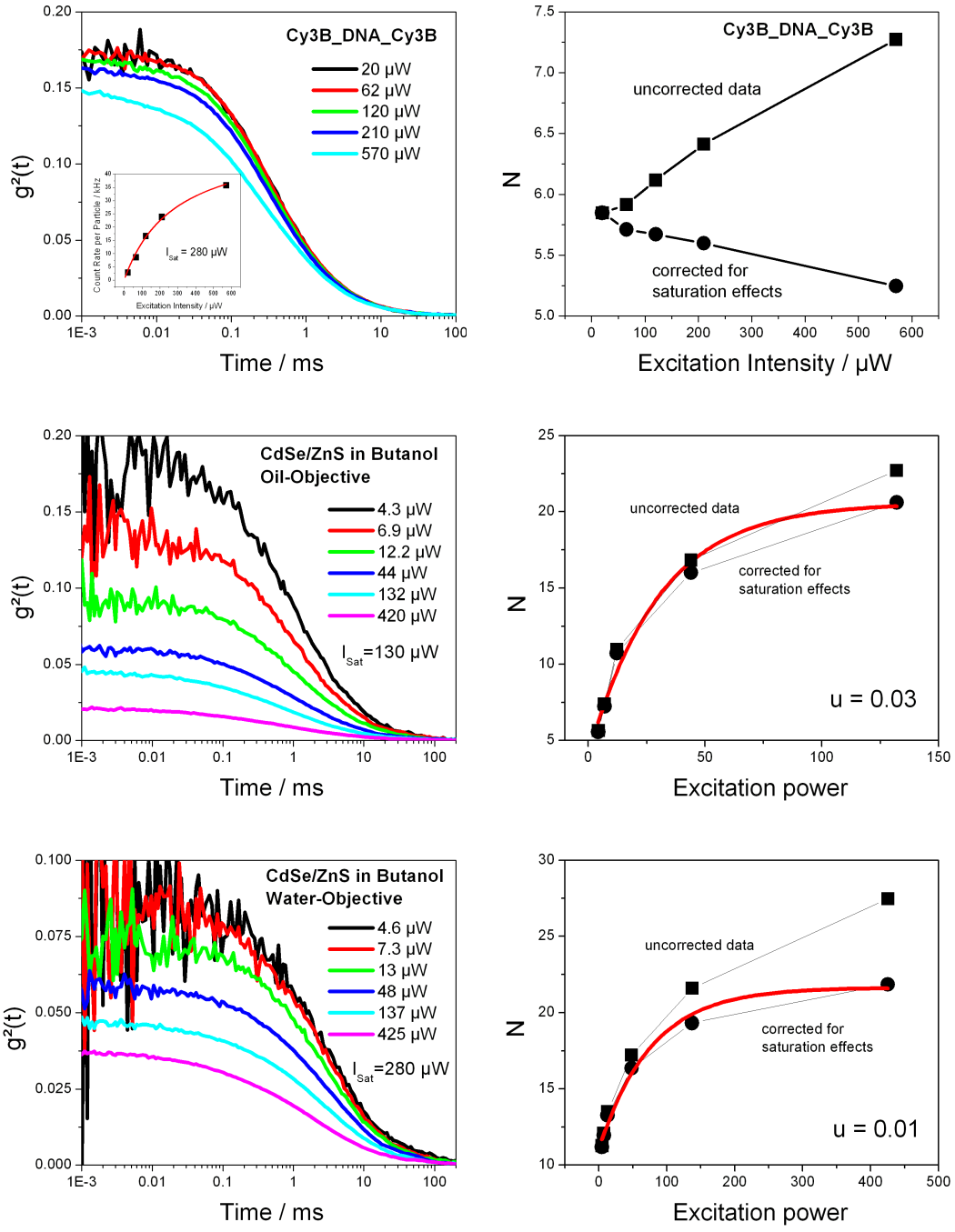

Figure 4.21: Intensity dependent correlation curves for Cy3B-labeled DNA (top) and CdSe/ZnS in butanol measured with both oil- (middle) and water-objective (bottom). Raw data is shown together with the estimated saturation intensity. The inlet in the top figure shows measured count rates per particle that were used to estimate I_{Sat}. This data is not shown for the other two measurements. (right) Occupancy values increase with higher excitation powers. Squares represent measured data; circles represent the data corrected for saturation influences. u is the fitting parameter from which polarizability can be extracted.

relocalization of free electrons.

For colloidal solutions a connection between polarizability and the index of refraction (n for the medium, m for the particle) is given by the Clausius-Mossotti relation, as long as the frequency is high enough that the particle (of radius r) cannot reorient:

$$\alpha = n(\frac{m^2-1}{m^2+2})r^3. \tag{4.7}$$

With these definitions in mind, expressions for two forces acting on small colloidal particles (so-called Rayleigh particles with $2r << \lambda$) can be derived *[Ashkin et al., 1986]*. The scattering and gradient force that acts on small colloids in a light field with a power density $I(\vec{r})$ (in $\frac{\mathrm{W}}{\mathrm{cm}^2}$) is ($c$: light velocity, I_0: maximum power density):

$$F_{scat} = \frac{I_0}{c}\frac{128\pi^5 r^6}{3\lambda^4}\frac{m^2-1}{m^2+2}n, \tag{4.8}$$

$$F_{grad} = -\frac{n}{2}\alpha\nabla E^2 = -\frac{n^3 r^3}{2}\frac{m^2-1}{m^2+2}\nabla E^2 \tag{4.9}$$

or with $I = \frac{1}{2}\int(\epsilon_0\vec{E}^2 + \frac{1}{\mu_0}\vec{B}^2)dV$:

$$F_{scat} = \frac{8\pi^3 n}{3\epsilon_0 c\lambda^4}\alpha^2 I_0, \tag{4.10}$$

$$F_{grad} = \frac{n^2}{2c\epsilon_r\epsilon_0}\alpha\nabla I(\vec{r}). \tag{4.11}$$

For NCs with sizes below 10 nm, scattering forces can be neglected, compared to gradient forces since $F_{scat} \sim r^6 \sim \alpha^2$ whereas $F_{grad} \sim r^3 \sim \alpha$. From the gradient force a trapping potential $U(\vec{r})$ can be derived, since $\nabla U(\vec{r}) = \vec{F}(\vec{r})$:

$$U(\vec{r}) = -\frac{n^2}{2c\epsilon_r\epsilon_0}\alpha I(\vec{r}). \tag{4.12}$$

Assuming that the probability to find a particle at position $\vec{r}$ in any potential is given by:

$$Prob(\vec{r}) = \frac{1}{A}\exp(-\frac{U(\vec{r})}{kT}), \tag{4.13}$$

and assuming that the number of detected particles is proportional to this probability, the apparent concentration of particles detected in a FCS measurement (depending on the excitation power P in W) can be derived as *[Chirico et al., 2002]*:

$$N_{obs} = N_0 + A(1 - \exp(-\frac{uP}{kT})), \tag{4.14}$$

where kT is the thermal energy, $P = I_0 \frac{\pi\omega_0^2}{2}$ in a Gaussian excitation volume $I(\vec{r}) = I_0 \exp(-\frac{2r^2}{\omega_{xy}^2} - \frac{2z^2}{\omega_z^2})$ and

$$u = \frac{n^2\alpha}{2\epsilon_0\epsilon_r c(\pi\omega_{xy}^2/2)} \cdot 6.25 \cdot 10^{18} = c \cdot \alpha. \tag{4.15}$$

Fitting the observed number of particles to Equation 4.14 a numerical value for u/kT and thus the polarizability of the particle can be estimated.

For the presented examples polarizabilities for CdSe/ZnS NCs of $6 \cdot 10^{(-24)}$ m^3 (using the oil-objective) and $2 \cdot 10^{(-24)}$ m^3 (using the water-objective) were calculated. In an additional measurement a polarizability for polymer-coated QDot^{TM} of $1 \cdot 10^{(-22)}$ m^3 was calculated. In all calculations the following numerical values were used: $n^{butanol} = 1.4$, $\epsilon_r^{butanol} = 17.8$, $\epsilon_0 = 8.85 \cdot 10^{-12}$ Fm^{-1}, $c = 3 \cdot 10^8$m/s and $\omega^{xy} = 260$ nm.

These values present nothing more but a crude estimation since large uncertainties are involved from the estimation of saturation intensities, experimental errors on the correlation amplitude and the fitting procedure performed on rather few data points. Nevertheless it provides an estimation to argue if an effect of optical trapping can contribute to the intensity dependence of the correlation amplitude. An observation that substantiates the influence of optical trapping is the 20–50 times larger polarizability of QDot^{TM} NCs. This observation follows the theoretically expected polarizability dependence on the particle volume (QDot^{TM} are estimated to be 2–5 times larger in diameter, thus 8–125 times larger in volume).

4.3.4 Photo-induced Activation in Solution

Now that the basic parameters that can be observed by FCS are well defined and validated for the case of semiconductor NCs, the technique can be used to address the problem of photo-induced activation. So far the question remains if the observed increase in fluorescent signal in a solution of NCs during illumination is due to a gradual increase in quantum yield or a change of the number of fluorescent particles.

A FCS measurement was performed on a solution of NCs. Afterwards the sample was illuminated through the objective with light from a Xe-lamp (400–450 nm) for

10 min. Illumination through the objective allowed a strong slightly uneven illumination throughout the field of view without changing the alignment of the laser illumination. The illuminated field is about 200 μm in diameter with the FCS observation volume in its center. As diffusion takes place, particles from non-illuminated areas of the much larger sample (the chamber has an approximated diameter of 5 mm and a hight of 0.5 mm) will be exchanged with those that have been exposed to UV light after the illumination is stopped. Therefore no long-term observations can be performed on illuminated molecules. Nevertheless a direct comparison of a FCS measurement before and after illumination can unravel changes in relative concentration of fluorescent particles simultaneously with changes in the brightness per particle. In Figure 4.22 a plot of these two parameters is shown as they change with time. The surprising result is that both the apparent concentration as well as the average brightness per particle change significantly during the illumination process. After the illumination is stopped a consecutive series of FCS measurements for around 10 min shows the relaxation to the initial parameters, due to diffusion of particles from outside the illumination area into the observation volume. This process is actually comparable to fluorescence recovery after photobleaching (FRAP) experiments and the time scale of this relaxation process can be estimated from the diffusion constant for NCs (on the order of $5 \times 10^{(-8)}$ cm^2/s) to be on the order of several minutes.

These results present a somewhat different situation compared to the observation of single NCs on a surface exposed to room atmosphere. Similar to what was guessed for consecutive confocal scans, a concentration change is accompanied by a change in brightness. The experiment points out the importance of characterization in the environment of interest — aqueous solution in the case of colloidal NCs that are used as biological probes — since a number of effects can have an influence. In this case it has to be kept in mind that the overall concentration is very different, and also the observed average brightness, compared to surface measurements. Brightness differences might be explained by different on/off time distributions. But also influences of the local environment might play a role.

4.3.5 Time-gated FCS

One of the advantageous optical properties of semiconductor nanocrystals is that the fluorescence lifetime is significantly longer than the lifetime of organic dyes

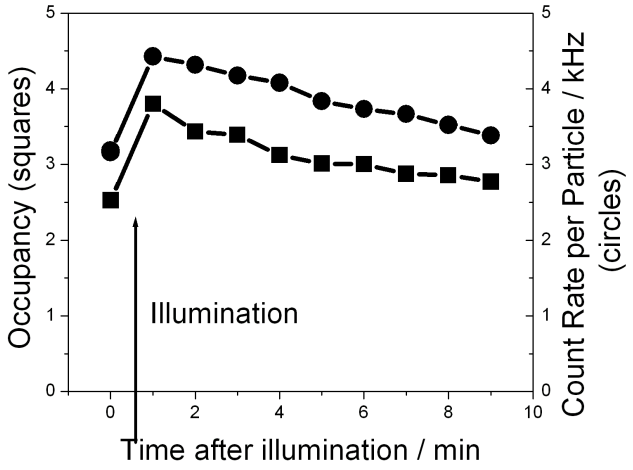

Figure 4.22: Brightness per particle (circles) and concentration of fluorescent particles (squares) as extracted from FCS measurements (excitation at 532 nm with 11 μW) before and after illumination of the confocal volume by a Xe-lamp (400–450 nm) for 10 min (arrow).

(usually 1–3 ns). As was presented on page 82 a single NC displays a lifetime that is not necessarily single-exponential at room temperature but at least has a major component that exhibits lifetimes on the order of 20 ns. As was discussed for the lifetime measurement of single NCs (page 86) this long lifetime component can be used in a time-gated detection scheme, where photons, which are emitted immediately after the excitation laser pulse, are discarded, and only those that are detected at later times are kept as signal. Since any radiation contributing to background originates either from instantaneously scattered light (Rayleigh- or Raman-scattering) or from fluorescence that is emitted by organic impurities with a lifetime on the order of a few nanoseconds, such time-gating reduces the background. Even though the signal is also reduced to a smaller amount, the SBR, and thus the SNR is significantly increased.

Here a FCS measurement is demonstrated that uses time-gating to reduce fluorescence originating from Rhodamine 6G (lifetime: 4 ns) and at the same time increase the relative signal contribution from NCs (long lifetime component: 16 ns). A mixture of R6G and polymer-coated Qdot^{TM} in addition to single component solutions with identical concentrations (nM) were prepared in water. Fluorescence

was collected on two channels of a confocal setup as described before. Excitation was provided by a pulsed Nd:YAG laser emitting at 532 nm. Single photon arrival times and the time delay to the previous laser pulse were recorded for each photon using a Becker & Hickl computer card. After the acquisition, photons with a time delay shorter than a given threshold were discarded and a software correlation algorithm was used to performed cross-correlation analysis on the remaining ones.

In a control experiment, the effect of pulsed excitation on the FCS data was investigated. Since ps-excitation pulses were provided at a rate of 68 MHz, no influence is expected at the timescales of interest to this experiment ($> \mu$s). The data presented in Figure 4.23 confirms this expectation. Slight differences in the occcupancy and measured brightness per particle can be attributed to small differences in the laser profile, but are of no concern to this experiment.

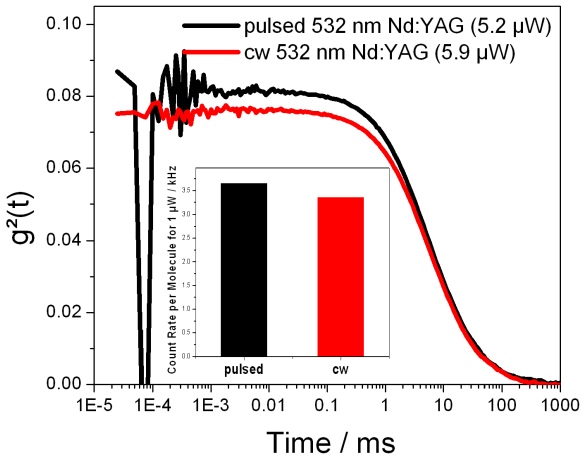

Figure 4.23: FCS data for 26 nm polystyrene beads using either pulsed or cw laser excitation at a wavelength of 532 nm and ~ 5 μW excitation power.

Figure 4.24 shows a histogram of the time delays between the photon arrival times and the corresponding laser excitation for a solution containing only R6G, only NCs or a mixture of R6G and NCs at the same concentrations. The data is consistent with expected lifetime values and illustrates the contribution from R6G and NCs to the lifetime that is measured for the mixture.

Correlation data on the corresponding samples taken with different time gating, illustrate the improvement of the SBR, when the NC fluorescence is considered signal

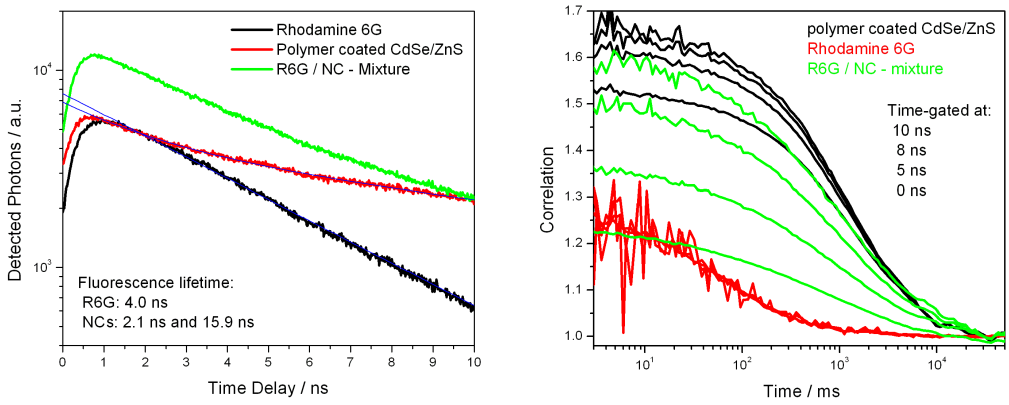

Figure 4.24: Correlation data recorded for various time gates (0–10 ns) for QDots^{TM} NCs alone (black), rhodamine 6G alone (red) and a mixture of both species with identical concentrations to the single-species solutions (green). As the time-gate is increased, $g^2(0)$ increases also, reaching almost the QDot-only concentration. Time-gating on single-species solutions changes only SNR but has no effect on $g^2(0)$.

and R6G background. As more photons are collected in a later time window, the contribution from R6G-background decreases for the mixed sample. At a time gating of 10 ns the concentration of NC particles almost equals the true concentration, as determined from a pure NC sample.

This first demonstration of a time-gated detection scheme in a solution-based measurement using NCs as the fluorescent probes of interest gives an idea of the advantages when used in systems where large background contributions from natural impurities are present. More work needs to be done to optimize the gating conditions, depending on the relative background concentration and its lifetime. As time gating is performed with longer time thesholds, the contribution from fast emitting impurities or scattered light is decreased, as shown. But at the same time the overall signal is also reduced, influencing the SNR of the FCS measurement. The optimal time gating should be determined depending on lifetime and relative concentration of all components.

4.3.6 Discussion

Characterization by FCS FCS has proven to be a valuable tool in the characterization process of colloidal semiconductor NCs after synthesis and chemical modification. The method provides feedback in a fast, accurate, reliable and easily implemented fashion. Extremely small sample volumes as well as preparation and acquisition times are required. The simultaneous accessibility of concentration, brightness and size in the solution environment makes FCS superior to many other techniques. By estimating the brightness normalized to the number of particles which actually contribute to the fluorescence signal, QY variations can be detected for modified samples (given that the absorption coefficient is comparable) independently from the ratio of dark particles. This is especially important to single-particle applications, as was discussed in the previous chapter. Saturation intensities can be estimated or compared between different NCs and dyes, thus providing evidence that NC fluorescence saturates at least an order of magnitude below most organic dyes. In addition, NC samples can be monitored for the undesired presence of aggregation, photobleaching and blinking.

Blinking and Photobleaching The fact that blinking does indeed effect the correlation data is not surprising. Also the fact that blinking was observed to be dependent on excitation power for immobilized NCs, and thus must be attributed to a photo-induced mechanism, is reflected in the correlation data. But also NC samples, that show blinking on surface-based measurements, but give no evidence of blinking in FCS data, were investigated. Up to this point additional information could not be extracted to unravel the mechanism for blinking because no model function is available to fit the data. *Verberg et al. [2002]* and *Verberg and Orrit [2003]* have recently derived a correlation function for power law blinking in immobilized particles. A similar analytical model for FCS could not be derived due to the lack of characteristic timescales in the blinking statistics. Separation of fluctuations caused by blinking or diffusion is impossible so that diffusion and rate equations cannot be solved analytically. To extract statistical parameters and make a quantitative comparison with surface-based measurements, a model was derived using Monte-Carlo simulations, which will be presented in the following chapter.

The same simulations will also provide a tool to distinguish blinking from photobleaching. One can already guess a fundamentally different influence on the shape

of the correlation function by looking at experimental data. This will be confirmed by simulations in the following chapter.

The Influence of Optical Trapping Correlation amplitudes were observed to decrease with increasing excitation power. A possible explanation could be the influence of an optical trapping effect, for which some evidence was collected:

(1) Observations have recently been reported for FCS measurements on R6G and polystyrene beads *[Osborne et al., 1998; Chirico et al., 2002]* that claim to detect optical trapping effects. In these experiments polarizability values have been measured for R6G that are several orders of magnitude larger than what would be expected for dielectric particles with a size on the order of nm. This is explained by a large difference in polarizability values under resonant and non-resonant conditions. From electromagnetic theory it is known, that polarizabilities at wavelength that are in resonance with allowed electronic transitions, can be orders of magnitude larger than at non-resonant wavelength *Agayan et al. [2002]*.

Polarizability values that were extracted for NCs show a similar behavior. They are one to two orders of magnitude larger than what has been measured from Stark effects for single CdSe ($2.38 \times 10^{(-25)}\mathrm{m}^3$, *Empedocles and Bawendi [1997]*) and CdSe/ZnS NCs ($7 \times 10^{(-26)}\mathrm{m}^3$ *Seufert et al. [2001]*).

(2) As mentioned before, a size dependence was observed that is in agreement with theory saying that polarizabilities are proportional to molecular volumes.

(3) A recent work using two-photon FCS on polymer-coated NCs does not report any occupancy changes larger than what can be explained by saturation *[Larson et al., 2003]*. This provides more evidence for a wavelength-dependent polarizability (in two-photon excitation near IR wavelength are used).

On the other hand these values present only a crude estimation due to a number of uncertainties that still need to be thoroughly quantified. Namely saturation effects have to be quantified for exactly measured saturation intensity values — so far the accuracy is for sure not better than a factor of two, as determined from simulations. In addition, saturation under non-Gaussian observation volumes might be significantly different. Since all corrections are derived from simulations using perfectly Gaussian excitation profiles, the effect has not been quantified for other profiles. And finally any influences attributed to NC photophysics, e.g. the influence of power law blinking, have to be ruled out.

Comparison between Surface- and Solution-Based Measurements A number of surface-based measurements like confocal scanning microscopy or wide-field techniques using lamp and TIR-excitation schemes were used to investigate fluorophores with single-particle sensitivity. These techniques have the inherent advantage that observations over long time scales are possible. Neither spectral shifts *van Sark et al. [2001]* nor spectral jumps *[Empedocles et al., 1996]* could have been observed otherwise. On the other hand the unavoidable influence of the surface itself or the surrounding atmosphere cannot be excluded. Interactions with a glass surface have not been thoroughly characterized for NCs, though influences have been reported for fluorescent dyes *[Ruckstuhl et al., 2000; Hellen and Axelrod, 1987]*. Since NCs are usually exposed to an atmosphere or embedded in a polymer matrix, the situation is in many respects not directly comparable to that in solution. The contrary results about photo-induced activation, resulting in variations of fluorescent particle concentrations (increase of apparent concentrations for both surface- and solution-based measurements), accompanied by gradual QY changes (only when measured in solution), point out the importance of this environmental influence.

Time-gated FCS Performing FCS in a time-gated way decreases background fluorescence and scattering from the most common impurities in biological environments. Real concentrations of NCs could be recovered even under equally high concentrations of R6G impurities. This method is especially valuable for in vivo applications, where autofluorescence due to naturally fluorescent proteins with lifetimes of 1–3 ns is always present. A similar situation is given in fixed cells as was discussed above. Due to a lifetime around 20 ns, NC-probes are superior over organic dyes in time-gated FCS (even though under certain conditions time-gating on ns probes has also been shown to be valuable *[Lamb et al., 2000]*). Once the requirements of pulsed laser excitation and TCSPC electronics are met, software correlation can be performed on photon subsets without further complications.

4.4 Blinking Nanocrystals and FCS Addressed by Monte-Carlo Simulations

To further address the influence of blinking on FCS measurements, a model was developed that is based on Monte-Carlo simulations of the diffusion and photophys-

ical events of single NCs. Using a simulation scheme as outlined on page 65 and implemented in LabView code, it was shown that simulated data does correspond to measured correlation curves. A number of features not related to blinking, such as saturation effects, burst statistics, size distributions and photobleaching, were investigated in the course of the development of the code. The code proved to be easily applicable to address problems that are of relevance to a number of solution-based single-molecule experiments. The initial goal to extract numerical values for the parameters which describe power law blinking statistics was then addressed. This turned out to be impossible without further experimental knowledge about the involved statistics, namely the minimal time (cut-off time) that is allowed for on- and off-time durations. However, it was shown that a set of reasonable parameters exists for which blinking does not effect the correlation curve.

4.4.1 Emission from Immobilized Particles

In a first step, fluorescence from immobilized emitters was simulated to test excitation-emission schemes involving either triplet or power law blinking. The simulation of fluorescence from an immobilized emitter provides the most straightforward way to test the simulated processes involving dark states. Figure 4.25 (A) is showing a time trace derived from simulated photon arrival times of a single nanocrystal over 1000 sec (bin time of 1 ms). To recover the blinking statistics that were plugged into the simulation code, a threshold was applied to the time trace in order to determine off periods (threshold=1 photon per bin). The resulting distribution (Figure 4.25 (B - circles)), plotted on a log-log scale, illustrates the power law dependence of off-times. A power law fit recovers the off-time exponent of 1.6, that was used in the simulation. An important result, which is of importance to the determination of on/off-time distributions from experimental data, can be found when increasing the threshold to determine off times. As displayed in Figure 4.25 (B - triangles) there is an influence of the threshold on the derived distribution, even in the absence of any additional background photons. The plot does not display an exact power law dependence any longer. This can be explained by the finite bin time, which can lead to intensity values in between the on-intensity and the off-intensity (which in the absence of background equals zero), when blinking times shorter than the bin time are possible (dependent on the cut-off time). Due to these intermediate intensity values an increase of the threshold intensity results in a distorted distribution of

blinking durations. Since in any real experiment there is always a background contribution which has to be exceeded by the threshold level, this distortion can easily influence experimentally determined on/off-time distributions.

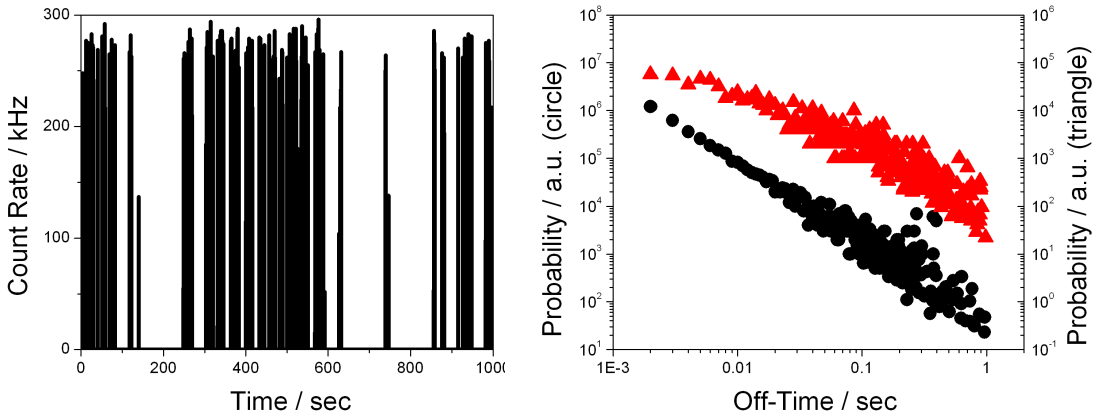

Figure 4.25: Simulated NC fluorescence with power law blinking ($m_{on} = 1.8$, $m_{off} = 1.6$, $\tau_{on/off} = 1E(-8)$) over 1000 sec (bin time 1 ms). Off-time histograms were determined with 1 count (circles) or 100 counts (triangles) threshold. The off-time histogram was converted into probability values by weighting each element of the on-time histogram by the average time between nearest neighbors.

4.4.2 Diffusion through a Confocal Volume

In the next step diffusion of non-blinking fluorophores was simulated. Diffusion is a process due to collisions with the surrounding solution molecules *[Einstein, 1905]*, which is not easily imagined due to its rare visualization in everyday life. Single-molecule measurements made it possible to follow the diffusion of a single molecule through an observation volume by observing the fluorescence signal. Since the detected signal depends on the position in the observation volume, any signal variation reflects motion of the molecule. Photon arrival times, originating from a single particle with a specified excitation and emission rate, are simulated. The individual particles show up as bursts in a time trace (Figure 4.26 (A)).

The simulation takes place in three dimensions with a zero probability to have more than one molecule per time in a Gaussian observation volume. Several methods

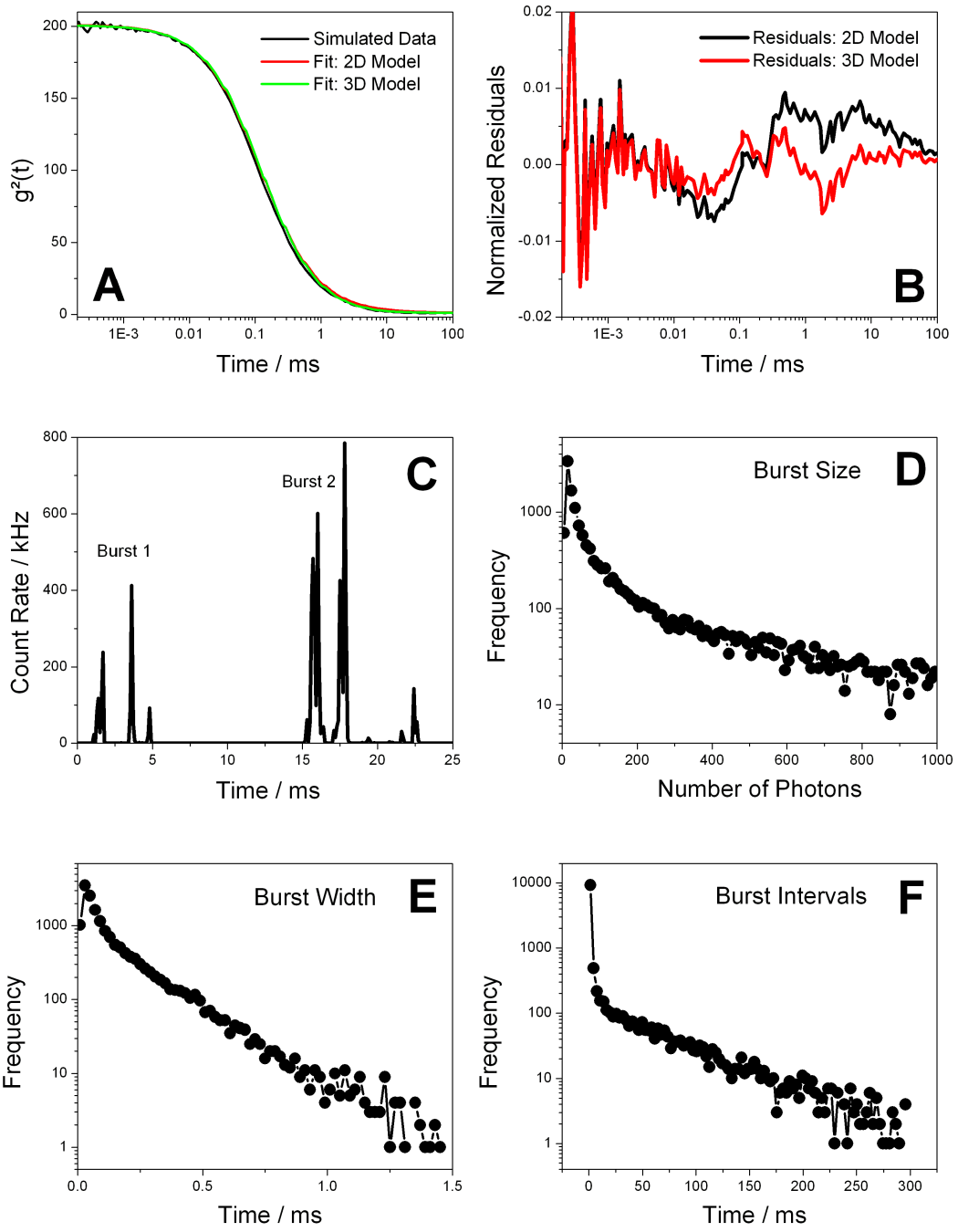

Figure 4.26: (A) Correlation curves of diffusing particles fitted with 2D- and 3D diffusion model. (B) Residuals show an advantage of a 3D fit, but prove that 2D fitting is applicable to a Gaussian excitation volume with $\omega_{xy}/\omega_z = 260$ nm/3000 nm. (C) Time trace showing individual bursts, most likely from two molecules. For each burst, the burst size (total number of photons (D)), burst width (time from burst start to end (E) and burst interval (time between successive bursts (E)) can be determined.

can then be applied to analyze such time traces and extract molecular information. The autocorrelation function, as already discussed, recovers the diffusion constant and occupancy. In this case a diffusion constant was extracted using a 3D (Equation 2.27) or 2D diffusion model (Equation 2.29) that fell within 1 % of the simulation parameter. The deviations between correlation data $g^2(t)$ and the fitted curves $\tilde{g}^2(t)$ are presented in the form of normalized residuals:

$$Res_{norm} = \frac{g^2(t) - \tilde{g}^2(t)}{g^2(0)} \tag{4.16}$$

Residuals provide a visual method to compare data and simulations under changing conditions by comparing it e.g. to the 2D diffusion model.

Another possibility is the analysis of individual bursts, which are identified by a thresholding algorithm. For each burst, a burst size (the total number of photons) and a burst width (the duration of passage) can be extracted and the time between successive bursts can be determined. (i) The burst size is related to the fluorophore's brightness and analytical expressions have been derived for specific experimental conditions by *Enderlein et al. [1997]* and *Fries et al. [1998]* to fit the burst size distribution (Figure 4.26 (D)). (ii) The burst width (Figure 4.26 (E)) on the other hand is a measure of the diffusion constant, which has been successfully determined from such distributions *[Ko et al., 1997]*. (iii) The burst intervals can be of interest in the context of optical trapping effects. The distribution of burst intervals displays exponential behavior up to a minimum duration (Figure 4.26 (B)). Below this duration burst intervals become more likely than an exponential distribution predicts. In an investigation by *Chiu and Zare [1996]* it was shown that the deviation increases when fluorophores are exposed to an IR-laser focus that is overlaid with the excitation laser. They interpret the deviation to be due to re-crossings of the same molecule and explain the increase of re-crossings by an optical trapping effect of the IR-laser. They argue that also without IR light, an optical trapping effect is present and might be the cause for any deviation. These simulations clearly show that a non-exponential distribution at short interval durations originates from diffusion alone, possibly expressing fast re-crossings of the same molecule, even if observed through a perfect Gaussian observation volume without any optical trapping effect.

Two technical parameters that enter the diffusion simulation are the box size in which the diffusion takes place and the time step for an individual random diffusion step. Both were varied (data not shown) to prove that the estimated sizes are large

enough for the box size (a minimal size is desired, so that invisible diffusion outside the observation volume, and therefore simulation time, is minimized) and small enough for the diffusion time step (the smaller the diffusion time step the more simulation steps are required to traverse the observation volume). Both parameters need to be optimized to keep the simulation time to a minimum. All further simulations were performed with a box size of 6 μm and a diffusion time step of 1 μs.

4.4.3 The Effect of Saturation

As blinking effects become increasingly important at higher excitation intensities (compare results for R6G *[Widengren et al., 1995]* and NCs *[Shimizu et al., 2001]*), any analysis will most likely have to include fluorescence saturation effects. Due to the non-constant excitation profile, saturation will always happen first at the center of the profile, extending towards its outer edges. Since the saturation effect is equivalent to a deformation (close to flattening) of the excitation profile, it will have an influence on the shape of the correlation curve. A series of simulations of purely diffusing particles excited with increasing intensities, can visualize the influence of saturation if the excitation rates exceed the emission rates of the particle. Correlation functions of simulated photon arrival times were calculated and fitted to a 2D-diffusion model. In Figure 4.27 the residuals of this fit are shown under the condition of saturation. The excitation power was increased from 0.04 to 20 times the saturation intensity I_{Sat} (determined from the average count rate of a simulation for an immobilized particle). The residuals show that no significant effect on the shape of the curve takes place up to at least 20 times I_{Sat}. This is an important result, since it allows the investigation of the influence of blinking processes on the correlation function without further correcting correlation curves for saturation effects.

The situation becomes different when the correlation amplitude is investigated. These simulations have already been referred to in the context of the determination of absolute concentration values and optical trapping. The apparent concentration of particles is, in fact, quite sensitive to saturation effects as is shown in Figure 4.27. Over a range of 1 to 20 times I_{Sat}, the occupancy increases by a factor of $1 + 1.7\frac{I}{(I+7.3I_{Sat})}$. The saturation intensity itself can be recovered from the count rate per particle (determined by dividing the average count rate from the total simulation by the occupancy) as a function of the excitation intensity. It turns out

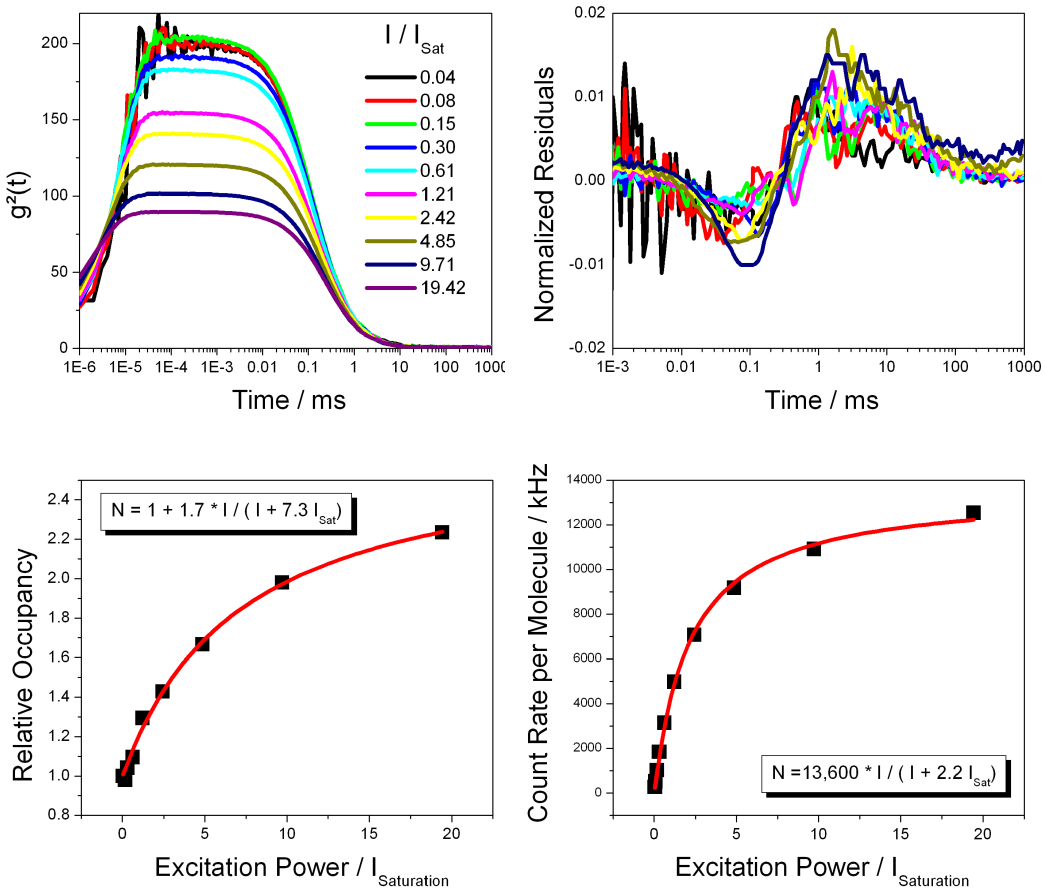

Figure 4.27: (top-left) Changes in the correlation amplitude ($\propto$ *occupancy*) are plotted (bottom-left) as a function of the excitation intensity (in units of I_{Sat} as determined from immobilized emitter) and fitted to a saturation function. (top-right) Residuals from a 2D diffusion fit to the simulated correlation curves show no significant variation for excitation intensities up to $20 \cdot I_{Sat}$. (bottom-right) Count rate per molecule is extracted and plotted as a function of excitation intensity, yielding a FCS saturation intensity that is $2.2 \cdot I_{Sat}$.

that when fitting the count rate per particle to the function $A\frac{I}{I+I_{Sat}}$, the saturation intensity is underestimated by a factor of 2.2. Since saturation increases the apparent occupancy, a measurement of I_{Sat} that uses this occupancy should deviate from the real value. But the fact that I_{Sat} can be determined from an FCS measurement under the influence of saturation within an error margin of around 2.2 times the true saturation intensity makes this method still usable.

4.4.4 The Effect of Size Distributions

Another simple extension to the simulation of purely diffusing particles, which is relevant for the characterization of NCs is taking a size distribution of particles into account. Assuming that the diffusing objects are spherical particles for which the Stokes-Einstein relation holds (Equation 4.5), a Gaussian distribution of the radius r will result in a non-Gaussian distribution of the diffusion constant D, since $r \propto D^{-1}$. The calculation of correlation functions from simulations, which take such a distribution of D into account, yields no significant effect on the shape of the correlation function for Gaussian distributions of the radius up to a standard deviation of 150 % (illustrated by residuals with an almost constant amplitude in Figure 4.28). For a STD of more than 50 %, only the diffusion time is shifting significantly towards larger values. The shift occurs because the distribution of D becomes more skewed towards smaller values with increasing broadening of the radius-distribution. Since NCs exhibit extremely small size distributions between 5 and 20 % for core-shell particles, going up to values around 100 % for modified particles (measured by atomic force microscopy and transmission electron microscopy; compare Figure 4.3.2), the simulated data proves that a diffusion model, assuming a fixed diffusion constant is consistent with the experimental size distribution of NCs and can be used in FCS on NCs.

4.4.5 The Effect of Photobleaching

The simulation was taken one step further to include the possibility of irreversible photo-destruction. An additional pathway from the excited state was included giving the possibility of destroying the fluorophore in addition to photon emission or inter-system crossing. The chances were determined by an exponential rate constant (equivalent to a bleaching quantum yield), such that the photobleaching pathway

is in direct competition to radiative and non-radiative relaxation processes. Upon photo-destruction of a given particle a new particle was introduced at a random position in the simulation box. The chances for a newly introduced particle to start directly inside the observation volume were extremely small. Figure 4.29 presents a series of simulations with increasing photobleaching rates, resulting in a larger number of particles being destroyed during their translation through the focal volume.

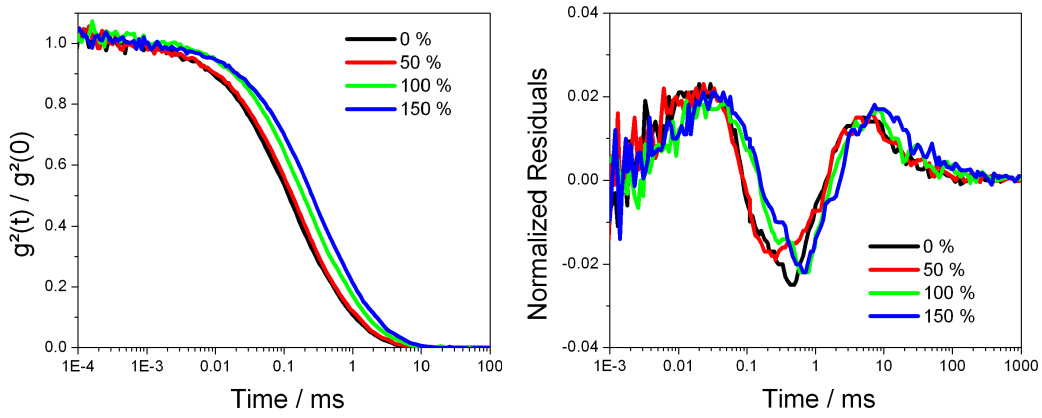

Figure 4.28: (left) Correlation functions for NCs with a Gaussian size distribution in radius of 0–150 %. (right) Residuals from a 2D diffusion fit show no variations in the shape of the correlation function besides shifting towards larger times for broader size distributions. Simulations were performed using a non-Gaussian excitation volume (as discussed further down on page 129) causing an overall different form for residuals compared to previous figures.

A comparison with experimental data (page 103) was done through fitting similar correlation curves with an analytical model which includes 2D diffusion and an additional exponential decay to account for a bleaching rate constant. The diffusion time was fixed to values determined at low bleaching rates. The residuals follow a similar time dependence but are shifted with respect to each other. It is evident that the analytical model deviates significantly at small times (residuals approach -0.04 as compared to 0 for diffusion without bleaching). Besides the shift, which is caused by differences in the diffusion constants, the residuals give evidence that simulation and experimental data are in better accordance with each other than with

the analytical model (since residuals for experiment and simulation both follow a very similar trend). In other words simulations can better describe experimental data than the proposed analytical model. Deviations for the analytical model can probably be explained by the fact that the real bleaching rate depends on the exact position in the excitation volume and therefore can not be estimated by just one constant bleaching rate.

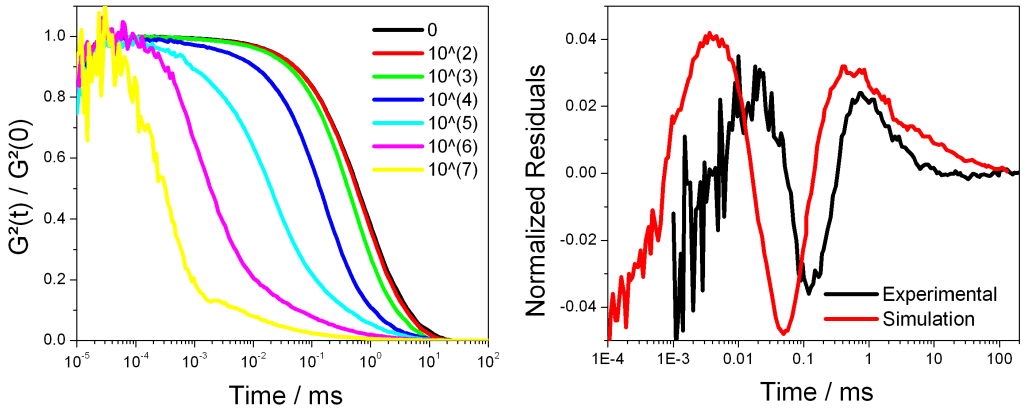

Figure 4.29: (left) Simulated FCS curves for increasing photobleaching rates. Photobleaching rate constants vary from 0 to 10^7 Hz. The rate constant for fluorescence emission was kept at 10^8 Hz. (right) Residuals of a fit including diffusion and exponential bleaching decays for experimental NC data (1.1 mW on page 103) and simulated data ($10^(4)$ Hz).

4.4.6 The Effect of Non-Gaussian Observation Volumes

The exact shape of both the excitation intensity distribution and the detection efficiency function is having a significant influence on the autocorrelation function. This was shown in the analytical derivation of various models (page 41) as well as in the experimental comparison between water- and oil-immersion objectives (page 91). Since it is impossible to incorporate the profile of almost any non-gaussian observation volume into an analytical model, Monte-Carlo simulations provide the only way to derive an exact correlation function, provided that a numerical representation of the observation profile is given. Numerical approximations derived from first principles of the involved optical components are currently investigated.

In Figure 4.30 the problem is illustrated by comparing the influence of a Gaussian observation volume and of a profile, calculated for a high NA oil-immersion objective using scalar diffraction theory, on the correlation curve. Diffusion of fluorescing particles through these two types of excitation volumes was simulated and the correlation data was calculated. Residuals from fits using a 2D diffusion model are shown for both cases. Simulations using the non-Gaussian profile show a flattening of the correlation decay which results in larger deviations to the 2D diffusion model. This can be seen from the opposite sign and larger amplitudes for residuals from the non-Gaussian profile simulation. The extracted diffusion time shifts from 113 μs (Gaussian) to 159 μs (non-Gaussian) for a simulation input of 112.7 μs.

In Figure 4.31 the calculated profiles are shown. An elongated Gaussian profile with a ω_{xy} to ω_z ratio of 260 to 3000 is displayed in comparison to a non-Gaussian profile with much more pronounced lobes. Even though this calculation is only approximating an experimental excitation profile, since it is calculated using scalar diffraction theory, it gives an idea of the effects that have to be taken into account.

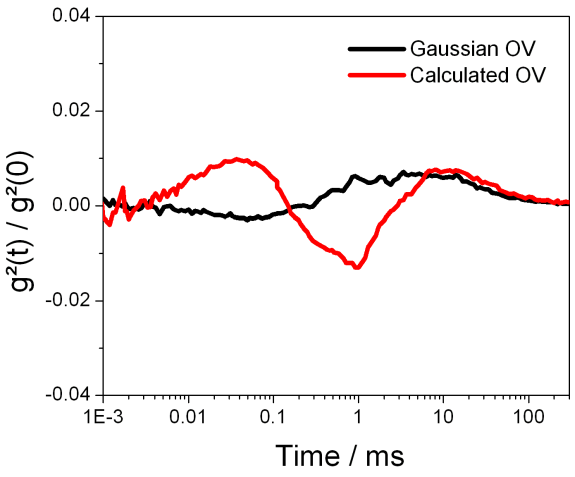

Figure 4.30: Residuals of fits using a 2D diffusion model for simulations with either a Gaussian excitation profile or a calculated excitation profile (1.3 NA oil-immersion objective, calculated using scalar diffraction theory).

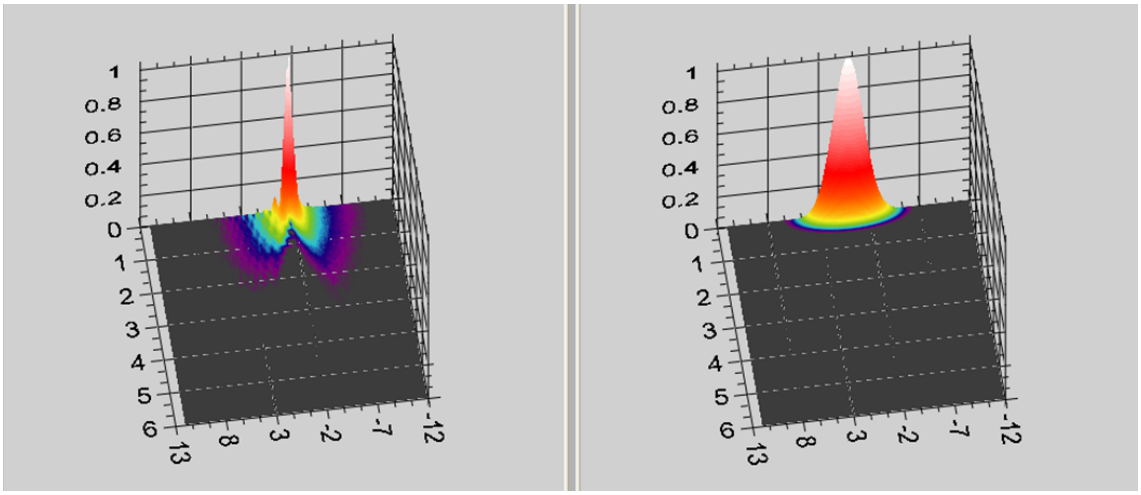

Figure 4.31: Calculated excitation profiles: (left) modelled 1.3 NA oil-immersion objective; (right) perfectly Gaussian profile. Axial and lateral components are given in μm. The intensity is normalized to the peak value.

4.4.7 The Influence of Power Law Distributed Blinking

The statistics inherent to on- and off-time distributions in the emission of NCs are described by a power-law (page 36) with an exponent m for both on- and off-time distributions and a lower cut-off time which ensures convergence when the probability distribution is integrated over all possible events. Whereas the on and off-exponents $m_{on/off}$ have been experimentally determined to be between 1 and 2, there is no experimental evidence for cut-off times t_0. For physical reasons it is reasonable to assume a finite t_0, that would correspond to a minimal on/off-time, on the order of the fluorescence lifetime. But there is no argument to reject the possibility of larger t_0. This is even more the case since t_0 turned out to influence the correlation data in similar ways as the exponents do. The smaller t_0 is, the higher the probability for short on/off-times and the more pronounced the influence on the slope of the correlation curve becomes. This practically leaves 4 free parameters to define power law statistics for on- and off-times: $m_{on/off}$ and $t_0^{on/off}$. Figure 4.32 shows the influence of each variable under otherwise constant parameters. The exponents influence the curve opposite to each other: whereas m_{on} increases the slope on the curve, m_{off} decreases it.

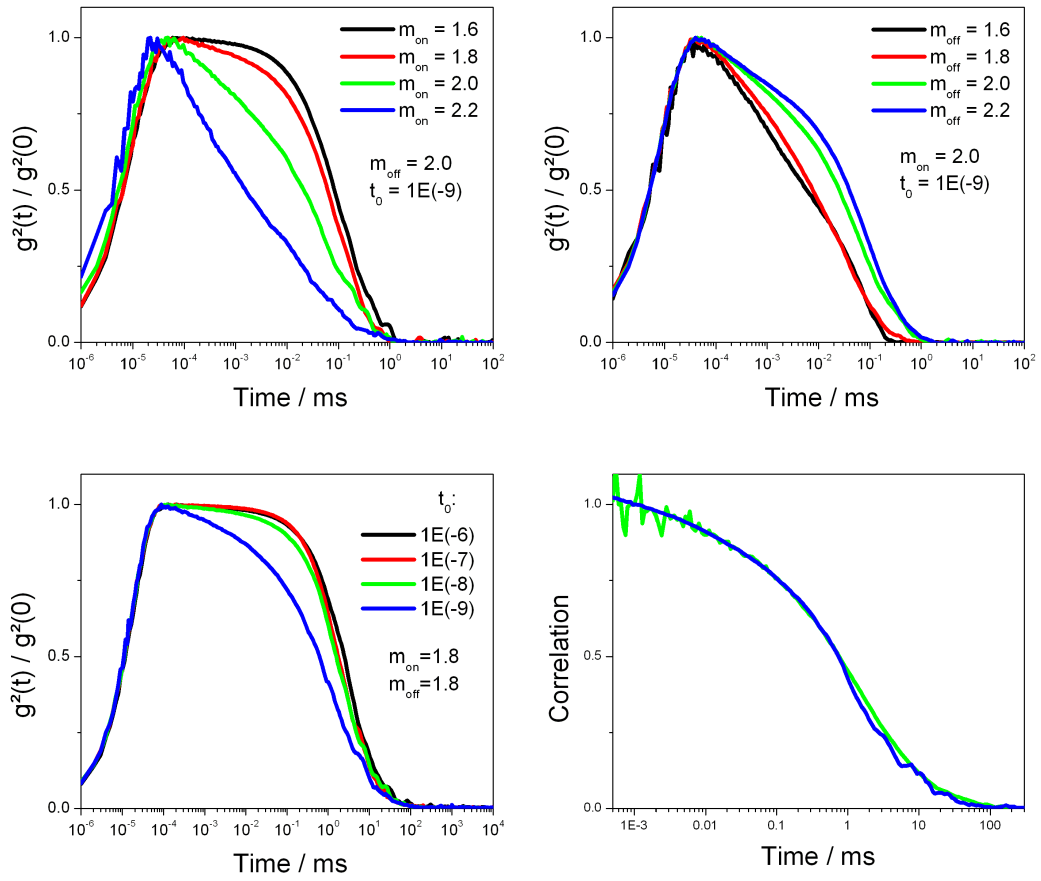

Figure 4.32: (top) Simulated FCS curves for diffusing particles that undergo power law blinking with the specified parameters. (bottom-left) Simulations for constant exponents but varying cut-off time. (bottom-right) FCS data on peptide-coated NCs (450 μW, 532 nm) and simulated FCS data for power law blinking NCs ($m_{on} = 1.9$, $m_{off} = 1.8$, $t_0 = 10^{-9}$).

A direct comparison between simulated data and experimental data is presented in Figure 4.32 (D). The general shape, as measured for peptide-coated CdSe/ZnS NCs under high excitation powers (450 μW at 532 nm), is reflected in simulated data with $m_{on} = 1.9$, $m_{off} = 1.8$ and $t_0 = 10^{-9}$ for on- and off-time statistics. Deviations at longer time delays are due to noise in the simulated data, resulting from the simulation of too few particles due to time constraints. The simulation took about one hour on a 2 GHz Pentium 4 processor. Even though this comparison is rather arbitrary, it does prove that the influence of power law blinking appears similar in experiment and simulation.

Since the choice of t_0 turned out to critically influence the shape and therefore the exponents, needed to fit experimental data, the simulations at this point do not provide the means to extract $m_{on/off}$ from solution-based measurements and compare them to surface observations. However, the fact that power law blinking with a certain set of parameters (e.g. $m_{on} = 1.8$, $m_{off} = 1.8$, $t_0 = 10^{-8}$ or $m_{on} = 1.6$, $m_{off} = 2.0$, $t_0 = 10^{-9}$) has almost no influence on the correlation curve is remarkable. This means that FCS experiments which do not show any blinking influence cannot provide evidence for non-blinking NCs. For large enough t_0 power law exponents which were measured on surface will not effect a correlation curve for diffusing particles.

4.4.8 Discussion

As NCs exhibit blinking which can be monitored by FCS, the method provides a tool to characterize blinking under variations of synthesis or surface modifications. Significant differences have already been observed for different batches of NCs. Since biological applications require NCs that in a best case scenario do not blink, FCS is valuable for optimization processes in NC preparation. Higher-sensitivity methods, like scanning-stage confocal microscopy, allow collecting data over longer times from a single NC. But on the other hand, such experiments require a large amount of preparation and acquisition time and provide only very limited statistics (one might be able to collect time traces from a few 10s of NCs per day).

These simulations were developed to provide a tool to perform quantitative analysis of blinking behavior using FCS. Having a virtual confocal microscope in which fluorophores' diffusion and photophysical properties can arbitrarily be adjusted and their effect on FCS (or other solution-based single-molecule methods, like burst

analysis) can be studied, is extremely helpful. Influences form multiple overlapping effects can be deciphered which cannot be investigated one by one in experiment. The developed LabView code allows studying effects from saturation, photobleaching, size distributions and non-gaussian observation volumes on time traces and their various analysis methods, like burst analysis and FCS.

Simulations showed that saturation does effect the correlation amplitude but has negligible effects on the shape of the correlation curve up to 20 times the saturation intensity. Results for amplitude variations were used to correct experimental data and help unravel the effect of optical trapping. Photobleaching was studied to reassure experimental observations and discriminate bleaching from blinking. The size distribution of typical NC samples was shown to have negligible effects on FCS data. Simulation of FCS data under various observation volumes confirmed what was shown in an experimental comparison for water- and oil-immersion objectives. And most importantly, it was shown how correlation curves depend on power law parameters. Simulations proved, that for certain power law parameters blinking NC can appear as purely diffusing particles. No observation of alterations in the FCS curve does not imply non-blinking NCs. For those parameters which induce alterations in the correlation curve, these alterations were shown to be qualitatively identical with experimental data at higher excitation powers, proving that experimental observations are not due to saturation or photobleaching.

One drawback so far is, that FCS cannot be used to extract quantitative information about the involved blinking statistics. The simulations showed that absolute values of power law exponents cannot be determined without further knowledge of a lower cut-of time. Assuming that t_0 is on the order of the fluorescence lifetime, one can monitor changes in blinking exponents for different NCs. But for a thorough comparison to surface-based measurements, a physical argument or more experimental evidence is needed.

The other limitation is that no simple scaling laws (e.g. $g^2(a \cdot D, \tau) = g^2(D, a^n \cdot \tau)$ — D: sample parameter like power law exponents or diffusion time; a: arbitrary factor; n: exponent which depends on the exact function g^2; τ: time delay) with respect to either blinking parameters or diffusion time have been found. In other words, the correlation curve has to be derived from completely simulated data for each set of parameters. This makes it impossible to perform real fitting of experimental data. A feasible approach to perform quasi-fitting is to simulate enough data to built up a database for a given parameter-matrix. By comparison between simulated and

experimental data and further extrapolation of correlation curves in between matrix elements, the closest match could be found and parameters determined. However this requires a large number of performed simulations and therefore a fast code. With simulation times of up to 2 hours per correlation curve the approach is not practical at this point. Code optimization and implementation in fast C++ code offer a future perspective.

5

Conclusion and Outlook

5.1 Conclusion

Fluorescence microscopy is an important tool for structural and functional analysis of macromolecules in the cell *[Weiss, 1999; Michalet, 2003]*. In addition to various organic fluorophores, colloidal semiconductor nanocrystals (NCs), also called quantum dots, have recently been introduced as biocompatible labels *[Bruchez et al., 1998; Chan and Nie, 1998]*. Unique photophysical properties *[Michalet et al., 2001]* render NCs especially suitable for observations in the live cell: (i) a narrow emission spectrum that can be tuned throughout the visual wavelength range by varying the size of the NCs during synthesis; (ii) a broad absorption spectrum enabling multicolor detection schemes with a single wavelength excitation source; (iv) a large total number of emitted photons (100–1000 times larger than for rhodamine fluorophores), prerequisite for observations at long timescales; (iv) a fluorescence lifetime of 20–30 ns, $\sim$ 10 times longer than the lifetime of naturally-occurring fluorescent proteins (autofluorescence), allowing background reduction by a time-gated detection (selection of photons that are emitted with a certain delay to excitation). By use of NCs as fluorescent labels a number of fluorescence microscopy techniques can be applied

that in principle allow increasing sensitivity in a biological environment up to the single-molecule level. Single molecule detection can resolve subpopulations in a heterogenous sample and record asynchronous dynamics that are otherwise hidden due to ensemble averaging *[Xie and Trautman, 1998; Michalet and Weiss, 2002]*.

As convincing as first experiments have been, they also showed alterations of optical properties from chemical treatments. Due to the vast amount of different synthesis routes and the need for various surface modifications to enable solubility in aqueous solution and binding to biological macromolecules, colloidal NCs are exposed to diverse chemistries. Large surface to volume ratios cause any surface modification to significantly influence NC photophysics. Protocols to render NCs water-soluble and apply specific labeling schemes very often decrease the fluorescence quantum yield, increase irreversible photo-destruction or cause spectral shifts. In order to develop reliable chemistries for highly fluorescent NCs, such effects have to be minimized.

In this work, a variety of fluorescent semiconductor NCs were investigated with ensemble and single-molecule methods. Fluorescence correlation spectroscopy (FCS) was applied to characterize photophysical and colloidal properties of NCs. It was demonstrated that FCS can recover basic parameters that allow a systematic comparison of NCs in terms of particle sizes, brightness per particle η and concentration of fluorescent particles. Results acquired by FCS were correlated with observations of single-particle fluorescence from immobilized NCs. Monte-Carlo simulations were performed to interpret the effects of various mechanisms on the correlation function. Both approaches helped validating the method and extracting parameters which are difficult to acquire by other means.

Single NCs on Surface In a first step, the unique optical properties of NCs were confirmed for various samples. Fluorescence intermittency (blinking) was observed in fluorescence time traces using confocal and total-internal-reflection (TIR) microscopy and followed power law statistics. Fluorescence lifetimes were measured to be around 20 ns for single NCs. To prove that single particles were observed, the signature of antibunching was observed simultaneously with lifetime measurements. The lifetime distribution showed varying components resulting in a multi-exponential decay that is different for each NC. Although this complicates quantitative fluorescence-lifetime-imaging-microscopy (FLIM), a time-gated detection

scheme that reduces background contributions is possible.

An increase in the fluorescence signal with time of illumination (light-induced activation) was observed in ensemble and single-particle measurements. TIR-measurements for NCs immobilized on a glass surface and exposed to air revealed an increase in the concentration of fluorescent particles while at the same time the brightness per particle stayed constant.

Characterization using FCS FCS was used to measure diffusion constants for various NCs. The diffusion constant was related to particle radius using Stokes-Einstein equation. A comparison with TEM measurements proved that the Stokes-Einstein equation is valid for particles down to at least 7 nm in diameter. A measurement of particle sizes will also provide evidence for the presence of aggregates, when the colloidal particle radius is known by other means (e.g. aggregation under various buffer conditions can be observed for a well characterized sample). Aggregates would show larger diffusion times due to increased particle radius and also increase the observed brightness per particle.

The estimation of brightness per particle yields an important parameter for the optical performance of NCs since it allows comparison of various NCs in terms of their brightness or quantum yield. Since η is determined from the average fluorescence and the concentration of fluorescent particles (not being sensitive to dark particles), it does not underestimate the brightness in the presence of a dark NC subpopulation. The concentration of emitting NCs was measured to be smaller than the total concentration of absorbing NCs. Therefore FCS-QY is more relevant to single-molecule applications than the ensemble QY.

The brightness per particle was also used to evaluate the saturation intensity. NC fluorescence saturates at excitation powers one to two orders of magnitude lower than that of rhodamine 6G, posing a limitation on the maximum observable signal (which is compensated by larger absorption cross sections, making NC probes no less bright than organic dyes).

FCS can monitor relative concentration changes over more than two orders of magnitude. Absolute concentration measurements confirmed that the number of fluorescent particles is in general smaller than absorption measurements suggest. In addition, it was shown that a subpopulation of non-fluorescent NCs is not static, but that light-induced activation can render dark NCs fluorescent. Light-induced activation was observed to change the concentration of fluorescent particles at the

same time as it increases the quantum yield for each particle.

The opposite process of photobleaching is rarely observed in NC samples. Nevertheless, substantial photobleaching was shown for CdTe cores at high excitation powers.

A second effect that can distort the overall shape of the correlation function is blinking. It was observed for most NCs at excitation intensities above the saturation intensity. However certain batches also showed no significant influence from blinking even at high excitation intensities in spite of the fact that blinking was observed for these particles on surface. The effect of blinking was clearly distinguished from photobleaching and further elucidated via Monte-Carlo simulations.

Time-gated FCS Solution-based measurements were combined with TCSPC to perform time-gated FCS. Fluorescence lifetimes of $\sim$ 20 ns enable a reduction of signal contributions from organic dyes with 1–5 ns lifetimes by time-gating after 10 ns. It was demonstrated, that "real" NC concentrations could be determined even in the presence of high levels of background fluorescence from rhodamine 6G.

Optical Trapping When performing FCS measurements at various excitation powers, the correlation amplitude was found to change independently from the sample concentration. An increase in apparent concentrations was observed for increasing excitation powers which could not be explained by saturation effects. Optical trapping, which can explain such variations in N, was discussed and quantified. Whereas the influence of saturation turned out to be sufficient to explain amplitude variations for organic dyes, a larger increase in measured occupancy for increasing excitation powers was found for NCs. Assuming trapping polarizability values were extracted that are one to two orders of magnitude larger than literature values (estimated via Stark shifts) suggest. This is expected when resonant wavelength are used (meaning the absorption coefficients are high). Even though numerical values for NC polarizability could be extracted, uncertainties for the measured saturation intensity and effects due to non-Gaussian observation volumes make it premature to give these results a precise physical meaning.

Monte-Carlo Simulations FCS was simulated using Monte-Carlo simulations of diffusing particles that undergo excitation-emission cycles with specified rate constants and exhibit blinking in their emission. Simulations were used to interpret the

influence of power-law distributed blinking on FCS data. The effect of various on/off exponents and a cut-off time t_0, required to ensure a finite probability for all possible time durations, was studied. The influence of t_0 on correlation data was found to be significant, when set to physically meaningful time scales on the order of the fluorescence lifetime (ns). Since t_0 is not known experimentally, exponents cannot be extracted from FCS data without ambiguity. However reasonable blinking parameters were found for which blinking did not effect the correlation curve. Monte-Carlo simulations were also used to quantify size-distribution, saturation, photobleaching and the influence of non-Gaussian observation volumes on FCS data.

5.2 Perspectives

Improvement in synthesis and conjugation schemes NC synthesis, modification to render them water-soluble and chemistries to provide specific bio-conjugation schemes are under steady development. However, until now most modifications deteriorate the optical performance with respect to QY and to the ratio of dark NCs (which can be lightened up by photo-induced activation). Efforts to eliminate these negative influences will be pursued until bio-conjugated NCs approach brightness and photostability that the best core-shell systems exhibit right after synthesis. Some photophysical properties that become evident on the single-particle level, like blinking and spectral jumps, are also disturbing for a number of applications; e.g. the observation of single diffusing particles in a cell is severely complicated by long off-states. All these effects need to be minimized.

On the other hand NCs with properties tailored to particular requirements of an experiment emerge. For example linearly-polarized emitting nanorods have been synthesized *Hu et al. [2001]* and promise to be useful in polarized light emitting diodes or as reporters for rotary motion in a number of biological systems.

The quest for IR-emitting NCs is just as large as the quest for red organic dyes, because of reduced autofluorescence in the red spectral range whenever biological buffer or even a living cell environment is given. Since tissue absorbs much less between 600 and 900 nm and at higher IR wavelength, emission at such wavelength would also be easier to observe at greater depth. The same effect makes two photon excitation such a powerful tool in tissue imaging.

Established methods to modify photophysical properties, like band-gap engineer-

ing, can be further explored. Due to the large number of semiconductor materials, new compositions of multiple materials are constantly proposed and demonstrated. Also the geometries in which various components are combined, e.g. to build gradient shells, are further developed.

Additional layers of organic matter are used to protect crystals from deterioration over time, to decrease non-radiative pathways and to provide sites specific labeling. As Qdot Corp. has demonstrated, additional layers of e.g. polymers, can help to protect the NC from its environment and thus improve optical properties. Other concepts or compositions of ligands will be developed.

This huge field of current and very "hot" research is dependent on reliable methods to characterize modified samples fast and by as many simultaneously observed parameter as possible. FCS together with related high-sensitivity methods offer an extremely fast and easily implemented technique to observe colloidal and optical properties and provide feedback for synthesis and surface modifications.

PAID — Photon Arrival-Time Interval Distribution FCS can be used to observe a number of parameters — occupancy and diffusion constant being the most important ones — that are useful for sample characterization. Even though an average brightness per particle can be estimated from the overall detected count rate and the occupancy, it is not possible to directly observe brightness distributions using FCS. The brightness information is lost in the calculation of the correlation function. Photon arrival-time interval distribution, or PAID, is one method that allows extracting brightness, occupancy and diffusion constants simultaneously for single-component solutions or show some evidence that a distribution of molecules with different brightness and/or diffusion constants is present in the sample. Very recently a numerical model was demonstrated that can fit PAID data and extract parameters for samples containing a single or multiple species *[Laurence, 2002]*.

PAID visualizes characteristic features by histogramming photon arrival-times in a two dimensional way. Counting photons in a monitor channel, that arrive between a start- and stop-photon in a start and stop channel, respectively (in most configuration the start and stop channel are given by one detector and the monitor channel by the other; but also one detector serving all three channels is possible), a histogram is built up with a time axis (the time difference between start and stop photon) and a photon number axis (the number of photons counted). The projection of this two dimensional histogram on the time axis equals the well known correlation

function. With access to the photon number axis, additional brightness information is available. The difficult part is to derive a model function that can be fitted to the data to actually extract numerical values.

Figure 5.1 gives a flavor of the power of PAID when used with NCs. Peptide-coated CdSe/ZnS NCs are observed at four different excitation powers, reaching far into saturation conditions. As we know that blinking at these high powers is a major contributor, it is difficult to conclude anything from a qualitative interpretation of the PAID histogram. Nevertheless some common characteristics of PAID histograms can be pointed out (see figure caption). A quantitative analysis has to be performed via fitting of precise numerical models and can hopefully reveal more of NC's photophysical peculiarities.

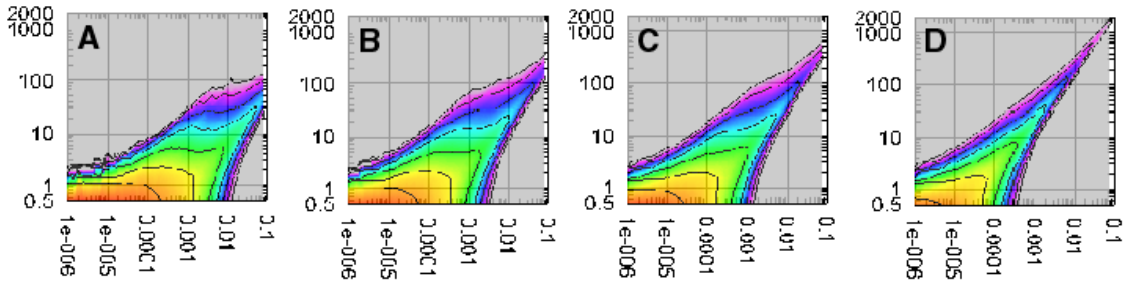

Figure 5.1: PAID histograms for peptide-coated CdSe/ZnS NCs at various excitation power (A: 8 μW, B: 43 μW, C: 100 μW, D: 470 μW). All axis, including the color table, show a logarithmic scale (x in sec, y in counts, and z in counts per time bin). The change in the overall slope towards higher values indicates an increase in brightness; the constant color gradient along this slope indicates a non-changing diffusion constant; a parallel shift towards the left is an indicator for an increase in apparent concentration, as has already been discussed for FCS measurements. The very pronounced shoulder at low excitation powers might be influenced by brightness distributions. Quantitative fitting is needed to obtain more information.

Biological applications One application for colloidal semiconductor NCs lies in specific labeling of biological macromolecules, membranes or cells. A successful bioconjugation scheme, that leaves optical properties unchanged, promises impact on many biological questions were long observations (minutes to hours) or multi-color observations are required. Proof-of-principle experiments have recently been

carried out in vitro and in vivo *[Bruchez et al., 1998; Chan and Nie, 1998; Mattoussi et al., 2000; Goldman et al., 2002; Dubertret et al., 2002; Jaiswal et al., 2003; Wu et al., 2003]*.

A straightforward application is to stain live cells and follow cellular development over time. To date this is performed by loading cells with large amounts of organic dyes, to perform minute-scale observations in spite of photobleaching. If smaller numbers of fluorescent probes are sufficient to extract the same information, probe-induced toxicity or perturbations can be reduced. Observations on mouse 3T3 fibroblast cells loaded with NCs via endocytosis showed that cells survive the uptake of NCs for hours and days.

Another application is fluorescence in situ hybridization (FISH). In this assay typically metaphase chromosomes are exposed to fluorophore-labeled DNA probes with a designed sequence. The DNA probes can be specific to one or several genes, or to centromeric or telomeric regions of a chromosome. Not only have all 24 human chromosomes been identified with this assay, but also the presence or absence of individual genes can be tested. The human genome consists of 3 billion base pairs. Assuming that at least 30,000 genes are encoded in this sequential information, diagnostic tests for only a few genes already requires massive parallel screening. Multi-colored probes, that can be accessed simultaneously under single-wavelength excitation, would benefit diagnostic tests extremely. An increase in resolution for mapping individual genes on the chromosome can be achieved at the same time as throughput can be speeded up by simultaneous observation of several colors. Applying the recently developed technology of DNA combing *Michalet et al. [1997]*, similar hybridization assays can be developed with oligonucleotide probes, rather than kilobase-pair probes in FISH, on stretched DNA. This allows reassuring distances, sizes and rearrangement of gene sequences down to the level of a few base-pairs. NC-labeled oligonucleotides would improve in similar ways as mentioned for FISH.

A whole battery of applications is awaiting, when specific labeling schemes are established. The recent commercialization of bioconjugated NCs promises ever more biologically relevant demonstrations [1].

[1] Just very recently the first bio-conjugated NCs became commercially available (QDots Inc., Hayward, CA). These polymer-coated, streptavidin-conjugated CdSe/ZnS particles have already proven valuable in a number of applications. CdSe/ZnS NCs, dissolved in non-polar solvents or aqueous buffers, are also distributed by other companies. Since every research group by now can have access to these novel fluorescent labels more interesting experiments will soon be

In the course of this work NCs have already been observed in live cells. Peptide-coated NCs, with certain peptide motives, were observed to diffuse freely in the cell as pictured in Figure 5.2. The cells did not show alterations from toxicity caused by NCs over several days.

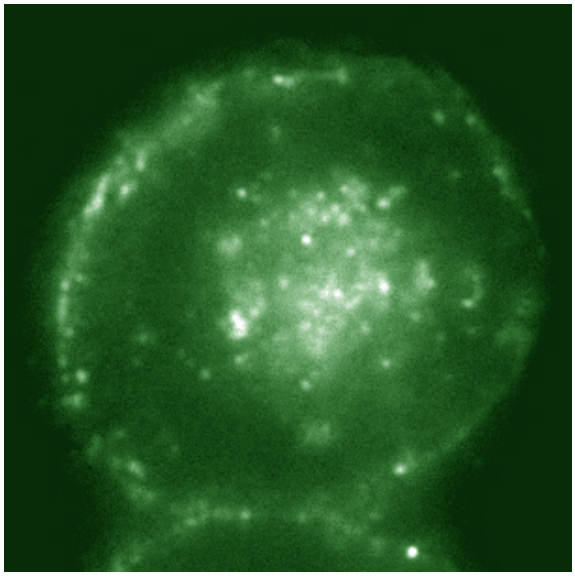

Figure 5.2: A live Hela cell is loaded with peptide-coated NCs and observed over several minutes using wide-field microscopy. Single NCs can be seen to diffuse freely in various compartments of the cell.

Movies of such images over several minutes can be analyzed to extract diffusion parameters in various compartments of the cell. One way to investigate diffusion behavior in live cells is by fitting the PSF of single NCs in successive frames and extracting the position in two or three dimensional space. The most severe complication is given by the blinking behavior of NC fluorescence, which increases at higher excitation powers. FCS might offer an alternative to extract diffusion constants at lower power and possibly, though not necessarily, at higher concentrations. The application of FCS in a live cell environment has been demonstrated by *Schwille [2001]*. The application of FCS to NCs, as was demonstrated the presented work, provides some tools and further evidence that FCS is a valuable technique to in-

demonstrated and further bio-conjugation schemes are going to be applied. Nevertheless the quality in terms of colloidal and photophysical properties of NCs is still far from being uniform or characterized in a standardized way.

vestigate the diffusion of NCs in a live cell environment. With the help of various labeling schemes, useful information about pathways and molecular interactions can be gained.

Molecular interactions are manifold in a cell. The field of proteomics is just as much concerned about individual proteins, their structure and function, as it is about how proteins interact with each other and form larger complexes. Almost every process that is essential to the life cycle of a cell, like transcription, replication, translation, photosynthesis, signaling pathways is carried out by a large number of proteins acting together. To observe these interactions or just co-localization, one needs non-invasive, therefore optical, methods that allow resolving distances from a few nm to hundreds of nm. As mentioned on page 13, Förster resonance energy transfer (FRET) provides a distance-dependent observable in the range of 1–10 nm. One recent experiment, which disproved a long time established hypothesis in transcription, was performed in our laboratory:

Promoters, specific DNA sequences that precede individual genes, are recognized in bacteria by specific proteins (σ factors). It was believed that σ factors lead the transcription machinery to specific genes, and subsequently dissociate upon maturation of the initial transcribing complex to the elongation complex. It has been shown on single-molecule level, that the primary σ factor (σ^{70}) is not released from the whole transcription complex after initiation, as was believed from ensemble observations. The essential ingredient in this experiment was probing the presence of donor and acceptor dyes simultaneously with observing distances via FRET. NCs could be helpful in such experiments as perfectly tunable donors. By adjusting the emission wavelength, R_0, the distance where FRET is most sensitive to distance changes, can be fine-tuned to the desired value. In addition, donor(NC)-acceptor(dye) pairs can be chosen independently of the available excitation source, since NC-donors can be excited in a wide spectral range. One limitation is given by the size of NCs, which requires precise constraints on the NC position, and thus reliable labeling chemistries. This constitutes a plausible reason why no molecular ruler using a NC-dye pair has yet been implemented.

In between 10 nm and the resolution limit of light microscopy, co-localization has been demonstrated by fitting PSF to two-color labels and measuring center-to-center distances. NCs are an ideal probe for this task, since they can be excited by a single wavelength, minimizing the influence of chromatic aberrations that otherwise reduce the resolution. The technique has been demonstrated on NCs immobilized on a glass

surface *[Lacoste et al., 2000]*, and with specific labeling schemes, the application to biological systems is straightforward.

Semiconductor NCs are fascinating probes that display a large number of advantageous optical properties compared to conventional dyes. As nanoscale objects, they exhibit just as many peculiarities which are less desirable, when used as single-photon sources or reporters in biological experiments. Questions about blinking, dark particles and photo-induced activation, to name a few, open up a wide field for physicists and chemists who like to explore nature at the interface between the quantum and the macroscopic world. Nanocrystals will continue to be investigated on a fundamental level and used in ever more diverse applications. And when surface effects become utterly mind-boggling, a look at the rainbow and its glowing colors is worthwhile.

Bibliography

Each reference is followed by numbers referring to the pages of citation.

R. R. Agayan, F. Gittes, R. Kopelman, and C. F. Schmidt. Optical trapping near resonance absorption. *Applied Optics*, 41(12):2318–27, 2002. 119

A. P. Alivisatos. Semiconductor clusters, nanocrystals, and quantum dots. *Science*, 271(5251):933–937, 1996. 29

W. P. Ambrose and W. E. Moerner. Fluorescence spectroscopy and spectral diffusion of single impurity molecules in a crystal. *Nature*, 349:225–227, 1991. 24

W. P. Ambrose, P. M. Goodwin, J. Enderlein, D. J. Semin, J. C. Martin, and K. A. Keller. Fluorescence photon antibunching from single molecules on a surface. *Chemical Physics Letters*, 269(3-4):365–70, 1997. 26

W. P. Ambrose, P. M. Goodwin, and J. P. Nolan. Single-molecule detection with total internal reflection excitation: comparing signal-to-background and total signals in different geometries. *Cytometry*, 36(3):224–31, 1999. 54

A. Ashkin, J. M. Dziedzic, J. E. Bjorkholm, and S. Chu. Observation of a single-beam gradient force optical trap for dielectric particles. *Optics Letters*, 11(5):288–29, 1986. 112

D. Axelrod. Total Internal Reflection Fluorescence Microscopy in Cell Biology. *Traffic*, 2(11):764–774, 2001. 21, 53

K. Bacia and P. Schwille. A dynamic view of cellular processes by in vivo fluorescence auto- and cross-correlation spectroscopy. *Methods*, 29(1):74–85, 2003. 41

K. Bahlmann and S. W. Hell. Electric field depolarization in high aperture focusing with emphasis on annular apertures. *Journal of Microscopy*, 200 (1):59–67, 2000. 51

U. Banin, C. J. Lee, A. A. Guzelian, A. V. Kadavanich, A. P. Alivisato, W. Jaskkolski, G. W. Bryant, A. L. Efros, and M. Rosen. Size-dependent electronic level structure of InAs nanocrystal quantum dots: Test of multiband effective mass theory. *Journal of Chemical Physics*, 109(6):2306–2309, 1998. 32

U. Banin, M. Bruchez, A. P. Alivisatos, T. Ha, S. Weiss, and D. S. Chemla. Evidence for a thermal contribution to emission intermittency in single CdSe/CdS core/shell nanocrystals. *Journal of Chemical Physics*, 110(2):1195–1201, 1999. 36, 71

T. Basché, W.E. Moerner, M. Orrit, and H. Talon. Photon antibunching in the fluorescence of a single dye molecule trapped in a solid. *Physical Review Letters*, 69:1516–1519, 1992. 26

T. Basche, S. Kummer, and C. Bräuchle. Direct spectroscopic observation of quantum jumps of a single-molecule. *Nature*, 373(6510):132–134, 1995. 24

W. Becker, A. Bergmann, K. König, and U. Tirlapur. Picosecond fluorescence lifetime microscopy by TCSPC imaging. *Proceedings SPIE*, 4262:414–419, 2001. 17, 19

E. Betzig and R. J. Chichester. Single molecules observed by near-field scanning optical microscopy. *Science*, 262(5138):1422–1425, 1993. 21, 22, 24

G. Binning, H. Rohrer, Ch. Gerber, and E. Weibel. Surface Studies by Scanning Tunneling Microscopy. *Physical Review Letters*, 49:57–61, 1982. 2

G. Binning, C.F. Quate, and Ch. Gerber. Atomic Force Microscope. *Physical Review Letters*, 56(9):930–933, 1986. 2

M.A. Bopp, Y. Jia, L. Li, R.J. Cogdell, and R.M. Hochstrasser. Fluorescence and photobleaching dynamics of single light-harvesting complexes. *Proceedings of the National Academy of Sciences USA*, 94:10630–10635, 1997. 25

J. E. Bowen Katari, V. L. Colvin, and A. P. Alivisatos. X-ray photoelectron spectroscopy of CdSe nanocrystals with applications to studies of the nanocrystal surface. *Journal of Physical Chemistry*, 98:4109–4117, 1994. 32

X. Brokmann, J. P. Hermier, G. Messin, P. Desbiolles, J. P. Bouchaud, and M. Dahan. Statistical aging and nonergodicity in the fluorescence of single nanocrystals. *Physical Review Letters*, 90(12):120601, 2003. Journal Article. 37, 77

M. Bruchez, M. Moronne, P. Gin, S. Weiss, and A. P. Alivisatos. Semiconductor nanocrystals as fluorescent biological labels. *Science*, 281:2013–2015, 1998. 5, 34, 137, 144

M. Bruchez. *Luminescent Semiconductor Nanocrystal — Intermittent Behavior and Use as Fluorescent Biological Probes.* PhD thesis, University of California at Berkeley, 1998. 34

C. Brunel, B. Lounis, P. Tamarat, and M. Orrit. Triggered source of single photons based on controlled single molecule fluorescence. *Physical Review Letters*, 83(14):2722–5, 1999. 26

L. E. Brus. A simple model for the ionization potential, electron affinity, and aqueous redox potentials of small semiconductor crystallites. *Journal of Chemical Physics*, 79(11):5566–5571, 1983. 29

S. A. Burgess, M. L. Walker, H. Sakakibara, P. J. Knight, and K. Oiwa. Dynein structure and power stroke. *Nature*, 421(6924):715–8, 2003. 3

V. Buschmann, K. D. Weston, and M. Sauer. Spectroscopic study and evaluation of red-absorbing fluorescent dyes. *Bioconjugate Chemistry*, 14(1):195–2, 2003. 28

T. A. Byassee, W. C. Chan, and S. Nie. Probing single molecules in single living cells. *Analytical Chemistry*, 72(22):5606–11, 2000. 27

B. Campbell and X. Michalet. Personal Communication, 2003. 101

W. C. W. Chan and S. Nie. Quantum dot bioconjugates for ultrasensitive nonisotopic detection. *Science*, 281:2016–2018, 1998. 5, 34, 137, 144

Y. Chen, J. D. Muller, P. T. C. So, and E. Gratton. The photon counting histogram in fluorescence fluctuation spectroscopy. *Biophysical Journal*, 77(1):553–567, 1999. 41

Y. Chen. *Analysis and applications of fluorescence fluctuation spectroscopy.* PhD thesis, University of Illinois at Urbana-Champaign, 1999. 41

G. Chirico, C. Fumagalli, and G. Baldini. Trapped brownian motion in single- and two-photon excitation fluorescence correlation experiments. *Journal of Physical Chemistry B*, 106(10):2508–2519, 2002. 110, 112, 119

D. T. Chiu and R. N. Zare. Biased diffusion, optical trapping, and manipulation of single molecules in solution. *Journal of the American Chemical Society*, 118(27):6512–6513, 1996. 110, 124

S. Chu, J. E. Bjorkholm, A. Ashkin, and A. Cable. Experimental observation of optically trapped atoms. *Physical Review Letters*, 57(3):314–317, 1986. 110

V. Colvin, M. Schlamp, and A. P. Alivisatos. Light-emitting diodes made from cadmium selenide nanocrystals and a semiconducting polymer. *Nature*, 370:354–357, 1994. 28

S. R. Cordero, P. J. Carson, R. A. Estabrook, G. F. Strouse, and S. K. Buratto. Photo-activated luminescence of CdSe quantum dot monolayers. *Journal of Physical Chemistry B*, 104:12137–12142, 2000. 75

R. O. Dabbousi, J. Rodriguez-Viejo, F. V. Mikulec, J. R. Heine, H. Mattoussi, R. Ober, K. F. Jensen, and M. G. Bawendi. (CdSe)ZnS core-shell quantum dots: synthesis and characterization of a size series of highly luminescent nanocrystallites. *Journal of Physical Chemistry B*, 101:9463–9475, 1997. 30, 34

M. Dahan, T. Laurence, F. Pinaud, D. S. Chemla, A. P. Alivisatos, M. Sauer, and S. Weiss. Time-gated biological imaging by use of colloidal quantum dots. *Optics Letters*, 26(11):825–7, 2001. 18, 82, 88, 89

S. Damjanovich, G. Vereb, A. Schaper, A. Jenei, J. Matko, J. P. Starink, G. Q. Fox, D. J. Arndt-Jovin, and T. M. Jovin. Structural hierarchy in the clustering of HLA class I molecules in the plasma membrane of human lymphoblastoid cells. *Proceedings of the National Academy of Sciences USA*, 92(4):1122–1126, 1995. 18

W. Denk, J. H. Strickler, and W. W. Webb. Two-photon laser scanning fluorescence microscopy. *Science*, 248(4951):73–6, 1990. 19

R. M. Dickson, A. B. Cubitt, R. Y. Tsien, and W. E. Moerner. On/off blinking and switching behaviour of single molecules of green fluorescent protein. *Nature*, 388(6640):355–358, 1997. 24

P. S. Dittrich and P. Schwille. Photobleaching and stabilization of fluorophores used for single-molecule analysis with one- and two-photon excitation. *Applied Physics B-Lasers and Optics*, 73(8):829–837, 2001. 19, 24, 47

B. Dubertret, P. Skourides, D. J. Norris, V. Noireaux, A. H. Brivanlou, and A. Libchaber. In vivo imaging of quantum dots encapsulated in phospholipid micelles. *Science*, 298(5599):1759–62, 2002. 34, 144

R. C. Dunn. Near-Field Scanning Optical Microscopy. *Chemical Review*, 99:2891–2927, 1999. 22

D. Duonghong, J. Ramsden, and M. Grätzel. Dynamics of interfacial electron-transfer processes in colloidal semiconductor systems. *Journal of the American Chemical Society*, 104(11):2985–2988, 1982. 33

Y. Ebenstein, T. Mokari, and U. Banin. Fluorescence quantum yield of CdSe/ZnS nanocrystals investigated by correlated atomic-force and single-particle fluorescence microscopy. *Applied Physics Letters*, 80(21):4033, 2002. 76, 98

Al. L. Efros and A. L. Efros. Interband absorption of light in a semiconductor sphere. *Soviet Physics-Semiconductors*, 16(7):772–775, 1982. 29

Al. L. Efros and M. Rosen. Random telegraph signal in the photoluminescence intensity of a single quantum dot. *Physical Review Letters*, 78(6):1110–1113, 1997. 37

Al. L. Efros and M. Rosen. The electronic structure of semiconductor nanocrystals. *Annual Review of Material Science*, 30:475–521, 2000. 31

C. Eggeling, J. Widengren, R. Rigler, and C. A. M. Seidel. Photobleaching of fluorescent dyes under conditions used for single-molecule detection: Evidence of two-step photolysis. *Analytical Chemistry*, 70(13):2651–2659, 1998. 47

M. Eigen and R. Rigler. Sorting single molecules — application to diagnostics and evolutionary biotechnology. *Proceedings of the National Academy of Sciences USA*, 91(13):5740–5747, 1994. 40

A. Einstein. Die von der molekular kinetischen Theorie der Wärme geforderte Bewegung von in ruhenden Flüssigkeiten suspendierte Teilchen. *Annalen der Physik*, 17:549–560, 1905. 65, 104, 122

A. I. Ekimov and A. A. Onuschenko. Quantum size effect in the optical spectra of semiconductor microcrystals. *Soviet Physics-Semiconductors*, 16(7):775–778, 1982. 29

S. A. Empedocles and M. G. Bawendi. Quantum-confined stark effect in single CdSe nanocrystallite quantum dots. *Science*, 278:2114–2117, 1997. 119

S. A. Empedocles and M. G. Bawendi. Influence of spectral diffusion on the line shapes of single CdSe nanocrystallite quantum dots. *Journal of Physical Chemistry*, 103:1826–1830, 1999. 35

S. A. Empedocles, D. J. Norris, and M. G. Bawendi. Photoluminescence spectroscopy of single CdSe nanocrystallite quantum dots. *Physical Review Letters*, 77(18):3873–3876, 1996. 35, 120

S. A. Empedocles, R. Neuhauser, and M. G. Bawendi. Three-dimensional orientation measurements of symmetric single chromophores using polarization microscopy. *Nature*, 399:126–130, 1999. 25

Th. Enderle, T. Ha, D. S. Chemla, and S. Weiss. Near-field fluorescence microscopy of cells. *Ultramicroscopy*, 71:303, 1998. 22

J. Enderlein, D. L. Robbins, W. P. Ambrose, P. M. Goodwin, and R. A. Keller. Statistics of single-molecule detection. *Journal of Physical Chemistry B*, 101:3626–3632, 1997. 124

J. Enderlein. Path Integral Approach to Fluorescence Correlation Experiments. *Physics Letters A*, V221(N6):427–433, 1996. 47

A. Eychmüller, A. Mews, and H. Weller. A quantum dot quantum well: CdS/HgS/CdS. *Chemical Physics Letters*, 208:59–62, 1993. 34

A. Eychmüller. Structure and photophysics of semiconductor nanocrystals. *Journal of Physical Chemistry B*, 104:6514, 2000. 29

S. Fafard, K. Hinzer, S. Raymond, M. Dion, J. McCaffrey, Y. Feng, and S. Charbonneau. Red-emitting semiconductor quantum dot lasers. *Science*, 274(5291):1350–1353, 1996. 28

L. Fleury, J. M. Segura, G. Zumofen, B. Hecht, and U. P. Wild. Nonclassical photon statistics in single-molecule fluorescence at room temperature. *Physical Review Letters*, 84(6):1148–51, 2000. 26

J. R. Fries, L. Brand, C. Eggeling, M. Kollner, and C. A. M. Seidel. Quantitative identification of different single molecules by selective time-resolved confocal fluorescence spectroscopy. *Journal of Physical Chemistry A*, 102(33):6601–6613, 1998. 26, 124

T. Förster. Zwischenmolekulare Energiewanderung und Fluoreszenz. *Annalen der Physik*, 6:55–75, 1948. 14

T. Funatsu, Y. Harada, M. Tokunaga, K. Saito, and T. Yanagida. Imaging of single fluorescent molecules and individual ATP turnovers by single myosin molecules in aqueous solution. *Nature*, 374(6522):555–559, 1995. 21

T. W. J. Gadella and T. M. Jovin. Oligomerization of epidermal growth factor receptors on A431 cells studied by time-resolved fluorescence imaging microscopy — a stereochemical model for tyrosine kinase receptor activation. *Journal of Cell Biology*, 129(6):1543–1558, 1995. 18

T. W. J. Gadella, T. M. Jovin, and R. M. Clegg. Fluorescence lifetime imaging microscopy (FLIM) — spatial resolution of microstructures on the nanosecond time scale. *Biophysical Chemistry*, 48(2):221–239, 1993. 17

T. W. J. Gadella, G. N. van der Krogt, and T. Bisseling. GFP-based FRET microscopy in living plant cells. *Trends in Plant Science*, 4(7):287–291, 1999. 18

N. Gaponik, D. V. Talapin, A. L. Rogach, K. Hoppe, E. V. Shevchenko, A. Kornowski, A. Eychmüller, and H. Weller. Thiol-capping of CdTe nanocrystals: an alternative to organometallic synthetic routes. *Journal of Physical Chemistry B*, 106:7177–7185, 2002. 75

A. C. Gavin, M. Bosche, R. Krause, P. Grandi, M. Marzioch, A. Bauer, J. Schultz, J. M. Rick, A. M. Michon, C. M. Cruciat, M. Remor, C. Hofert, M. Schelder, M. Brajenovic, H. Ruffner, A. Merino, K. Klein, M. Hudak, D. Dickson, T. Rudi, V. Gnau, A. Bauch, S. Bastuck, B. Huhse, C. Leutwein, M. A. Heurtier, R. R. Copley, A. Edelmann, E. Querfurth, V. Rybin, G. Drewes, M. Raida, T. Bouwmeester,

P. Bork, B. Seraphin, B. Kuster, G. Neubauer, and G. Superti-Furga. Functional organization of the yeast proteome by systematic analysis of protein complexes. *Nature*, 415(6868):141–7, 2002. 3

D. Gerion, F. Pinaud, S. C. Williams, W. J. Parak, D. Zanchet, S. Weiss, and A. P. Alivisatos. Synthesis and properties of biocompatible water-soluble silica-coated CdSe/ZnS semiconductor quantum dots. *Journal of Chemical Physics*, 2001. 34

E. R. Goldman, E. D. Balighian, H. Mattoussi, M. K. Kuno, J. M. Mauro, P. T. Tran, and G. P. Anderson. Avidin: a natural bridge for quantum dot-antibody conjugates. *Journal of the American Chemical Society*, 124(22):6378–82, 2002. Journal Article. 34, 144

M. Gösch, H. Blom, J. Holm, T. Heino, and R. Rigler. Hydrodynamic flow profiling in microchannel structures by single molecule fluorescence correlation spectroscopy. *Analytical Chemistry*, 72(14):3260–3265, 2000. 46

T. Ha, Th. Enderle, D.S. Chemla, P.R. Selvin, and S. Weiss. Quantum jumps of single molecules at room temperature. *Chemical Physics Letters*, 271:1–5, 1997. 24

A. Hagfeldt and M. Grätzel. Light-induced redox reactions in nanocrystalline systems. *Chemical Review*, 95:49–68, 1995. 28, 29

Q. S. Hanley, D. J. Arndt-Jovin, and T. M. Jovin. Spectrally resolved fluorescence lifetime imaging microscopy. *Applied Spectroscopy*, 56(2):155–66, 2002. 19

R. P. Haugland. *Handbook of fluorescent probes and research products*. Molecular Probes, Eugene USA, 9th edition, 2003. 27

U. Haupts, S. Maiti, P. Schwille, and W. W. Webb. Dynamics of fluorescence fluctuations in green fluorescent protein observed by fluorescence correlation spectroscopy. *Proceedings of the National Academy of Sciences USA*, 95(23):13573–8, 1998. 40

A. A. Heikal, S. T. Hess, G. S. Baird, R. Y. Tsien, and W. W. Webb. Molecular spectroscopy and dynamics of intrinsically fluorescent proteins: coral red (dsRed) and yellow (Citrine). *Proceedings of the National Academy of Sciences USA*, 97(26):14831, 2000. 28

S. Hell, G. Reiner, C. Cremer, and E. H. K. Stelzer. Aberrations in confocal fluorescence microscopy induced by mismatches in refractive index. *Jounal of Microscopy*, 169(3):391–405, 1993. 94

E. H. Hellen and D. Axelrod. Fluorescence emission at dielectric and metal-film interfaces. *Journal of the Optical Society of America B*, 4(3):337–349, 1987. 13, 120

A. Henglein. Photochemistry of colloidal cadmium sulfide. 2. Effects of adsorbed methyl viologen and of colloidal platinum. *Journal of Physical Chemistry*, 86:2291–2293, 1982. 29

J. F. W. Herschel. On a case of superficial colour presented by a homogeneous liquid internally colourless. *Philosophical Transactions of the Royal Society of London*, 135:143–145, 1845. 1

S. T. Hess and W. W. Webb. Focal volume optics and experimental artifacts in confocal fluorescence correlation spectroscopy. *Biophysical Journal*, 83(4):2300–17, 2002. 95

B. C. Hess, I. G. Okhrimenko, R. C. Davis, B. C. Stevens, Q. A. Schulzke, Q. A. Wright, C. D. Bass, C. D. Evans, and S. L. Summers. Surface transformation and photoinduced recovery in CdSe nanocrystals. *Physical Review Letters*, 86(14):3132–3135, 2001. 75

M. A. Hines and P. Guyot-Sionnest. Synthesis and characterization of strongly luminescing ZnS-capped CdSe nanocrystals. *Journal of Physical Chemistry*, 100:468–471, 1996. 30, 34

T. Hirschfeld. Optical microscopic observation of single small molecules. *Applied Optics*, 15(12):2965–2966, 1976. 4, 21

Y. Ho, A. Gruhler, A. Heilbut, G. D. Bader, L. Moore, S. L. Adams, A. Millar, P. Taylor, K. Bennett, K. Boutilier, L. Yang, C. Wolting, I. Donaldson, S. Schandorff, J. Shewnarane, M. Vo, J. Taggart, M. Goudreault, B. Muskat, C. Alfarano, D. Dewar, Z. Lin, K. Michalickova, A. R. Willems, H. Sassi, P. A. Nielsen, K. J. Rasmussen, J. R. Andersen, L. E. Johansen, L. H. Hansen, H. Jespersen, A. Podtelejnikov, E. Nielsen, J. Crawford, V. Poulsen, B. D.

Sorensen, J. Matthiesen, R. C. Hendrickson, F. Gleeson, T. Pawson, M. F. Moran, D. Durocher, M. Mann, C. W. Hogue, D. Figeys, and M. Tyers. Systematic identification of protein complexes in Saccharomyces cerevisiae by mass spectrometry. *Nature*, 415(6868):180–3, 2002. 3

J. Hofkens, M. Maus, T. Gensch, T. Vosch, M. Cotlet, F. Kohn, A. Herrmann, K. Mullen, and F. De Schryver. Probing photophysical processes in individual multichromophoric dendrimers by single-molecule spectroscopy. *Journal of the American Chemical Society*, 122(38):9278–9288, 2000. 25

A. Hopt and E. Neher. Highly nonlinear photodamage in two-photon fluorescence microscopy. *Biophysical Journal*, 80(4):2029–36, 2001. 19

J. Hu, Ls Li, W. Yang, L. Manna, Lw Wang, and A. P. Alivisatos. Linearly polarized emission from colloidal semiconductor quantum rods. *Science*, 292(5524):2060–3, 2001. 141

T. Huser, M. Yan, and L. J. Rothberg. Single chain spectroscopy of conformational dependence of conjugated polymer photophysics. *Proceedings of the National Academy of Sciences USA*, 97(21):11187–91, 2000. 25

R. Iino, I. Koyama, and A. Kusumi. Single molecule imaging of green fluorescent proteins in living cells: E-cadherin forms oligomers on the free cell surface. *Biophysical Journal*, 80:2667–2677, 2001. 27

J. K. Jaiswal, H. Mattoussi, J. M. Mauro, and S. M. Simon. Long-term multiple color imaging of live cells using quantum dot bioconjugates. *Nature Biotechnology*, 21(1):47–51, 2003. 34, 144

L. Jürgens, D. Arndt-Jovin, I. Pecht, and T. M. Jovin. Proximity relationships between the type I receptor for Fc epsilon (Fc epsilon RI) and the mast cell function-associated antigen (MAFA) studied by donor photobleaching fluorescence resonance energy transfer microscopy. *European Journal of Immunology*, 26(1):84–91, 1996. 18

A. N. Kapanidis and S. Weiss. Fluorescent probes and bioconjugation chemistries for single-molecule fluorescence analysis of biomolecules. *Journal of Chemical Physics*, 117(24):1095310964, 2002. 28

P. Kask, K. Palo, D. Ullmann, and K. Gall. Fluorescence-intensity distribution analysis and its application in biomolecular detection technology. *Proceedings of the National Academy of Sciences USA*, 96(24):13756–61, 1999. 41

P. Kask, K. Palo, N. Fay, L. Brand, U. Mets, D. Ullmann, J. Jungmann, J. Pschorr, and K. Gall. Two-dimensional fluorescence intensity distribution analysis: theory and applications. *Biophysical Journal*, 78(4):1703–13, 2000. 41

H. J. Kimble, M. Dagenais, and L. Mandel. Photon Antibunching in Resonance Fluorescence. *Physical Review Letters*, 39(11):691, 1977. 26

V. I. Klimov, A. A. Mikhailovsky, Su Xu, A. Malko, J. A. Hollingsworth, C. A. Leatherdale, H.-J. Eisler, and M. G. Bawendi. Optical gain and stimulated emission in nanocrystal quantum dots. *Science*, 290:314–317, 2000. 28

J. P. Knemeyer, D. P. Herten, and M. Sauer. Detection and identification of single molecules in living cells using spectrally resolved fluorescence lifetime imaging microscopy. *Analytical Chemistry*, 75(9):2147–2153, 2003. 27

D. S. Ko, M. Sauer, S. Nord, R. Müller, and J. Wolfrum. Determination of the diffusion coefficient of dye in solution at single molecule level. *Chemical Physics Letters*, 269(1-2):54–58, 1997. 124

D. E. Koppel. Statistical accuracy in fluorescence correlation spectroscopy. *Physical Review A*, 10:1938–1945, 1974. 48

A. R. Kortan, R. Hull, R. L. Opila, M. G. Bawendi, M. L. Steigerwald, P. J. Carroll, and L. E. Brus. Nucleation and growth of CdSe on ZnS quantum crystallite seeds, and vice versa, in inverse micelle media. *Journal of the American Chemical Society*, 112:1327–1332, 1990. 33

O. Krichevsky and G. Bonnet. Fluorescence correlation spectroscopy: the technique and its applications. *Reports on Progress in Physics*, 65(2):251–97, 2002. 39, 44, 48

M. Kuno, J. K. Lee, B. O. Dabbousi, F. V. Mikulec, and M. G. Bawendi. The band edge luminescence of surface modified CdSe nanocrystallites: Probing the luminescing state. *Journal of Chemical Physics*, 106(23):9869–9882, 1997. 32

M. Kuno, D. P. Fromm, H. F. Hamann, A. Gallagher, and D. J. Nesbitt. Nonexponential "blinking" kinetics of single CdSe quantum dots: A universal power law behavior. *Journal of Chemical Physics*, 112(7):3117–3120, 2000. 25, 36, 81

M. Kuno, D. P. Fromm, H. F. Hamann, A. Gallagher, and D. J. Nesbitt. On/off fluorescence intermittency of single semiconductor quantum dots. *Journal of Chemical Physics*, 115(2):1028–1040, 2001. 36

T. D. Lacoste, X. Michalet, F. Pinaud, D. S. Chemla, A. P. Alivisatos, and S. Weiss. Ultrahigh-resolution multicolor colocalization of single fluorescent probes. *Proceedings of the National Academy of Sciences USA*, 97(17):9461–6, 2000. 147

M. Lakadamyali, M. J. Rust, H. P. Babcock, and X. Zhuang. Visualizing infection of individual influenza viruses. *Proceedings of the National Academy of Sciences USA*, 100(16):9280–5, 2003. 27

J. R. Lakowicz and K. W. Berndt. Lifetime-Selective Fluorescence Imaging Using an Rf Phase-Sensitive Camera. *Review of Scientific Instruments*, 62(7):1727–1734, 1991. 17

J. R. Lakowicz, H. Szmacinski, K. Nowaczyk, and M. L. Johnson. Fluorescence lifetime imaging of free and protein-bound NADH. *Proceedings of the National Academy of Sciences USA*, 89(4):1271–5, 1992. 17

J.R. Lakowicz. *Principles of Fluorescence Spectroscopy.* Kluwer Academic/Plenum Publishers, New York, USA, 2nd edition, 1999. 5, 27, 52

Don C. Lamb, Andreas Schenk, Carlheinz Rocker, C. Scalfi-Happ, and G. Ulrich Nienhaus. Sensitivity enhancement in fluorescence correlation spectroscopy of multiple species using time-gated detection. *Biophysical Journal*, 79(2):1129–1138, 2000. 120

D. R. Larson, W. R. Zipfel, R. M. Williams, S. W. Clark, M. P. Bruchez, F. W. Wise, and W. W. Webb. Water-soluble quantum dots for multiphoton fluorescence imaging in vivo. *Science*, 300(5624):1434–6, 2003. 106, 119

T. A. Laurence. *Photon-counting single-molecule spectroscopy for studying conformational dynamics and macromolecular interactions.* PhD thesis, University of California at Berkeley, 2002. 41, 142

C. A. Leatherdale, W. K. Woo, F.V. Mikulec, and M. G. Bawendi. On the absorption cross section of CdSe nanocrystal quantum dots. *Journal of Physical Chemistry B*, 106(5346):7619–7622, 2002. 71, 98

B. Lounis and W. E. Moerner. Single photons on demand from a single molecule at room temperature. *Nature*, 407:491–493, 2000. 26

B. Lounis, H. A. Bechtel, D. Gerion, A. P. Alivisatos, and W. E. Moerner. Photon antibunching in single CdSe/ZnS quantum dot fluorescence. *Chemical Physics*, 329:399–404, 2000. 84, 101

H. P. Lu and X. S. Xie. Single-molecule spectral fluctuations at room temperature. *Nature*, 385(6612):143–6, 1997. 24

H. P. Lu, L. Xun, and X. S. Xie. Single-molecule enzymatic dynamics. *Science*, 282:1877–1882, 1998. 27

J. J. Macklin, J. K. Trautman, T. D. Harris, and L. E. Brus. Imaging and time-resolved spectroscopy of single molecules at an interface. *Science*, 272:255–258, 1996. 21

D. Magde, E. L. Elson, and W. W. Webb. Fluorescence correlation spectroscopy. II. An experimental realization. *Biopolymers*, 13(1):29–61, 1974. 6, 39

H. Mattoussi, J. M. Mauro, E. R. Goldman, G. P. Anderson, V. C. Sundar, F. V. Mikulec, and M. G. Bawendi. Self-assembly of CdSe-ZnS quantum dot bioconjugates using an engineered recombinant protein. *Journal of the American Chemical Society*, 122, 2000. 34, 144

U. Meseth, T. Wohland, R. Rigler, and H. Vogel. Resolution of fluorescence correlation measurements. *Biophysical Journal*, 76(3):1619–1631, 1999. 39

U. Mets, J. Widengren, and R. Rigler. Application of the antibunching in dye fluorescence: measuring the excitation rates in solution. *Chemical Physics*, 218(1-2):191–8, 1997. 26, 46

X. Michalet and S. Weiss. Single-molecule spectroscopy and microscopy. *Comptes Rendus Physique*, 3(5):619–644, 2002. 138

X. Michalet, R. Ekong, F. Fougerousse, S. Rousseaux, C. Schurra, N. Hornigold, M. Slegtenhorst, J. Wolfe, S. Povey, J. S. Beckmann, and A. Bensimon. Dynamic molecular combing: stretching the whole human genome for high-resolution studies. *Science*, 277(5331):1518–1523, 1997. 144

X. Michalet, F. Pinaud, T. D. Lacoste, M. Dahan, M. P. Bruchez, A. P. Alivisato, and S. Weiss. Properties of fluorescent semiconductor nanocrystals and their application to biological labeling. *Single Molecules*, 2(4):261–276, 2001. 5, 16, 29, 137

X. Michalet. Personal Communication, 2003. 101, 137

P. Michler, A. Imamoglu, M. D. Mason, P. J. Carson, G. F. Strouse, and S. K. Buratto. Quantum correlation among photons from a single quantum dot at room temperature. *Nature*, 406(6799):968–70, 2000. 26, 29

J. N. Miller. *Standards in Fluorescence Spectroscopy*. Ultraviolet Spectrometry Group. Chapman and Hall, London, New York, 1st edition, 1981. 90

W. E. Moerner and L. Kador. Optical detection and spectroscopy of single molecules in a solid. *Physical Review Letters*, 62(21):2535–2538, 1989. 21

W. E. Moerner and M. Orrit. Illuminating single molecules in condensed matter. *Science*, 283:1670–1676, 1999. 4

W. E. Moerner. Examining nanoenvironments in solids on the scale of a single, isolated impurity molecule. *Science*, 265:46–53, 1994. 21

W. E. Moerner. A dozen years of single-molecule spectroscopy in physics, chemistry, and biophysics. *Journal of Physical Chemistry B*, 106(5):910–27, 2002. 24

J. D. Muller, Y. Chen, and E. Gratton. Resolving heterogeneity on the single molecular level with the photon-counting histogram. *Biophysical Journal*, 78(1):474–486, 2000. 41

C. B. Murray, D. J. Norris, and M. G. Bawendi. Synthesis and characterization of nearly monodisperse CdE (E = S, Se, Te) semiconductor nanocrystallites. *Jounal of the American Chemical Society*, 115:8706–8715, 1993. 33

E. Neher and B. Sakmann. Single-channel currents recorded from membrane of denervated frog muscle fibres. *Nature*, 260:799–802, 1976. 2

R. G. Neuhauser, K. T. Shimizu, W. K. Woo, S. A. Empedocles, and M. G. Bawendi. Correlation between fluorescence intermittency and spectral diffusion in single semiconductor quantum dots. *Physical Review Letters*, 85(15):3301–3304, 2000. 35

S. Nie and R. N. Zare. Optical detection of single molecules. *Annual Review of Biophysics and Biomolecular Structure*, 26:567–96, 1997. 24

S. Nie, D. T. Chiu, and R. N. Zare. Probing individual molecules with confocal fluorescence microscopy. *Science*, 266:1018–1021, 1994. 21

M. Nirmal, D. J. Norris, M. G. Bawendi, Al. L. Efros, and M. Rosen. Observation of the "dark exciton" in CdSe quantum dots. *Physical Review Letters*, 75(20):3728–3731, 1995. 31, 32

M. Nirmal, B. O. Dabbousi, M. G. Bawendi, J. J. Macklin, J. K. Trautman, T. D. Harris, and L. E. Brus. Fluorescence intermittency in single cadmium selenide nanocrystals. *Nature*, 383:802–804, 1996. 35, 36, 37

D. J. Norris and M. G. Bawendi. Measurement and assignment of the size-dependent optical spectrum in CdSe quantum dots. *Physical Review B*, 53(24):16338–16346, 1996. 70, 71

D. J. Norris, M. Bawendi, and L. Brus. Optical properties of semiconductor nanocrystals. In J. Jortner and M. Ratner, editors, *Molecular Electronics*. Blackwell Science, USA, 1997. 31

M. Orrit and J. Bernard. Single pentacene molecules detected by fluorescence excitation in a p-terphenyl crystal. *Physical Review Letters*, 65(21):2716–2719, 1990. 24

M. A. Osborne, S. Balasubramanian, W. S. Furey, and D. Klenerman. Optically biased diffusion of single molecules studied by confocal fluorescence microscopy. *Journal of Physical Chemistry B*, 102:3160–3167, 1998. 110, 119

K. Palo, U. Mets, S. Jäger, P. Kask, and K. Gall. Fluorescence intensity multiple distributions analysis: concurrent determination of diffusion times and molecular brightness. *Biophysical Journal*, 79(6):2858–66, 2000. 41

G. H. Patterson and D. W. Piston. Photobleaching in two-photon excitation microscopy. *Biophysical Journal*, 78(4):2159–62, 2000. 19

J. B. Pawley, editor. *Handbook of Biological Confocal Microscopy*. Plenum Press, New York, USA, 1995. 23

X. Peng, M. C. Schlamp, A. V. Kadavanich, and A. P. Alivisatos. Epitaxial growth of highly luminescent CdSe/CdS core/shell nanocrystals with photostability and electronic accessibility. *Journal of the American Chemical Society*, 119(30):7019–7029, 1997. 30, 34

A. Periasamy. *Methods in Cellular Imaging*. Oxford University Press, UK, 2001. 17

Francis Perrin. Théorie quantique des transferts d'activation entre molécules de même espèce. Cas des solutions fluorescentes. *Annales de Physique*, 17:283–313, 1932. 14

R. Peters. Introduction to the multiple tau correlation technique. *ALV-GmbH promotional literature*, 2000. 40, 67

F. Pinaud. Personal Communication, 2002. 71

D. W. Piston, D. R. Sandison, and W. W. Webb. Time-resolved fluorescence imaging and background rejection by two-photon excitation in laser scanning microscopy. *Proceedings SPIE*, 1640:379–389, 1992. 19

W. H. Press. *Numerical Recipes in C: The Art of Scientific Computing*. Cambridge University Press, UK, 2nd edition, 1993. 47

H. Qian and E. L. Elson. On the analysis of high order moments of fluorescence fluctuations. *Biophysical Journal*, 57(2):375–80, 1990. 41

H. Qian. On the statistics of fluorescence correlation spectroscopy. *Biophysical Chemistry*, 38(1-2):49–57, 1990. 48

R. Rigler and E.S. Elson. *Fluorescence Correlation Spectroscopy: Theory and Applications*. Springer-Verlag, Berlin, Heidelberg, New York, 1st edition, 2001. 39, 40, 46

R. Rigler, U. Mets, J. Widengren, and P. Kask. Fluorescence correlation spectroscopy with high count rate and low background — analysis of translational diffusion. *European Biophysics Journal*, 22(3):169–175, 1993. 22, 40

R. Rossetti and L. Brus. Electron-hole recombination emission as a probe of surface chemistry in aqueous CdS colloids. *Journal of Physical Chemistry*, 86:4470–4472, 1982. 33

T. Ruckstuhl, J. Enderlein, S. Jung, and S. Seeger. Forbidden light detection from single molecules. *Analytical Chemistry*, 72(9):2117–23, 2000. 120

S. Saffarian and E. L. Elson. Statistical analysis of fluorescence correlation spectroscopy: the standard deviation and bias. *Biophysical Journal*, 84(3):2030–2042, 2003. 48

Y. Sako, K. Hibino, T. Miyauchi, Y. Miyamoto, M. Ueda, and T. Yanagida. Single-molecule imaging of signaling molecules in living cells. *Single Molecules*, 1(2):159–163, 2000. 21, 27

E. J. Sanchez, L. Novotny, G. R. Holtom, and S. X. Xie. Room-temperature fluorescence imaging and spectroscopy of single molecules by two-photon excitation. *Journal of Physical Chemistry A*, 101(38):7019–23, 1997. 19

M. Sauer, K. H. Drexhage, C. Zander, and J. Wolfrum. Diode laser based detection of single molecules in solutions. *Chemical Physics Letters*, 254(3-4):223–228, 1996. 28

G. J. Schütz, G. Kada, V. P. Pastushenko, and H. Schindler. Properties of lipid microdomains in a muscle cell membrane visualized by single molecule microscopy. *EMBO Journal*, 19(5):892–901, 2000. 26

G. J. Schütz, V. P. Pastushenko, H. Gruber, H. G. Knaus, B. Pragl, and H. Schindler. 3D imaging of individual ion channels in live cells at 40 nm resolution. *Single Molecules*, 1(1):25–31, 2000. 21, 26

K. Schätzel. New concepts in correlator design. *Inst. Phys. Conf. Ser.*, 77:175–184, 1985. 40

P. Schwille, J. Korlach, and W. W. Webb. Fluorescence correlation spectroscopy with single-molecule sensitivity on cell and model membranes. *Cytometry*, 36(3):176–82, 1999. 26

P. Schwille, J. Korlach, and W. W. Webb. Fluorescence correlation spectroscopy with single-molecule sensitivity on cell and model membranes. *Cytometry*, 36(3):176–82, 1999. 47

P. Schwille. Fluorescence correlation spectroscopy and its potential for intracellular applications. *Cell Biochem Biophys*, 34(3):383–408, 2001. 47, 145

G. Seisenberger, M. U. Ried, T. Endreß, H. Büning, M. Hallek, and C. Bräuchle. Real-time single-molecule imaging of the infection pathway of an adeno-associated virus. *Science*, 294:1929–1932, 2001. 27

J. Seufert, M. Obert, M. Scheibner, N. A. Gippius, G. Bacher, A. Forchel, T. Passow, K. Leonardi, and D. Hommel. Stark effect and polarizability in a single CdSe/ZnSe quantum dot. *Applied Physics Letters*, 79(7):1033–1035, 2001. 119

E. B. Shera, N. K. Seitzinger, L. M. Davis, R. A. Keller, and S. A. Soper. Detection of single fluorescent molecules. *Chemical Physics Letters*, 174(6):553–557, 1990. 21

K. T. Shimizu, R. G. Neuhauser, C. A. Leatherdale, S. A. Empedocles, W. K. Woo, and M. G. Bawendi. Blinking statistics in single semiconductor nanocrystal quantum dots. *Physical Review B*, 6320(20):5316,U395–U398, 2001. 36, 125

P. T. C. So, T. French, W. M. Yu, K. M. Berland, C. Y. Dong, and E. Gratton. Time-resolved fluorescence microscopy using two-photon excitation. *Bioimaging*, 3(2):49–63, 1995. 19

P. T. So, C. Y. Dong, B. R. Masters, and K. M. Berland. Two-photon excitation fluorescence microscopy. *Annual Review of Biomedical Engineering*, 2:399–429, 2000. 19

L. Spanhel, M. Haase, H. Weller, and A. Henglein. Photochemistry of colloidal semiconductors. 20. Surface modification and stability of strong luminescing CdS particles. *Journal of the American Chemical Society*, 109:5649, 1987. 30

G. G. Stokes. On the change of refrangibility of light. *Philosophical Transactions of the Royal Society of London*, 142:463–562, 1852. 1

L. Stryer and R. P. Haugland. Energy transfer: a spectroscopic ruler. *Proceedings of the National Academy of Sciences USA*, 58:719–726, 1967. 14

K. Svoboda and S. M. Block. Biological applications of optical forces. *Annual Review of Biophysics and Biomolecular Structure*, 23:247–85, 1994. 51, 110

J. Sytsma, J. M. Vroom, C. J. DeGrauw, and H. C. Gerritsen. Time-gated fluorescence lifetime imaging and microvolume spectroscopy using two-photon excitation. *Journal of Microscopy*, 191:39–51, 1998. 19

P. Tamarat, A. Maali, B. Lounis, and M. Orrit. Ten years of single-molecule spectroscopy. *Journal of Physical Chemistry A*, 104(1):1–16, 2000. 24

E. Terpetschnig, H. Szmacinski, H. Malak, and J. R. Lakowicz. Metal-ligand complexes as a new class of long-lived fluorophores for protein hydrodynamics. *Biophysical Journal*, 68:342–350, 1995. 18

P. Tinnefeld, V. Buschmann, D.-P. Herten, K.-T. Han, and M. Sauer. Confocal fluorescence lifetime imaging microscopy (FLIM) at the single molecule level. *Single Molecules*, 1(3):215–223, 2000. 17

P. Tinnefeld, D. P. Herten, and M. Sauer. Photophysical dynamics of single molecules studied by spectrally-resolved fluorescence lifetime imaging microscopy (SFLIM). *Journal of Physical Chemistry A*, 105(34):7989–8003, 2001. 26

P. Tinnefeld, K. D. Weston, T. Vosch, M. Cotlet, T. Weil, J. Hofkens, K. Mullen, F. C. De Schryver, and M. Sauer. Antibunching in the emission of a single tetrachromophoric dendritic system. *J Am Chem Soc*, 124(48):14310–1, 2002. 26

P. Tinnefeld. *Multiparameter single-molecule spectroscopy based on spectrally-resolved fluorescence lifetime imaging microscopy.* PhD thesis, 2002. 28

J. K. Trautman, J. J. Macklin, L. E. Brus, and E. Betzig. Near-field spectroscopy of single molecules at room temperature. *Science*, 369:40–42, 1994. 24

R. Y. Tsien. The green fluorescent protein. *Annual Review of Biochemistry*, 67:509–544, 1998. 28

A. M. van Oijen, M. Ketelaars, J. Kohler, T. J. Aartsma, and J. Schmidt. Spectroscopy of individual light-harvesting 2 complexes of Rhodopseudomonas acidophila: diagonal disorder, intercomplex heterogeneity, spectral diffusion, and energy transfer in the B800 band. *Biophysical Journal*, 78(3):1570–7, 2000. 25

A. Van Orden, N. P. Machara, P. M. Goodwin, and K. A. Keller. Single-molecule identification in flowing sample streams by fluorescence burst size and intraburst fluorescence decay rate. *Analytical Chemistry*, 70(7):1444–1451, 1998. 26

W. G. J. H. M. van Sark, P. L. T. M. Frederix, D. J. Van den Heuvel, H. Gerrtsen, A. A. Bol, J. N. J. van Lingen, C. de Mello Donegá, and A. Meijerink. Photooxidation and photobleaching of CdSe/ZnS quantum dots probed by room-temperatur time-resolved spectroscopy. *Journal of Physical Chemistry B*, 105:8281, 2001. 37, 75, 120

D. A. Vanden Bout, W. T. Yip, D. Hu, D. K. Fu, T. M. Swager, and P. F. Barbara. Discrete intensity jumps and intramolcular electronic energy transfer in the spectroscopy of single conjugated polymer molecules. *Science*, 277(5329):1074–1077, 1997. 25

R. Verberg and M. Orrit. Photon statistics in the fluorescence of single molecules and nanocrystals: Correlation functions versus distributions of on- and off-times. *Journal of Chemical Physics*, 119:2214–2222, 2003. 106, 118

R. Verberg, A. M. van Oijen, and M. Orrit. Simple model for the power-law blinking of single semiconductor nanocrystals. *Physical Review B*, 66:233202, 2002. 106, 118

G. Vereb, E. Jares-Erijman, P. R. Selvin, and T. M. Jovin. Temporally and spectrally resolved imaging microscopy oflanthanide chelates. *Biophysical Journal*, 74:2210–2222, 1998. 18

T. Vossmeyer, L. Katsikas, M. Giersig, I. G. Popovic, K. Diesner, A. Chemseddine, A. Eychmüller, and H. Weller. CdS nanoclusters: synthesis, characterization, size dependent oscillator strength, temperature shift of the excitonic transition energy, and reversible absorbance shift. *Journal of Physical Chemistry*, 98:7665–7673, 1994. 33

X. F. Wang, T. Uchida, D. M. Coleman, and S. Minami. A 2-dimensional fluorescence lifetime imaging system using a gated image intensifier. *Applied Spectroscopy*, 45(3):360–366, 1991. 17

Shimon Weiss. Fluorescence spectroscopy of single biomolecules. *Science*, 283:1676–1683, 1999. 137

J. Widengren and R. Rigler. Mechanisms of photobleaching investigated by fluorescence correlation spectroscopy. *Bioimaging*, 4(3):149–57, 1996. 47

J. Widengren and P. Schwille. Characterization of photoinduced isomerization and back-isomerization of the cyanine dye Cy5 by fluorescence correlation spectroscopy. *Journal of Physical Chemistry A*, 104:6416–6428, 2000. 40

J. Widengren, U. Mets, and R. Rigler. Fluorescence correlation spectroscopy of triplet states in solution — a theoretical and experimental study. *Journal of Physical Chemistry*, 99(36):13368–13379, 1995. 40, 46, 109, 125

T. Wohland, R. Rigler, and H. Vogel. The standard deviation in fluorescence correlation spectroscopy. *Biophysical Journal*, 80(6):2987–2999, 2001. 48, 65

M. Wu, P. M. Goodwin, W. P. Ambrose, and R. A. Keller. Photochemistry and fluorescence emission dynamics of single molecules in solution - B-phycoerythrin. *Journal of Physical Chemistry*, 100(43):17406–17409, 1996. 25

X. Wu, H. Liu, J. Liu, K. N. Haley, J. A. Treadway, J. P. Larson, N. Ge, F. Peale, and M. P. Bruchez. Immunofluorescent labeling of cancer marker Her2 and other cellular targets with semiconductor quantum dots. *Nature Biotechnology*, 21(1):41–6, 2003. 35, 144

S. X. Xie and R. C. Dunn. Probing single molecule dynamics. *Science*, 265(5170):361–364, 1994. 24

X. S. Xie and J. K. Trautman. Optical studies of single molecules at room temperature. *Annual Reviews of Physical Chemistry*, 49:441–480, 1998. 24, 138

W. T. Yip, D. H. Hu, J. Yu, D. A. VandenBout, and P. F. Barbara. Classifying the photophysical dynamics of single- and multiple-chromophoric molecules by single molecule spectroscopy. *Journal of Physical Chemistry A*, 102(39):7564–7575, 1998. 25

T. Zimmermann, J. Rietdorf, and R. Pepperkok. Spectral imaging and its applications in live cell microscopy. *FEBS Letters*, 546(1):87–92, 2003. 16